

Compaction of silty sands through biogenic gas desaturation pretreatment

Author
G.M. Andrag

DELFT UNIVERSITY OF TECHNOLOGY
Faculty of Civil Engineering and Geosciences
Department of Geoscience & Engineering
Section Geo-Engineering

Front cover pictures:

Top left: One of Cofra's CDC (RIC) units at work. Project: Gorgon, Barrow Island, Australia (2009 - 2013)

Bottom right: Project Suez Canal, Dredging a 35-kilometers-long and 24-meters-deep shipping route. Sand deposit.

Pictures supplied by Boskalis Brand Centre

Compaction of silty sands through biogenic gas desaturation pretreatment

MSc thesis

by

G.M. Andrag

student number: 4520815

in partial fulfilment of the requirements for the degree of
Master of Science in Civil Engineering

October 2017

Graduation committee

Chair/daily supervisor

Prof. dr. C. Jommi
Geo-Engineering, TU Delft

Supervisor

Dr. ir. L. A. van Paassen
Center for Bio-mediated and Bio-inspired Geotechnics (CBBG),
Arizona State University
(formerly Geo-Engineering, TU Delft)

Supervisor

Dr. A. Askarinejad
Geo-Engineering, TU Delft

Supervisor Deltares

Dr. ir. W. R. L. van der Star
Subsurface and Groundwater Systems, Deltares

Supervisor Boskalis

Ir. B. Vos
Hydronic B.V., Boskalis

External supervisor

Prof. dr. ir. S. G. J. Aarninkhof
Coastal Engineering, TU Delft

An electronic version of this thesis is available at <http://repository.tudelft.nl/>

Acknowledgements

This thesis is the final assignment of the master Civil Engineering at the Delft University of Technology. Without the contribution and support of my committee, this study would not have been possible. This study is the brainchild of Leon van Paassen. The interesting topic gave me a taste of bio-mediated and bio-inspired geotechnics, which will undoubtedly be revolutionary. Without the support of Wouter van der Star at Deltares and Bas Vos at Boskalis and the knowledge they contributed from their respective fields, it would not have been possible to enter the labs, let alone integrate the fields of biochemistry and geotechnics. Thank you for providing direction. The guidance and discussions from Prof Jommi proved invaluable in the completion of this study. I would like to thank Vinh Pham for the opportunity to tap into her knowledge base on MIDP. As an expert in this process, she made it seem easy.

A number of parties contributed to the successful execution of this study: Arno Mulder and the staff at the TU and Vincent Franke and the Boskalis Environmental team. Thank you.

The support of friends and family, new and old, Southern and Northern hemisphere, proved unfaltering.

G. M. Andrag
Delft, October 2017



Summary

This thesis entitled “*Compaction of Silty Sands through Biogenic Gas Desaturation Pretreatment*” investigates a method to improve compactibility of an initially fully saturated soil body bringing it to a saturation corresponding to the optimum water content of the targeted soil layer. The process comprises two stages: a reaction phase to desaturate the soil body, and compaction phase where the necessary loading is applied to the system. The substrate solution with predetermined concentration, combined with a bacterial inoculum to convert the substrate into nitrogen gas, is injected into the soil and left to react. Gas is produced in-situ as a result of the stimulation of the bacteria which creates a local overpressure and expels water from the system. The desaturated soil body is subsequently compacted. The aim is to achieve a higher degree of compaction with the same energy, or the same degree of compaction with less energy input in the desaturated soil as opposed to the fully saturated case where energy is wasted on expelling water.

This study builds on the work of Pham (2017) who achieved an 80% saturation in a fine sand through denitrification of an engineered substrate solution. The denitrifying bacterial strand, commonly found in organic rich soil, use the organic carbon energy source to convert the nitrate into nitrogen gas. Based on the combination of stoichiometry of the biochemical reaction, Henry’s law and the Ideal gas law, the substrate solution can be engineered to produce the required volume of nitrogen gas to desaturate the soil body.

This study comprises a review of existing literature, enrichment of denitrifying bacteria, the design and execution of a test to evaluate gas formation at varying pressure conditions and consequent desaturation. Subsequent static compaction is performed under unchanging conditions and the work approach is used to evaluate the efficiency of the protocol in different tests. The results from various test configurations are compared and contrasted to the untreated counterpart. Conclusions are drawn and recommendations made based on the results.

The substrate concentrations are successfully engineered to achieve the target saturation of 80%, which correspond to the optimum water content of most soils to achieve a maximum dry density after compaction. However, the saturation of the specific uniform fine sand with varying fines fraction is not reached due to its inability to contain the gas. The pH of the soil and particle size distribution is found to have a major influence on the gas volume and production rates, as well as the initial lag period. Static compaction on a radially confined sample is only a partial approximation of compaction techniques in practice due to a uniform stress increment which also limits the migration of gas in the soil. The high placement densities in this experimental test limit the improvements in maximum dry densities achieved.

It was initially hypothesised that the method of biogenic gas desaturation could be introduced as an alternative drainage technique. Based on the results, this hypothesis cannot be proven or failed. No clear reduction in energy input is measured between the treated and untreated samples. It is however measured that no expansion of the soil skeleton occurs due to in-situ gas production under the given pressure conditions. For future research, three suggestions are made. Firstly, it is recommended to test a material that can contain sufficient gas to reach the saturation corresponding to the optimal water content. Secondly, an alternative placement method must be developed to allow for sufficient control over the placement density, the initial saturation and the substrate solution. Thirdly, a method to introduce dynamic loading into the system must be developed - either through impulse or vibratory loading of the existing set-up, or through a change of set-up.

Contents

Acknowledgements	i
Summary	iii
Contents	v
List of Figures	viii
List of Tables	x
Nomenclature	xii
1 Introduction	1
1.1 Problem Statement	1
1.2 Proposed solution	2
1.3 Hypothesis	2
1.4 Research Questions	4
1.5 Scope of Work	4
1.6 Report Layout	5
2 Review of Literature	7
2.1 Microbial soil improvement methods	7
2.1.1 Urea Hydrolysis Mechanics	8
2.1.2 Denitrification	8
2.1.2.1 Environmental effects	12
2.1.3 Gas in soil	13
2.1.4 Bubble formation	13
2.1.5 Critical degree of saturation	14
2.1.6 Estimation of gas volume in pore space through microbial desaturation	15
2.1.7 Desaturation through air injection	16
2.1.8 Unsaturated and gassy soils	17
2.1.8.1 Gassy soils	17
2.2 Compaction	17
2.2.1 Proctor test	19
2.2.2 Work input	20
3 Methodology	23
3.1 Research Methodology	23
3.2 Soil Sample	24
3.2.1 Particle size distribution	24
3.2.2 Minimum and maximum void ratio	25
3.2.3 Optimum water content	26
3.3 Bacteria Enrichment	27

3.3.1	Determination of substrate concentration	29
3.4	pH Buffering of soil	31
3.5	Hydraulic (Rowe) Cell Methodology	32
3.5.1	Preparation of cell	34
3.5.2	Sample placement	34
3.5.3	Fitting of cell cover	35
3.5.4	Saturation	36
3.5.5	Reaction phase (Bacterial solution for pore fluid)	38
3.5.6	Loading phase	39
3.5.7	Dismantling of test	40
3.5.8	Water content during loading phase	40
3.5.9	Compaction energy	41
4	Results and Discussion	43
4.1	Dry density - water content curves	43
4.2	Hydraulic Cell processed results	44
4.2.1	Evaluation in terms of work input	54
4.3	Discussion	54
4.3.1	Description of scenario	54
4.3.2	Diaphragm calibration	55
4.3.3	Gas production assumptions	55
4.3.4	Nitrogen Balance	56
4.3.5	Diffusion of substrate	57
4.3.6	$CaCO_3$ precipitation	57
4.3.7	Microbial Desaturation	59
4.3.8	Initial Relative Density	59
4.3.9	Reduction in work input	59
5	Conclusion	61
6	Recommendations	63
	Bibliography	65
A	Incubation tests	69
A.1	Incubation test results	69
B	Test Specimen	71
B.1	Particle size distribution - Sieving	71
B.2	Hydrometer M6	72
B.3	Chemical analysis	75
B.4	Proctor test data	76
C	Substrate solution	79
C.1	Treatment Composition	79
C.2	Areometer/Hydrometer density test	79
D	Hydraulic Cell test Results	81
D.1	Control1	82
D.2	Control2	83
D.3	Control3	84

D.4	Bac1	85
D.5	Bac2	86
D.6	Bac3	87
D.7	Nitrogen balance	88
D.8	$CaCO_3$ content	88
E	Alternative Test Set-ups	91
E.1	Adapted Proctor Cell	91
E.2	Hydraulic Cell with Flush Through	92

List of Figures

Figure 1.1:	Dry unit weight - water content curve indicating scenarios	3
Figure 1.2:	Proposed process on Dry unit weigh - water content curve	4
Figure 1.3:	Reader's Guide	5
Figure 2.1:	Urea hydrolysis process	8
Figure 2.2:	Denitrification process	10
Figure 2.3:	MIDP process analysis from Pham et al. (2016)	11
Figure 2.4:	Saturation and permeability of treated fine sand	11
Figure 2.5:	Classical homogeneous (top) and heterogeneous nucleation (bottom) (Jones et al., 1999)	13
Figure 2.6:	Type III pseudo-classical and Type IV non-classical nucleation Jones et al. (1999)	14
Figure 2.7:	Air flow through visco-elastic medium	15
Figure 2.8:	Gas saturation with depth at various concentrations	16
Figure 2.9:	The compaction range of techniques as applied by Keller (n.d.b)	18
Figure 2.10:	Range of compaction grouting techniques as applied by Keller (n.d.a)	19
Figure 2.11:	Dry density - water content plots for various types of soils	20
Figure 3.1:	Particle Size Distribution	25
Figure 3.2:	Dry density - water content relationship for Geba-M6 soils with air content	27
Figure 3.3:	Dry density - water content relationship of Geba-M6 soils with saturation	27
Figure 3.4:	Incubation test measurement set-up	29
Figure 3.5:	Saturation with depth	31
Figure 3.6:	pH Buffering of Soil	32
Figure 3.7:	Hydraulic cell set-up	33
Figure 3.8:	In-line Gas trap	34
Figure 3.9:	Fitting the cell cover	36
Figure 3.10:	Rowe Cell process	37
Figure 3.11:	Analysis of work input for undrained- and drained loading	42
Figure 4.1:	Dry density - water content plots to compare Geba-M6 combinations to various types of soils	43
Figure 4.2:	Rowe cell tests substrate consumption, precipitation and pH	49
Figure 4.3:	Tests comparison between untreated and treated Rowe cell tests 1	50
Figure 4.4:	Tests comparison between untreated and treated Rowe cell tests 2	51
Figure 4.5:	Tests comparison between untreated and treated Rowe cell tests 3	52
Figure 4.6:	Dry density-water content of Geba M6 84-16 Hydraulic cell and Proctor tests	53
Figure 4.7:	Dry density-water content of Geba M6 34-66 Hydraulic cell and Proctor tests	53
Figure 4.8:	Scenario in hydraulic cell vs Proctor cell	55
Figure 4.9:	Gas pockets on surface and bulging around edge	56

Figure 4.10: Nitrogen balance between the start and end of the treated Rowe cell tests . . . 57
Figure 4.11: Calcium balance between start and end of treated Rowe cell tests 58
Figure 4.12: Effect of placement density on displacement - Envisioned soil placement
condition vs actual placement condition 59

List of Tables

3.1	Particle size analysis. Results in <i>mm</i>	25
3.2	Soil samples e_{min} and e_{max}	25
3.3	Soil pH buffer regime	32
3.4	Hydraulic cell incremental loading regime	39
3.5	Hydraulic cell unloading regime	40
4.1	Properties for the range of Hydraulic cell samples (1/2)	44
4.2	Properties for the range of Hydraulic cell samples (2/2)	45
4.3	Measurements for treated specimens	45
4.4	Gas measurements for treated specimens	46
4.5	Gas measurements: Measured vs Predicted	46
4.6	Nitrogen balance for the treated Rowe cell tests	47
4.7	Evaluation of Rowe cell samples in terms of RD and axial strain increase for the measured amount of work input - smaller is better	54
4.8	$CaCO_3$ content for treated tests [g/kg dissolved solids]	58
4.9	Ca^{2+} balance for the treated tests	58
4.10	Evaluation of Rowe cell results in terms of initial relative densities prior to loading and percentage difference between treated and untreated samples	60

Nomenclature

A	Air content
A_ϕ	Cross section area
Ac/N	Ratio of Acetate to nitrate
atm	Unit of atmospheric pressure
APC	Automatic pressure controller
BPC	Back pressure controller
$^\circ\text{C}$	Temperature in degrees Celsius
$c_{\text{subscript}}$	Concentration
$c_{\text{subscript}}^g$	Concentration present in gas phase
$c_{\text{subscript}}^l$	Concentration present in liquid phase
Ca-Ac-N	Molar ratio Calcium to Acetate to Nitrate
C_c	Compression index
C_e	Expansion index
C_U	Coefficient of uniformity
C_Z	Coefficient of curvature
CR	Compression ratio
D	Depth of compaction
DPC	Diaphragm pressure controller
e	Void ratio
F	Force in [N], positive signifies compression by definition
g	Gravitational acceleration
G_s	Specific gravity of the soil particle
$H_{(\text{subscript})}$	Height from which weight is dropped
H	Height of sample
$^\circ\text{K}$	Temperature in degrees Kelvin
$k_{H_{\text{subscript}}}$	Henry's coefficient in [$\text{atm} \cdot \text{L} \cdot \text{mol}^{-1}$]
K_0	Ratio of effective horizontal stress to effective vertical stress
L	Power in [$\text{N} \cdot \text{m} \cdot \text{s}^{-1}$ or $\text{J} \cdot \text{s}^{-1}$]
M	Molar concentration, Molarity or Molar in [mol/L^{-1}]
$M_{(\text{subscript})}$	Mass
MICP	Microbial Induced Calcite Precipitation
MIDP	Microbial Induced Desaturation
MIDP	Microbial Induced Desaturation and Precipitation
n	Porosity
$n_{(\text{subscript})}$	Molar quantity
$N_{(\text{blows})}$	Number of blows
$p_{\text{subscript}}$	Partial pressure in [atm]
P	Pressure
pH	Measure of acidity or alkalinity on a log scale on which 7 is neutral
pK_a	Logarithmic acid dissociation constant
PSD	Particle size distribution

Q_{10}	temperature coefficient - increase of reaction rate with every 10°C
R	Ideal gas constant taken as $0.0821 \text{ L} \cdot \text{atm} \cdot \text{K}^{-1} \cdot \text{mol}^{-1}$
RD	Relative density
RIC	Rapid Impact Compaction
s_a	Axial displacement
S_g	Gas saturation
S_r	Water saturation
$S_{r;eorf}$	Water saturation at the end of reaction phase
$S_{r;l}$	Water saturation during the loading phase
STP	Standard temperature and pressure
u	Pore pressure
u_a	Pore air pressure
u_w	Pore water pressure
V or Vol	Sample volume
V_{BPC}	BPC volume
V_{DPC}	DPC volume
V_{diaph}	Diaphragm volume
V_g	Volume of gas
\dot{V}_g	Rate of change of gas volume
$V_{gastrap}$	Volume of gas in the gas trap
V_L	Volume of liquid
V_{pfv}	Pore fluid volume
V_{tot}	Total volume to be treated
V_v	Volume of voids
$V_{v;eorf}$	Volume of voids at the end of the reaction phase
W	Work [$N \cdot m$ or J]
w	Water content
w_{opt}	Optimum water content
$Y_{(subscript)}$	Stoichiometric ratio

Greek letters

ϵ_a	Axial strain
ϵ_r	Radial strain
μ	Diaphragm calibration coefficient
ρ	Density
ρ_b	Bulk density
ρ_d	Dry density
ρ_s	Particle density
ρ_w	Density of water
σ or σ_{tot}	Total stress
σ'	Effective stress
σ_a	Axial stress
σ_{DP}	Uncorrected diaphragm pressure
σ_r	Radial stress
χ	Partially saturated soil parameter related to S_r

Chapter 1

Introduction

Biogeochemical processes and their application in geotechnics has been extensively researched throughout the past decade on a bench scale. Several applications in this field were mentioned by DeJong et al. (2013), including erosion control, structural repair, soil liquefaction mitigation and ground improvement. It has been noted that biogeochemical-based soil improvements will never replace all conventional ground improvement techniques. However, some attributes can be more advantageous as in the following cases: They are non-disruptive to existing structures; they make use of natural processes leading to possible reduced costs and reduced environmental impact; optimisation of treatments by adjusting concentrations; hydraulic control and flexible treatment implementation.

Recent developments in microbial induced calcite precipitation (MICP) through denitrification by Pham et al. (2016), has led to the idea of using the Nitrogen (N_2) gas formed in the process to force the water from a saturated soil body and reduce the water saturation of a fine silty sand to 80%. This microbial induced soil desaturation led to the idea that a soil body can be brought closer to its optimal water content and thus better suited for compaction.

1.1 Problem Statement

The suitability of reclaimed deposits comprising out of silty sand mixtures highly depends on the present and future geometrical and loading conditions and, above all, on the present stress state and void ratio compared to the unique material characteristics. The bearing capacity of reclaimed soils is often insufficient to withstand overburden structures or traffic due to the loose state of the soil grains. The applicability of conventional soil improving techniques such as consolidation, preloading, static or dynamic compaction, electro osmosis, thermal energy or combinations thereof, may for various reasons not result in envisaged or optimal solutions. The efficiency of compaction vary in different materials and conditions. For the purpose of this investigation, a saturated fine grained soil will be investigated due to its vulnerability to pore pressure accumulation during compaction, which renders the method ineffective.

Consolidation is a time-consuming process due to the low permeability. The process of consolidation involves the dissipation of generated excess pore water pressures by the increase of an isotropic or deviatoric stress increment. The rate of consolidation is depending on the void ratio and permeability of the soil, of which the latter may be enhanced by application of vertical drains (stone columns or sand piles) or other drainage improving elements, which is a costly task. During this process, the soil remains fully saturated. The application of uniform static loading of unsaturated soils partially leads to immediate compression followed by a delayed settlement as water is expelled over time as the void ratio decreases, known as consolidation. Both consolidation and compaction result in a reduction of void space and increased interlocking.

An immediate solution is sought in compaction, but when redressing fully saturated fine grained

soil with fines content above 10-12%, compaction is often debated. Dynamic compaction is inefficient due to excess pore water pressure generation and the effectiveness of a static compaction is typically limited in fine grained soil with a high sand content. The former may result in immediate contraction of a loose soil, whereas the latter can result in consolidation over a longer period.

For this reason, alternative solutions are sought to increase the effectiveness of compaction and found in biogeochemical processes.

1.2 Proposed solution

If one is to decrease the water saturation of the pores and partially fill them up with gas, the expulsion of water during the first stage of treatment contributes to the decrease of water content. Previous studies have indicated theoretical optimal conditions of soils for compaction are commonly around 80% saturation. One could subsequently apply compaction techniques, such as dynamic compaction, Rapid Impact Compaction or vibro-compaction (vibroflotation), which will increase the shear resistance of the soil without the generation of excess pore water pressures due to pores only partially filled.

It is hypothesised that the first stage of the treatment (biogenic gas production) will reduce the energy and time requirements during the execution of the second phase (compaction). Instead of using energy that is used to expel water from pores during compaction, the energy is used for compression of the soil skeleton and possible expulsion of air voids.

Denitrification is the suggested process for in situ biogenic gas production. It is a process that can occur in anaerobic conditions, without having adverse by-products when the nitrate is completely reduced to nitrogen gas. The process has extensively been investigated by Pham et al. (2016) for the use in biocementation. By adding calcite to the process, calcium carbonate precipitates which decreases the pH to around 7 and produce additional CO_2 gas. Gas build-up commences instantly and reaches a peak depending on the confining pressure. The process is fully documented at lab scale.

1.3 Hypothesis

The compaction (Proctor) curves for different soils can be represented as seen in Figure 1.1. From these curves the maximum dry unit weight at a particular optimum water content, for a specific compactive effort, can be obtained.

Four scenarios are indicated on the dry density-water content graph, all of which start from a fully saturated condition A. Path AD indicates the route the density-moisture content ratio will follow when consolidated under fully saturated conditions. This is achieved through e.g. vacuum consolidation or the placement of static weight on top of the soil body. The soil body remains fully saturated as it consolidates under an increased energy level. Scenarios AB, AC and AE could occur through gas desaturation. Path AC will occur if the soil body is desaturated, together with a decrease in void ratio. This case is unlikely due to no increment in total or effective stress level. Scenario AB may occur when gas saturation occurs without a change in void ratio. Scenario AE may occur if the soil body is desaturated, together with an increase in void ratio. This can occur when the gas bubbles force the soil skeleton apart. This is observed for conditions of low overburden pressure by Pham et al. (2016). This case is conceived to be counter productive, as it has the opposite effect on the soil body, as what is to be accomplished through compaction. The actual path that is followed during biogenic desaturation remains to be established.

Figure 1.2 indicates the hypothesised process. The process can be divided into two steps; step AB indicating the path of desaturation of the soil sample if no expansion or contraction of the soil skeleton occurs and path BC indicating what could happen if the same compactive effort (energy level) is applied to the desaturated sample. Point A indicates a fully saturated sample at a given

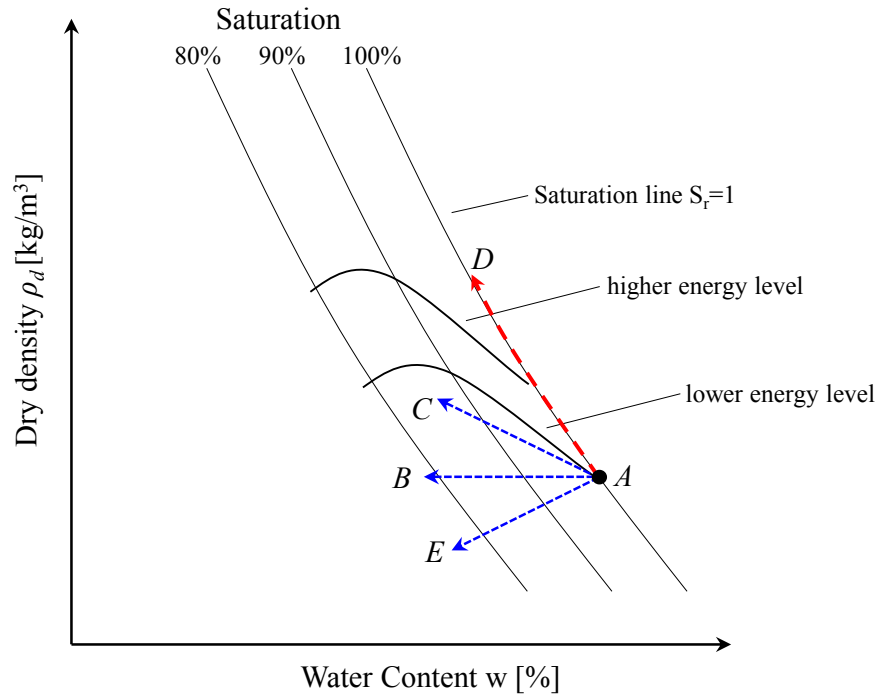


Figure 1.1: Dry unit weight - water content curve indicating the path of consolidation (AD) and possible scenarios during gas production: AC indicating a decrease in void ratio, AB suggesting no change in void ratio, and path AE indicating an increase in void ratio

energy level. When applying a certain compactive effort, the density cannot be increased above the level of point A, due to the fact that the soil body is fully saturated and possesses a low permeability (acts undrained). If the sample can be desaturated to point B, without increasing the void ratio, the soil body can be compacted to a higher density (point C) by applying the same compactive effort. It is suggested to induce desaturation via in-situ gas production through denitrification.

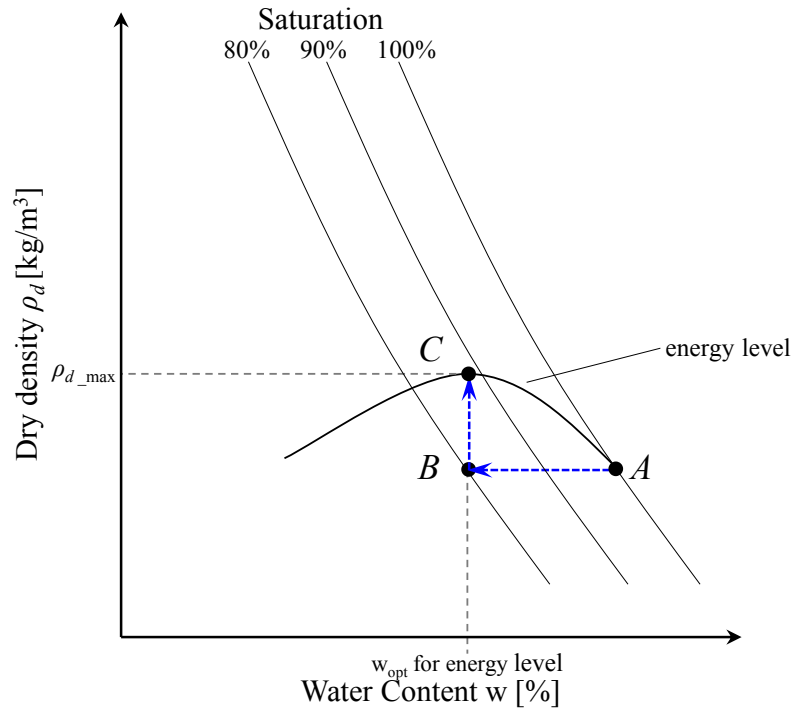


Figure 1.2: An indication of the expected route in two stages: Desaturation step AB and compaction step BC

1.4 Research Questions

A study is launched to attempt to answer the following research questions:

- Can *in-situ* gas formation be accomplished without inducing any expansion of the saturated soil skeleton? And,
- Can the gas created by denitrification reduce the amount of energy required to increase the density of a silty sand layer to a given target density through compaction?

1.5 Scope of Work

This research includes

- a review of existing literature on the topics of the improvement of engineering parameters using microbial treatments through MICP by urea hydrolysis and denitrification, with an in depth analysis of microbial induced desaturation (MID) through denitrification,
- a revision of the method proposed by Pham (2017) to predict and engineer a desaturation regime for a soil body,
- understanding the factors that have an influence on the behaviour of the biochemical reaction,
- a study of the formation of gas inside a soil structure and the influence on the mechanics of the soil,

- an assessment of the methods currently used in compacting fine grained soils and the analysis of the water content - dry density relationship,
- the procedures for incubation of the required bacterial inoculum to be used in the process,
- devising a bench scale test set-up to test if an increase in void ratio occurs as a result of gas production,
- the use of the same test set-up to evaluate if the *in-situ* gas formation as a result of denitrification can decrease the energy required to compact a saturated silty sand layer and
- an evaluation if MID is suitable as an alternative to conventional drainage techniques.

1.6 Report Layout

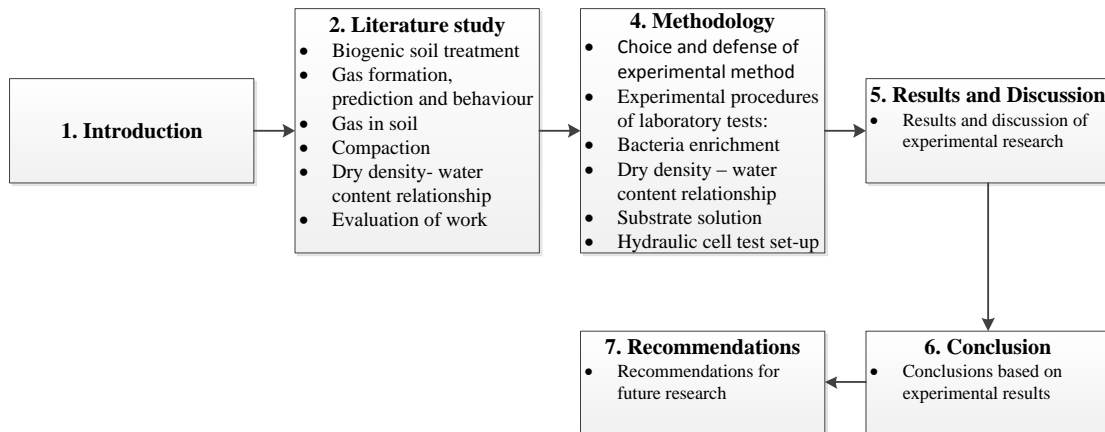


Figure 1.3: Reader's Guide

Chapter 2

Review of Literature

The improvement of soil parameters for practical application has been extensively researched throughout the last decade. To use nature to do the work for us becomes ever more appealing. Building with nature aims to result in a cleaner, greener way of adapting the environment to suit our needs.

It is common knowledge among geotechnical engineers that the large scale performance of soils depend on the micro scale conditions. DeJong et al. (2013) further mentions that harnessing biological processes in soils promises to be the next breakthrough in soil remediation. The paper further mentions that biogeochemical processes have the potential to alter several attributes: physical properties such as density, gradation, porosity and saturation; conductive properties including hydraulic-, electrical- and thermal conductivity; mechanical properties, e.g. friction angle, cohesion, cementation, erodibility, compressibility, stiffness, dilation, and soil-water characteristic curve; and the chemical composition of soils.

2.1 Microbial soil improvement methods

Biomineralisation, the precipitation of calcite, also known as microbially induced calcite precipitation (MICP) or bio clogging, the filling of pore space by microbial biomass, has successfully been implemented to improve mechanical properties of soil bodies (DeJong et al., 2013; Van Paassen et al., 2009, 2010; Chu et al., 2013). Two biological processes have been studied; urea hydrolysis and denitrification. In-situ Biogenic gas production is suggested as a mitigation measure for seismic liquefaction (Rebata-Landa and Santamarina, 2012; Zeybek and Madabhushi, 2016; Chu et al., 2013; Okamura et al., 2011; Yegian, 2007; Stabnikov et al., 2015; Yamamoto et al., 2009; Huang and Wen, 2015). Denitrification is suggested as the preferred biological process which results in nitrogen gas. When nitrogen bubbles are included in a soil body, excess pore pressure is reduced or may not generate, as the partially desaturated soil damps the development.

As the transport of microorganisms occur freely within a pore space, the use of bacteria is ideal in cohesionless soils. The passage is limited by the pore throats of a soil matrix which prohibits the spread of the substance by diffusion, advection, dispersion, sorption or self-propelled movement. Typically, the spread of bacteria is restricted by the pore throats with limit of 0.4 microns (DeJong et al., 2006). The pH of the environment is a critical factor, as calcium carbonate precipitation begins at a pH level of 8.3 and occurs at an increasing rate up to a pH value of 9.0.

Several different methods have recently been researched regarding the biological improvement of soil characteristics. In order to apply these solutions to subsoil improvement, a biological process that operates in anaerobic conditions must be sustained. Regarding soil cementation by means of calcium precipitation (MICP), attention is given to two biological processes:

- MICP by Urea Hydrolysis (urease)
- MICP by Denitrification

In both cases, calcium carbonate is precipitated from organic processes once the solution is oversaturated - i.e. the amount of calcium and carbonate ions exceed the solubility of the solution (Van Paassen et al., 2009).

2.1.1 Urea Hydrolysis Mechanics

The process is implemented to reduce liquefaction potential and increase soil cohesion, increase shear resistance and bearing capacity, and reduce the permeability of specimens through calcium carbonate precipitation. The result can be described as biologically formed grout .

The process of urea hydrolysis has been extensively researched by DeJong et al. (2006, 2010) and Van Paassen et al. (2009). The process has also been successfully subjected to field tests by Van Paassen et al. (2010). The soil is injected with a solution of ureum which is metabolised to form carbonate and ammonium ions. In the presence of the calcium ions from calcium chloride, calcium carbonate is precipitated and forms calcite crystals which act as cement.

As a result of bacterial metabolic activity, the pH increase leads to the creation of calcite cement. *Sporosarcina Pasteurii* is the bacteria responsible for the reaction which uses urea as energy source and produces ammonia, which increases the pH in the surroundings and results in Ca^{2+} and CO_3^{2-} to precipitate into $CaCO_3$. The bacterial suspension is injected or mixed into the soil and supplied with a solution of urea and calcium chloride. Through the hydrolysis of urea, ammonium and carbonate is produced. The carbonate ions bind with calcite ions to produce calcium carbonate crystals. Subsequently, the ammonium chloride is removed. The equilibrium reaction is indicated in Figure 2.1.

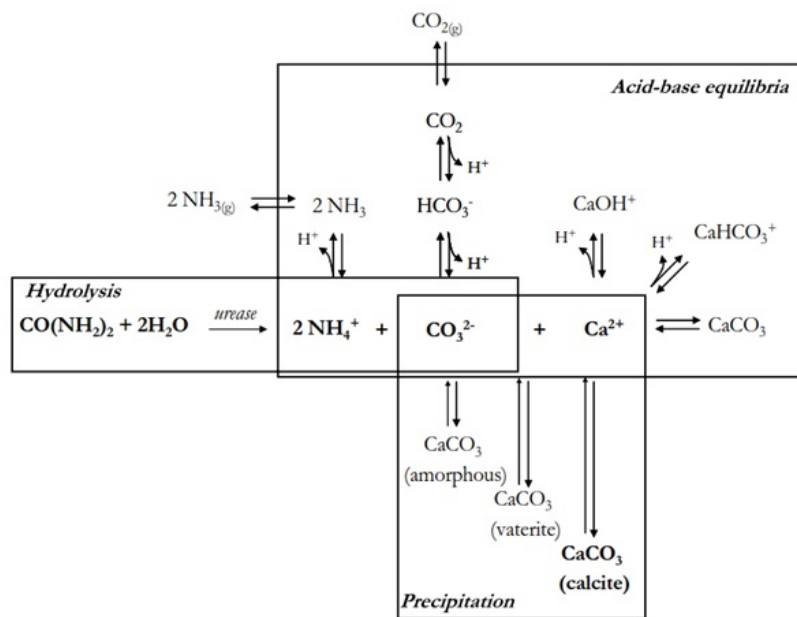


Figure 2.1: The process of urea hydrolysis and all its products according to Van Paassen et al. (2009)

2.1.2 Denitrification

Pham et al. (2016) describes denitrification as a biological process in which microbes use nitrates to break down organic matter and produce Nitrogen gas and biomass. By adding calcium to the process

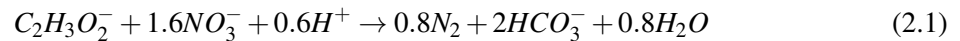
to buffer the pH, minor precipitation of calcium carbonate occurs which cements soil particles. Apart from the cementation effect, produced nitrogen gas enhances undrained response and acts as buffer to undrained dynamic loading due to the compressibility of the gas bubbles, resulting in an increased cyclic stress ratio and a reduction in P-wave velocity. Rebata-Landa and Santamarina (2012) also makes a connection between the aforementioned phenomena and the Skempton B-value. Through experiments, Pham et al. (2016) found that the volume of gas produced depends on the pressure conditions. The gas storage capacity, varying between 22% and 40% of the pore volume, depends on the grain size distribution of the material. The permeability is hardly affected by the presence of gas at up to 1 bar of pore pressure. Once the pore pressure is increased or the grain size of the material reduced, significant reductions in permeability are measured. Through varying the concentration of substrate and pore pressure, the gas volume and bubble size can be controlled at lab scale. Parameters such as confinement pressure and pore- and grain size distribution control the gas storage capacity of the soil.

Within a single flush of substrate through a specimen, Pham et al. (2016) achieves a decrease in saturation of an initially fully saturated fine sand in a triaxial cell set-up at 100 kPa back pressure and 200 kPa confinement pressure to around 80% within three days, after which the gas storage capacity was reached. In the following days, the permeability decreased by 70% due to the aggregated effect of carbonate precipitation, gas- and biofilm formation. Multiple treatments at a low concentration are required for sufficient calcium carbonate precipitation. Furthermore, Pham et al. (2016) found that the cohesive effect created by calcium carbonate is destabilised by venting.

No harmful by-products result from denitrification if nitrate (NO_3^-) is completely converted to nitrogen N_2 gas. For this to be the case, nitrate and acetate need to react in the correct ratios to refrain from generating nitrite NO_2^- , nitric oxide NO or nitrous oxide N_2O . The intermediate products should be limited due to its toxicity to the bacteria itself in high concentrations (van Spanning et al., 2006) and the environment. The organisms responsible for the denitrification process are abundant, stemming from organic rich soils or even waste streams. No shortage of the bacteria, which is a vital link in the nitrogen cycle, exists. The denitrification process is indicated in Figure 2.2.

The process can be expressed in terms of an anabolic- and catabolic reaction, the former expresses the production of biomass, whereas the latter describes the generation of energy in order to produce new biomass. The availability of substrate and nutrients controls the growth rates. Acetate ($C_2H_3O_2^-$) acts as the electron and carbon donor. Pham expresses the two reactions as in Equations 2.1 and 2.2.

Catabolic:

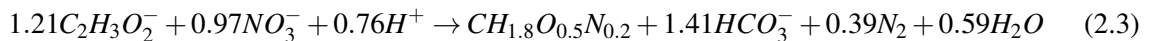


Anabolic:



The energy balance for maximum growth is solved to deliver Equation 2.3 for metabolic reaction.

Metabolic:



Pham suggests that the actual metabolic stoichiometry ranges between the catabolic reaction (zero growth) and the metabolic reaction (maximum growth).

In the presence of calcium ions (Ca^{2+}), bicarbonate reacts to form calcium carbonate (Equation 2.4)



Acidity is increased during the process at neutral pH which buffers the alkalinity production as a result of denitrification. The denitrification process is depicted in Figure 2.3 which explains what reaction

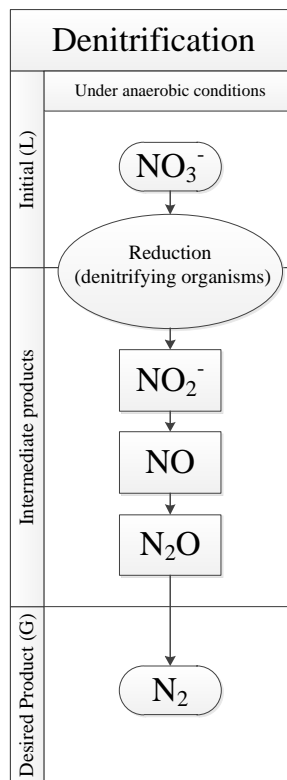


Figure 2.2: The reduction of nitrate in solution to dinitrogen gas through the process of denitrification (van Spanning et al., 2006)

is responsible for each phase; anoxic denitrification leads to the formation of nitrogen and carbon dioxide gas, bicarbonate reacts with calcium ions to precipitate calcium carbonate, the formation of biofilm as a result of the metabolic process, and the acid-base equilibrium responsible for the buffering of the pH. The gas phase is implemented in MID.

Pham et al. (2016) determined that the pH remained constant just below 7 when calcium ions are added to the process. When the calcium ions are replaced with sodium ions, the pH rides to about 9.5. The precipitation of carbonate acts as a buffer, which also limits the production of nitrite.

The procedures used by Pham to prepare the inoculum for the batch cultivation comprise of 30g of soil sampled from two bore holes. The substrate (Ca-Ac-N concentration mM 55:60:50) and nutrients were added to the sample and was left to incubate. The subsequent incubations use the inoculum from the previous incubation (0.25l/l) with more substrate to stimulate bacteria growth further. The liquid from the bottles are regularly sampled to analyse the electrical conductivity, pH and concentrations in the solute. Nitrate, nitrite and calcium are determined spectrophotometrically. Gas production is measured using a water clock/ eudiometer set-up.

In Pham's experiments it is noted that the most efficient acetate to nitrate ratio (Ac/N) is identified as 0.8. It is also noticed that the residual nitrite concentration does not reduce to zero as is the case in a Ac/N experiment with ration 1.2. The closer the reaction get to the catabolic reaction (Ac/N of 0.6), the greater the rate of gas production is albeit at a greater residual nitrite concentration.

Several sand column experiments were conducted of which the objective was cementation though calcite precipitation. The columns were flushed multiple times and the effluent analysed to determine the constituents in the column through mass balance, together with the displaced pore liquid as a

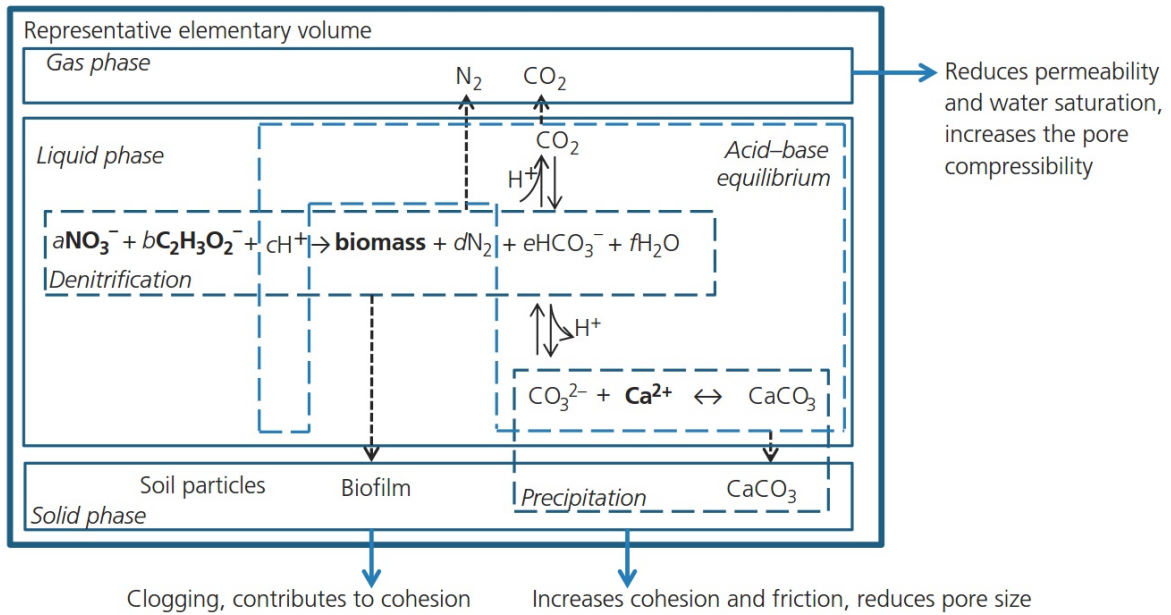


Figure 2.3: MIDP process analysis from Pham et al. (2016)

result of gas production. The permeability was also measured and compared between flushes. During a flush, an increase in permeability was recorded. The significant drop in permeability (K/K_{ini} - Figure 2.4) is a result of gas venting from the system during flushing. The gas phase is not recorded in the balance monitored vessel the pore fluid is displaced into.

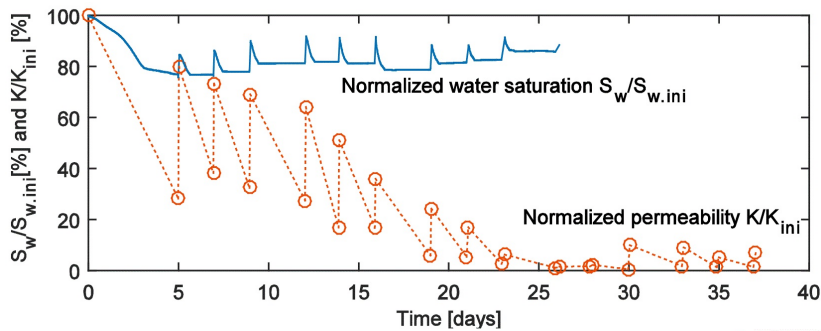


Figure 2.4: Saturation and permeability of treated fine sand during multiple flushes of denitrifying bacteria and substrate solution (10mM $Ca(NO_3)_2$ and 12mM $Ca(C_2H_3O_2)_2$) in a triaxial cell at 100 kPa back pressure and 200 kPa cell pressure (Pham et al., 2016)

Pham suggested that the treated material will have a significant increase in liquefaction resistance due to the dampening of pore pressure build-up. It is considered that gas desaturation also facilitates formation of calcite cementation, as substrate solutions are concentrated at pore throats, where cementation can more easily occur. Pham found that gas bubbles migrate toward the top of the gas column, whereas calcium precipitation was higher at the bottom of the column, which counters the consideration that calcium forms in pore throats. This is attributed to the lack of substrate available due to its displacement by gas bubbles.

2.1.2.1 Environmental effects

The conversion rate of substrate is attributed to the type of denitrifying organism, the substrate and product concentrations and environmental effects. A study of Knowles's (1982) work delivers an explanation of how different parameters influence the characteristics of the metabolic reaction (Equation 2.3). Factors studied by Knowles shows that the presence of oxygen, organic carbon availability, pH and temperature conditions are prominent influential factors. According to Knowles (1982), denitrification is the reduction of nitrogen oxides (NO_3^- , NO_2^-) to gaseous oxides (NO , N_2O) which may further reduce to dinitrogen (N_2). A number of routes could be followed, depending on the conditions and type of organism. Knowles mentions that most genera of denitrifying bacteria possess the ability to reduce NO_3^- to N_2 .

Oxygen presence

The presence of low concentrations of O_2 in soil reduce the rate of denitrification and simultaneously result in a larger mole fraction of harmful N_2O . Transient changes in N_2O metabolism result in a change of N_2O and N_2 being the dominant product. However, ultimately N_2 dominates in most cases (depending on the genus) (Knowles, 1982). Denitrifying organisms show preference to the respiration of O_2 . The presence of oxygen could allow for assimilatory nitrate reduction to take place, which will result in residual NO or NH_4^+ (van Spanning et al., 2006).

Organic carbon availability

The availability of organic carbon is one of the most important factors controlling the activity of heterotrophs (organisms that derive their nourishment and carbon requirements from organic substances). The overwhelming majority of denitrifying bacteria can only rely on organic carbon (covalent compounds containing carbon, excluding some simple compounds like CO_2) as electron donor. Pham's research states that the concentration of nitrate and acetate, combined with the ratio in which they occur in the system, is an influential factor in the concentration of residual nitrite. In the presence of abundant carbon (Acetate NO_3^- energy source) and anaerobic conditions, ammonium NH_4^+ is the product, instead of N_2 .

pH

Knowles indicates that the optimum pH range for denitrification to occur, is between 7.0 and 8.0. The upper limit is set to be pH 11.0 in waste streams. Lower pH values progressively inhibit denitrification. The product also shifts towards N_2O and at pH 4, N_2O constitutes the main component generated. Rebata-Landa and Santamarina (2012) stated that the reduction of N_2O to N_2 is more in an environment with pH between pH 6.0 to 8.0 due to the accelerated rate of denitrifiers.

Effect of temperature

The reaction is temperature dependant. In soil with a temperature range between 10°C to 35°C, the Q_{10} temperature coefficient ranges between 1.5 to 3.0 which means that for every 10 degrees increase, the reaction rate is 1.5 to 3.0 times higher. Denitrification in soil is known to take place at temperatures of 0 to 5 degrees, albeit at reduced rates. At extreme reaction temperatures, the mole fraction of N_2O is significantly higher with additional NO formation at the lower end of the spectrum. Maggi and Riley (2015) confirmed that the reaction adheres to Arrhenius' law with an inverse logarithmic relationship to temperature.

An Ac/N ratio lower than 0.8 leads to residual nitrite, whereas a higher ratio results in residual calcium acetate in solution. The gas volume can successfully be predicted by following a thermodynamic approach involving pore pressure and a mass balance according to stoichiometry of

the metabolic reaction. At high pressure, the pore water is successfully displaced. The same could be said for low pore pressures, although the gas storage capacity (the point where gas vents from the sample) is reached earlier.

2.1.3 Gas in soil

Several phenomena, physical and chemical, may result in gas formation in soil. Rebata-Landa and Santamarina (2012) found that bubbles can nucleate due to depressurisation of the vapour pressure; due to a temperature increase where the vapour becomes more stable; or due to gas dissolution in a supersaturated liquid due to a chemical change. An external air source may also result in lasting air bubbles.

2.1.4 Bubble formation

In research conducted by Jones et al. (1999) it is stated that gas bubbles are the result of supersaturation of a liquid, where the rate of bubble growth is governed by the concentration gradient. Four types of bubble nucleation have been identified: Type I and II classical homogeneous and heterogeneous nucleation where the initial nucleation energy is overcome (Figure 2.5), and Type III and IV where existing bubbles grow larger (Figure 2.6). These cases are discussed for autogenous bubble creation through gas desorption. Type II nucleation, the presence of nucleation sites, is also stated by Pham (2017) as a reason for a faster rate of gas production within a soil skeleton, compared to in solution. Type IV nucleation may be a reason for non-homogeneous gas distribution, as no nucleation energy needs to be overcome to form new bubbles. The term “Ostwald ripening” is used by van Paassen et al. (2017).

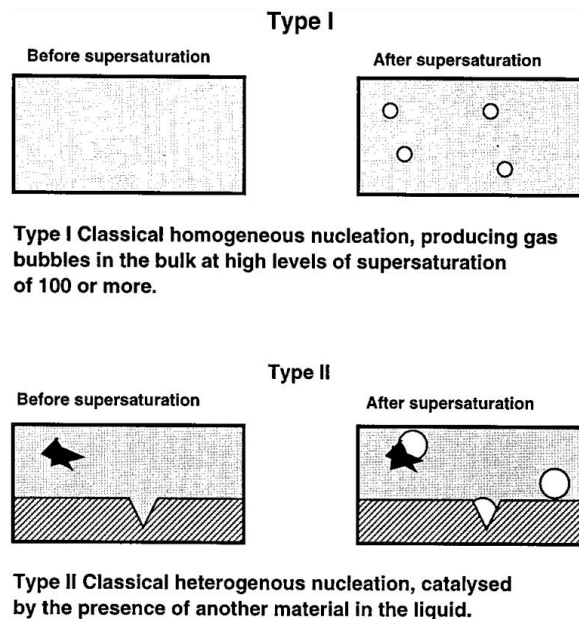


Figure 2.5: Classical homogeneous (top) and heterogeneous nucleation (bottom) (Jones et al., 1999)

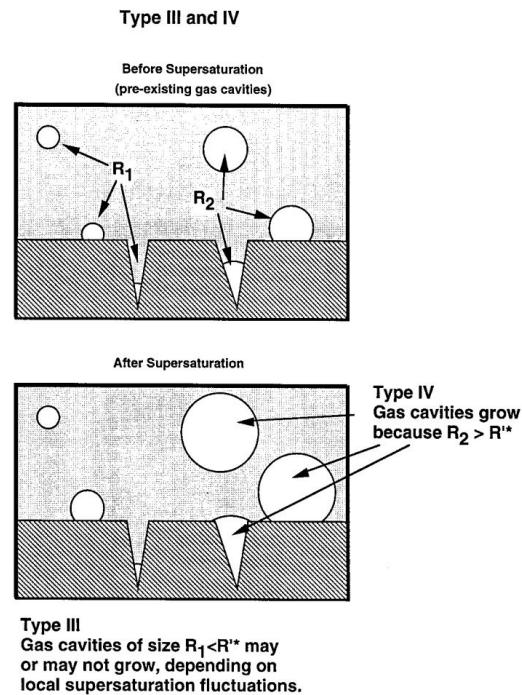


Figure 2.6: Type III pseudo-classical and Type IV non-classical nucleation Jones et al. (1999)

2.1.5 Critical degree of saturation

In the study of gas migration through cement, a viscoelastic medium, Bonett and Praftis (1996) identified four cases of gas pocket migration depicted in Figure 2.7: Bubble flow - the rise of separated gas pockets in the medium, Slug flow - where the gas rises as a continuous pocket, interface flow - the formation of gas pockets at the interface of the medium and a different material, and as a rising plume - where a rising gas pocket is connected to a trailing umbilical passage. Similar phenomena are thought to occur in a fine, silty material. Bubble flow may occur at first, coagulate and form slugs which, due to its larger buoyancy, can overcome tensile forces more easily. Interface flow could occur easily in laboratory experiments where boundary effects cannot be ignored. A rising plume may result in the increase of material permeability.

At low confinement (near the surface), fissures form as a result of gas bubbles coagulating into larger gas pockets which migrate upwards if a critical buoyancy is reached i.e. when the buoyancy of the gas pocket exceeds that of the surrounding fluid and overcome surface tension.

Nageswaran (1983) studied the effect of gas bubbles in silty marine formations. The critical degrees of saturation typically range between 85 to 90 % for fine materials. Pham (2017) terms this critical degree of saturation as the gas percolation threshold, the saturation at which gas starts venting from the system. A sensitivity study launched by Pham (2017) found that the gas percolation threshold is a function of grain size, effective- and total stress. A material with a larger D_{50} is typically found to have a significantly lower critical degree of saturation, corresponding to Nageswaran's (1983) work. A relatively coarser material is capable of containing a larger fraction of gas in its pore space. A lower total stress was also shown to result in a lower gas percolation threshold.

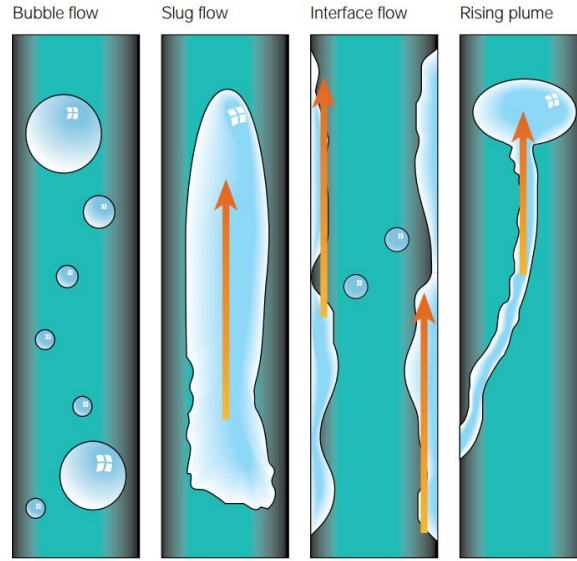


Figure 2.7: Scenarios of air flow through a viscoelastic medium (concrete) similar to a loose granular material (Bonett and Praftis, 1996)

2.1.6 Estimation of gas volume in pore space through microbial desaturation

Pham (2017) suggests the following assumptions to predict the gas production in porous media generated through denitrification:

- It is assumed that nitrate is directly reduced to nitrogen gas without accumulating intermediates such as nitrite, nitric oxide or nitrous oxide
- Inorganic carbon (CO_2) can be present in the gas phase. It is assumed that the fraction of CO_2 is negligible. Due to the neutral pH, the system opts to produce bicarbonate instead. Compared to N_2 gas (Henry's coefficient of $1542.6 \text{ atm} \cdot L \cdot \text{mol}^{-1}$), CO_2 is soluble to a far greater extent (Henry's coefficient of $28.53 \text{ atm} \cdot L \cdot \text{mol}^{-1}$).

From the assumptions, the subsequent procedures can be implemented. When the substrate consumption rate and state of microbial metabolism is known, the amount of N_2 produced can be predicted from stoichiometric ratios (Y_X) for the reaction in Equation 2.3.

$$c_{N_{2\text{tot}}} = \left[\frac{Y_{N_2}}{Y_{NO_3^-}} \right]_{\text{metabolic}} \cdot c_{NO_3^- \text{ consumed}} \quad (2.5)$$

Henry's law is implemented to calculate the fraction of N_2 in the liquid phase due to its partial pressure with $c_{N_{2\text{dissolved}}}$ in $\text{mol} \cdot L^{-1}$ indicating the concentration of dissolved N_2 in the system. In Equation 2.6, p_{N_2} represents the partial pressure in atm which acts on the gas. k_{HN_2} corresponds to the Henry coefficient of N_2 gas in $\text{atm} \cdot L \cdot \text{mol}^{-1}$.

$$c_{N_{2\text{dissolved}}} = \frac{p_{N_2}}{k_{HN_2}} \quad (2.6)$$

The molar quantity of the required N_2 in gas phase is calculated through Equation 2.7, with V_L representing the liquid volume occupying pore space.

$$n_{N_2^g} = (c_{N_{2\text{total}}} - c_{N_{2\text{dissolved}}}) \cdot V_L \quad (2.7)$$

The ideal gas law (Equation 2.8) can be implemented to calculate the volume the gas will occupy under known pressure (P in atm) and temperature (T in °Kelvin) conditions. The partial pressure is assumed to be equal to the pore pressure (negation of bubble surface tension).

$$V_g = \frac{n_{N_2}^g \cdot R \cdot T}{P_{N_2}} \quad (2.8)$$

With R, the ideal gas constant, taken as $0.0821 \text{ L} \cdot \text{atm} \cdot \text{K}^{-1} \cdot \text{mol}^{-1}$

It is found that the behaviour of N_2 gas does not deviate much from the ideal behaviour at STP (273.15 °K, 1 atm). At operating pressures and temperatures of around 293 °K and 2 atm (circa 10 m below phreatic level), the difference between ideal behaviour and real behaviour of N_2 gas occupying the same volume in molar quantities, is about 1%. Figure 2.8 serves as combined result of Equations 2.1, 2.3 and Equations 2.5 to 2.8.

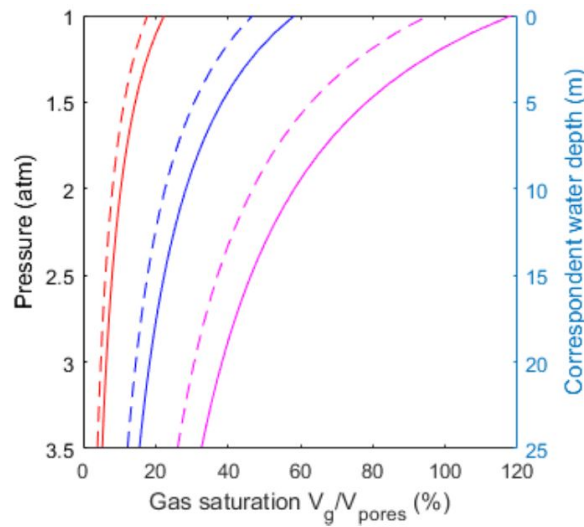


Figure 2.8: The gas saturation with depth as a function of pore pressure for stoichiometric reactions of maximum growth (dashed) and zero growth (solid), for varying concentrations of NO_3^- ; 20mM (red), 50mM (blue) and 100mM (magenta) Pham (2017)

At elevated pressure conditions in triaxial tests, Pham (2017) found that the amount of gas deviated from the predicted volume. This is allocated to the volume change with pressure, the increased gas concentration and higher pressure in small bubbles and the ease at which dissolved gas escapes through diffusion.

2.1.7 Desaturation through air injection

Okamura et al. (2011) evaluated in-situ desaturation through air injection, a method similar to air sparging. In situ air sparging is a technique developed for remediating contaminated groundwater. The method was tested to increase the liquefaction resistance of a saturated sand layer. A degree of saturation between 65-98% was obtained in the 4 metre radius around the point of injection. A lower saturation was achieved in a gravely fine sand compared to a silty sand (65-88% and 88-98% respectively). Electric resistivity tomography was successfully implemented and showed comparable results to a two-phase simulation and gravimetric saturation measurements. The homogeneous distribution of gas was not achieved.

2.1.8 Unsaturated and gassy soils

The presence of gas bubble inside soil changes the behaviour of the soil. The terms unsaturated or partially saturated soils are often used in geotechnical engineering. Craig (2004) describes a partially saturated soil as a soil where the pore space is occupied partly by water, partly by air. Due to surface tension, the pore water pressure u_w is always lower than the pore air pressure u_a . The size of the air voids is determined by the size of the pore space, unless the soil skeleton is nearly fully saturated, where air voids occur in the form of bubbles separated by the surface tension instead of the menisci influenced by soil particles. Pore water is concentrated around the interparticle contacts. Partially saturated soils can be found in the top few metres of land soil due to evaporation or the lowering of the water table. Terzaghi's principle of effective stress for fully saturated soils was adapted with a factor χ to formulate Equation 2.9, where χ is determined experimentally and ranges between $\chi = 0$ when $S_r = 0$ and $\chi = 1$ when $S_r = 1$.

$$\sigma = \sigma' + u_a - \chi(u_a - u_w) \quad (2.9)$$

The term $(u_a - u_w)$ represents matric suction and can potentially result in an increase of soil stability as a consequence of the additional tensile strength caused by pore water below atmospheric pressure, or capillary action, at interparticle contacts. It is noted that when the soil is close to saturation and the air exists in the form of bubbles, the soil can be considered as fully saturated with additional compressibility due to the presence of air bubbles. The term "gassy soil" is used by Nageswaran (1983) for this state.

2.1.8.1 Gassy soils

In the study of marine soils containing gas bubbles, Nageswaran (1983) terms a gassy soil as a partially saturated soil with sufficiently high degrees of saturation for the gas to form bubbles, spherical- or irregularly shaped. Due to the compressibility of the pore fluid, the behaviour of a partly saturated soil is different than that of a saturated soil. During undrained loading the undissolved gas bubbles undergo volume change. The initial degree of saturation is calculated using Boyle's law and Henry's law. When a load is applied, the degree of saturation increases immediately due to pore pressure increase, then decreases to the initial value as pore pressure dissipates. The gas permeability increases if the gas pores are interconnected, thus as the gas content increases, the gas permeability increases rapidly and the soil body consolidates faster. Pham (2017) describes this as venting.

2.2 Compaction

Monahan (1994) states the definition of compaction as the reduction of void spaces of a fill through the induction of a load, impact and/or vibration through appropriate equipment or processes. This results in a densification of the soil structure to improve engineering parameters. The process should not be confused with consolidation, which is the densification of normally natural fully saturated soils such as silts and clays below the water table. Compaction is an immediate process, as opposed to consolidation which lead to a long term reduction of void ratios through the expulsion of pore water from the subsurface. Compaction is a method of ground improvement achieved through the increase in density of a soil by eliminating air (Fredlund and Rahardjo, 1993). Fredlund and Rahardjo (1993) further cites the objective of compaction to be to decrease compressibility, increase soil shearing strength and decrease permeability. The same outcome is achieved through consolidation, but an extended time frame is required.

Cohesionless materials are normally compacted through vibratory rollers or other dynamic methods, such as rapid impact compaction, with no moisture content control required (Terzaghi et al.,

2.2. COMPACTION

1996). Compaction of soils with moderate cohesion is greatly affected by the moisture content. Moisture-content control is deemed critical to result in a higher dry density after compaction. Not only is the density of the soil increased during compaction, but also the ratio of effective horizontal to effective vertical pressures (K_0) resulting in an effect similar to overconsolidation Terzaghi et al. (1996).

Several techniques to compact soil in place are discussed by Terzaghi et al. (1996). This includes vibration combined with water jetting (vibro flotation), compaction by dropping weights, pile driving, sand piles and stone columns. The range of application of vibro flotation is limited to a relatively well graded material with less than 10% fines content as indicated in Figure 2.9 and has a reduced penetration rate in gravel (Terzaghi et al., 1996). Techniques using the dropping of weights (including rapid impact compaction and dynamic compaction) are inefficient in fine-grained soils. Trenches filled with permeable material are required to facilitate drainage. The depth to which the technique is effective is estimated to be $D = \sqrt{M_w H_w}$, where D signifies the depth of compaction, M_w the mass of the weight in tonnes and H_w represents the height of the fall in metres. The actual depth of compaction, however is found to be 50% to 80% of the value of D. Pile driving results in a reduction of porosity of cohesionless materials. The effect is significantly reduced in the presence of cohesive sandy soils below the water table, where the decreased permeability of the soil is governing. Terzaghi et al. (1996) states that compaction of fully saturated silty layers below the water table can only be achieved by surcharge and/or some form of drainage. In this case sand piles can be used in place of structural piles, where the sand pile also serves as a drainage element. Vibro replacement, a form of compaction where a vibroflot is used in combination with a backfill material of angular gravel, is also used to compact soft soils. A hole is created with an auger and filled with the highly permeable material and compacted using a vibroflot. The spacing of the columns range between 1.5 and 3 meters, depending on the material.

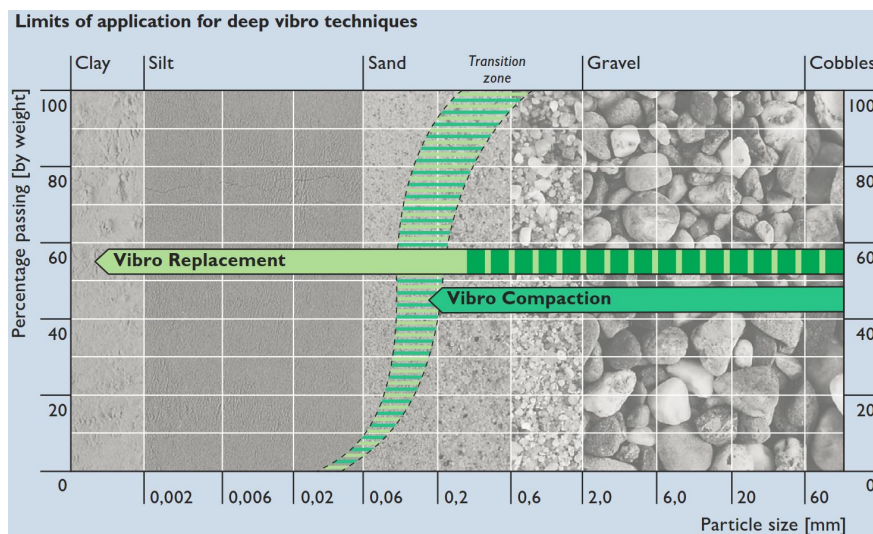


Figure 2.9: The compaction range of techniques as applied by Keller (n.d.b)

Compaction grouting is also implemented to achieve a denser soil structure. Grout varying in stiffness is injected into the soil under pressure. In fine grained soils, the technique is considered as a form of consolidation grouting. The various types of compaction grouting are indicated in Figure 2.10 with the ranging soil types application.

When evaluating the applicability of the different compaction methods, it is important that it is assumed that below the groundwater level the soils are saturated. MID can generate an unsaturated soil below the groundwater level. The presence of occluded air may alter the applicability of the traditional ground improvement methods. Four scenarios are identified (van Paassen, personal

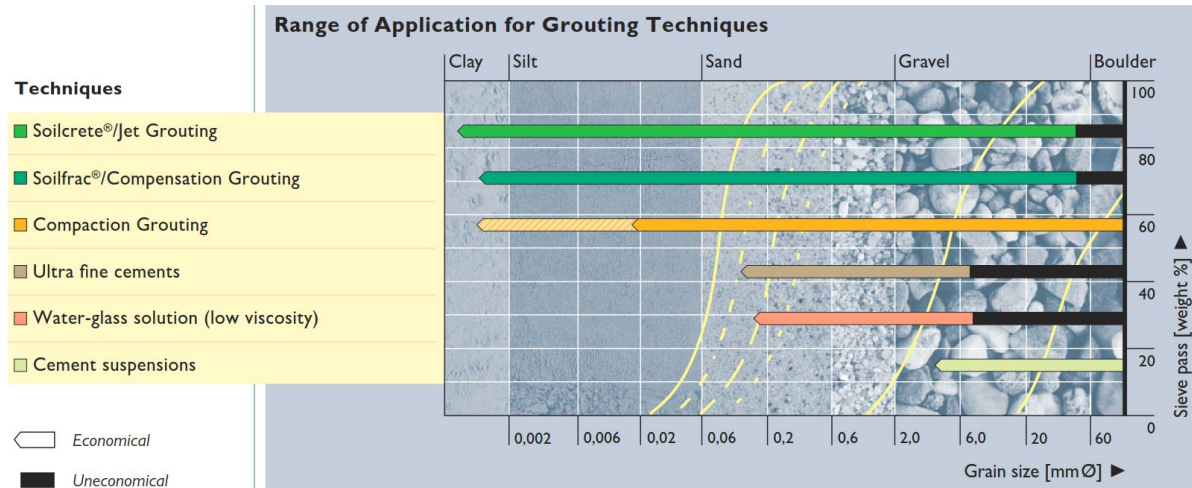


Figure 2.10: Range of compaction grouting techniques as applied by Keller (n.d.a)

communication, October, 2017). Firstly, the gas can escape during compaction, leading to irreversible compaction. Secondly, if the gas does not escape during compaction, but the compaction is irreversible due to interlocking particles, an increased gas pressure is generated which extends gas driven dissipation of pore pressures. Thirdly, the gas is elastically compressed and does not result in a lasting effect. Finally, partial saturation due to gas formation result in a lower hydraulic conductivity preventing the water to escape. The first two scenarios specify a positive outcome, the third defines a neutral outcome and in the fourth scenario, the problem is exacerbated.

2.2.1 Proctor test

The test is designated to measure the effectiveness of compaction on a specific soil and to identify the optimal efficiency conditions. The effectiveness of compaction is measured in dry mass per unit volume and is highly influenced by the water content. The maximum density and optimum water content, located at the peak of the curve, are not intrinsic soil properties and vary with the compaction energy applied.

At low water content values, most soils act stiff. As the water content increases towards the optimum water content (the particular value of water content at which the dry density is highest for a particular work input), the soil becomes more workable. Progressively higher dry densities can be achieved. When the water content increases past the optimum value, a reduction in dry density for a given amount of energy is measured, due to an increasing proportion of soil volume being occupied by water (Craig, 2004). The saturation dry density is unattainable in practice. Not all air can be expelled.

Fredlund and Rahardjo (1993) found that the theory of unsaturated soil mechanics can explain the behaviour of a soil when compacted. The matric suction is highest at low water contents (2% residual water content for uniformly graded fine Toyoura sand under 49 kPa of confinement pressure (Gallage et al., 2016)), preventing soil particles to move into a more dense state. As the water content increases, the suction reduces. The results for light Proctor tests (both 2.5 kg ASTM D698 and EN 13286-2) for a range of soil types are depicted in Figure 2.11 with saturation plotted for $G_s = 2.65$ as reference.

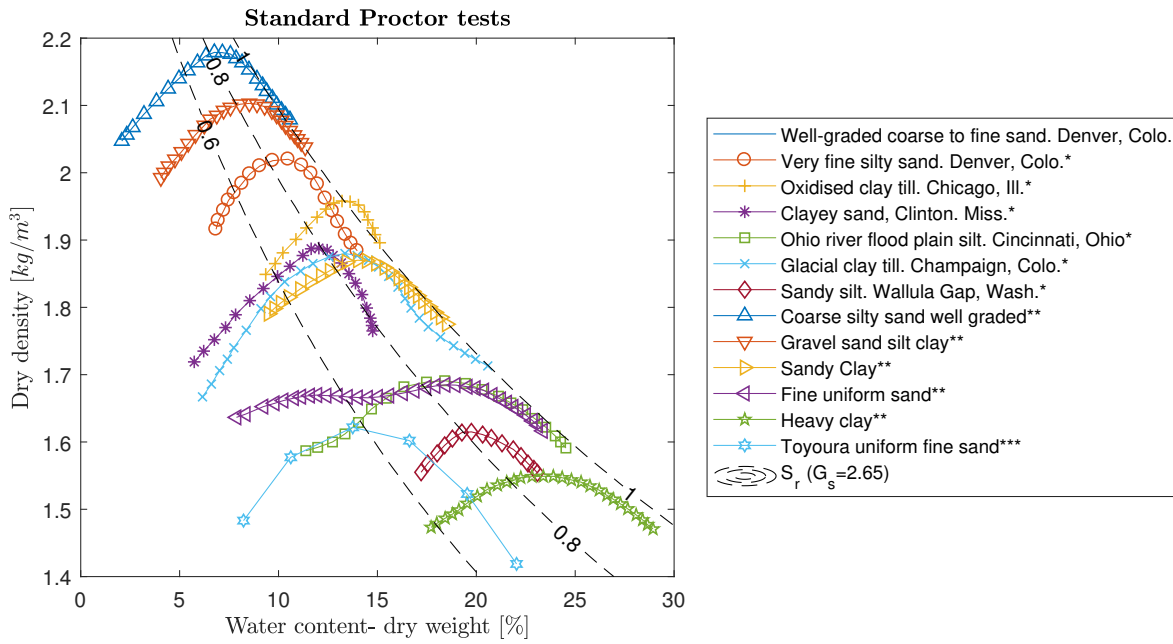


Figure 2.11: Dry density - water content Standard Proctor (light 2.5 kg hammer) test results for various types of soils. The saturation contours are indicated for $G_s = 2.65$.

*From Terzaghi et al. (1996)

**From Head (2006)

***From Gallage et al. (2016)

2.2.2 Work input

In a study of comparing static and dynamic compaction, Hafez et al. (2010) found that a similar amount of work input in a static compaction test resulted in a higher maximum density compared to the dynamic counterpart. The work input is calculated according to Equation 2.10 for a radially constrained sample and normalised to the sample volume to obtain a measure of work input in $[\frac{J}{m^3}]$.

$$W = \int F \cdot ds_a = [N \cdot m] = [J] \quad (2.10)$$

The energy input applied to a proctor test was found to be as in Equation 2.11. The work per unit volume is a function of the mass of the Proctor hammer head (M_{proc}), gravitational acceleration (g), the amount of blows (N_{blows}) and the Proctor cell volume (Vol_{proc}).

$$\frac{W}{Vol} = \frac{M_{proc}gH_{proc}N_{blows}}{Vol_{proc}} \quad (2.11)$$

A similar principle can be applied to Rapid Impact Compaction (RIC). In a case study, a 12 tonne hammer delivers 60 blows to compact the soil at 7 metres depth. A few simplifications are made: The drop height was assumed to be 0.5 metres without downward impact assistance (gravity only); the head diameter was assumed to be 2 metres; and the zone of influence was assumed to be a cylinder of 7 metres high and a diameter of 2 metres (overlapping and unrealistic, non-bulging influence zone). When Equation 2.11 is implemented, the work per unit volume amounted to 163.70 kJ/m^3 .

In Fredlund and Rahardjo's (1993) review of the comparison between the predicted and measured compaction curves for both static and dynamic compaction, the equal-energy input is calculated by integrating the applied stress over the volumetric strain.

In a triaxial cell, the work input per unit volume in $J \cdot m^{-3}$ is calculated as in Equation 2.12, with the radial strain ϵ_r being deduced from the volumetric strain. In an unsaturated material, a calibrated

double cell triaxial set-up is required to measure volumetric strain accurately. In a radially confined set-up, the radial strain is zero. Compaction can only occur vertically.

$$\frac{W}{Vol} = \int \sigma_a d\varepsilon_a + 2 \int \sigma_r d\varepsilon_r \quad (2.12)$$

In Hously's (1979) investigation into the work input to granular materials, it is stated that the power input per unit volume [$J \cdot m^{-3} s^{-1}$] is the product of the stresses and the strain rates, which is not the case for a multiphase material. The total power input depends on the skeleton displacement and the pore fluid displacement. The effective stress is responsible for work input, and not the total stress. In a multiphase material, the two processes of deformation and pore fluid seepage occur simultaneously. The work input is analysed for a fully saturated material, i.e. consolidation, the case where both phases are incompressible. The expression for power input per unit volume of soil is shown to be the product of the effective stress and the strain rate, combined with the product of excess pore pressure gradient and the artificial seepage velocity (Equation 2.13).

$$L = \sigma_{ij} \dot{\varepsilon}_{ij} - u'_{,i} w_i \quad (2.13)$$

Hously (1981) adapted the formulation for unsaturated soils by an additional term for the compressibility of the pore fluid, as in Equation 2.14, with n representing porosity and \dot{v}^w the volumetric strain rate in the pore fluid.

$$L = \sigma_{ij} \dot{\varepsilon}_{ij} - u'_{,i} w_i + n u \dot{v}^w \quad (2.14)$$

The formulation for a three-phase compressible medium is significantly more complex than at first thought and was further expanded in Hously's (1997) work to Equation 2.15. The latest formulation accounted for the energy dissipated by air and water flow through the soil (first two terms), the work connected to suction s (third term), the power input to compress the air phase (fourth term) and the input due to deformation of the skeleton due to the effective stress defined as per Equation 2.9 (fifth term).

$$L = -u'_{,j} w_j^w - u'_{,j} w_j^a - n s \dot{S}_r + n(1 - S_r) u^a \dot{v}^a + \sigma'_{ij} \dot{\varepsilon}_{ij} \quad (2.15)$$

Chapter 3

Methodology

3.1 Research Methodology

The method of desaturation and compaction is a two-stage process. However, a single experimental set-up was devised to test the coupled process.

For further investigation, the method of biogenic gas production through denitrification was implemented to desaturate a soil specimen before compactive effort was applied. *In situ* biogenic gas formation is chosen over air sparging, as the in-place created gas is more stable than the gas injected into the soil under pressure. Air sparging may cause a change in the local environment of existing denitrifying bacteria if air is injected. Higher levels of nitric- and nitrous oxide may occur. Nitrogen sparging may be implemented to maintain anaerobic conditions. However, it is chosen to stimulate a natural process with appropriate concentrations and correct ratios of substrate solution to desaturate a soil. A predictable amount of molecular nitrogen gas can be produced through denitrification of a nitrate rich substrate without resultant harmful intermediates.

To investigate the compactive effort required to achieve a higher density, the Rowe cell (hydraulic consolidation cell) was chosen. A triaxial may be more representative, but the lack of access to a calibrated double walled cell with hydraulic pressurised and monitored controller entailed that the volumetric strain cannot be measured accurately. The radial strain is in turn estimated from the volumetric strain. The radially confined Rowe cell allows for the work input to be calculated from the axial strain and overburden pressure. Additionally, the Rowe cell offers the possibility of flush through treatment and permeability tests and various drainage conditions.

Initially a set-up was designed based on the Proctor test (Appendix E.1). However, dynamic loading was sacrificed for the Rowe cell's ability to maintain pressure conditions. Adequate confinement and the sample pressure conditions play a cardinal role in the behaviour of the gas phase. Accurate measurement of the produced gas, expelled pore fluid and surface displacement is possible in an adapted Rowe cell, during the desaturation- and loading phase. The loading steps in the hydraulic cell was increased up to the maximum pressure within calibration limits to aim for a similar work input to that of a Proctor test or the RIC case study. Static compaction over the entire sample surface does not allow for a similar shearing and bulging effect as is found in a Proctor test. Smaller displacements are expected with limited grain rearrangement. Another significant difference between the calculation of work input of the Rowe cell compared to the Proctor test. The energy input in a Proctor cell is determined through the number of times a known mass is dropped from a controlled height. In a Rowe cell, the work input is a function of the axial displacement under a controlled constant overburden pressure.

The adapted Rowe cell set-up was initially designed to allow for substrate flush through of the sample (Appendix E.2). The set-up was simplified to its final form to reduce the complexity and equipment requirements. It was instead opted to mix the inoculated substrate solution in place for

optimal distribution.

From Figure 2.11 it is evident that the optimum water content for most materials can be reached by desaturating the sample to 80% saturation. The material that was chosen for the study was a fine sand with a fines fraction ($< 63\mu m$) of 16%. The clean, inert material had the added benefit of not having an influence on the denitrification process. Due to pore pressure accumulation caused by the low permeability directly influenced by fines content, a silty fine sand with 16% fines was chosen. It is found that a material with a fines content above 10 to 12% is the practical limit of the compactible range of Rapid Impact Compaction. The fines was increased to 66% because the location of the maximum dry density - optimum water content point for the particular material was at a saturation significantly below the aimed 80% saturation.

The anaerobic denitrifying bacterial strain inoculum was obtained from a previous study. A sample from the targeted soil body is preferred to serve as base for the inoculum enrichment. This prohibits the introduction of foreign bacteria into a soil body in practice.

From experience, Pham (2017) found that the time it takes to consume all nitrate within soil is halved compared to the same concentrations in solution. This was not initially observed and consequently an additional study into the pH of the soil was launched.

The procedures that were followed during the experimental investigation are described in the following section. The sample composition and properties are delineated, enrichment of the bacteria is reported, procedures for phosphate buffering of the soil are described and the method followed during hydraulic cell tests and subsequent data conversion are outlined.

3.2 Soil Sample

Two different specimens were prepared for the investigation made from varying ratios of a uniformly graded fine sand (Geba - Sibelco Benelux) combined with a silica flour silt (M6 MILLISIL - Sibelco Benelux).

3.2.1 Particle size distribution

The particle size distributions (PSDs) for the Geba sand and M6 MILLISIL were determined separately and combined in two ratios; one at 84-16 (84%Geba and 16% M6 silt) to obtain a material with 18% passing the $63\mu m$ sieve, and the other at 34-66 to obtain a material with 61% passing the $63\mu m$ sieve. The PSD for Geba sand was obtained from Krapfenbauer's (2016) work and the PSD for M6 MILLISIL was determined through a hydrometer test (based on BS1377, Appendix B). The first material is uniformly graded and classified as a silty sand (SM). The second mixture can be described as a sandy silt. The particle size distribution curves can be seen in Figure 3.1. The Geba uniform fine sand fraction is similar to Toyoura and Karlsruhe sand.

The effective size of the particles for both soils are determined from Figure 3.1 and presented in Table 3.1. The coefficient of uniformity (C_U) and coefficient of curvature (C_Z) are determined through Equations 3.1 and 3.2:

$$C_U = \frac{D_{60}}{D_{10}} \quad (3.1)$$

$$C_Z = \frac{D_{30}^2}{D_{60} \cdot D_{10}} \quad (3.2)$$

According to Craig (2004), a higher C_U indicate a larger range of particle sizes in the soil. A material with C_Z between 1 and 3 is considered well-graded. Neither one of the materials conform to this criterion.

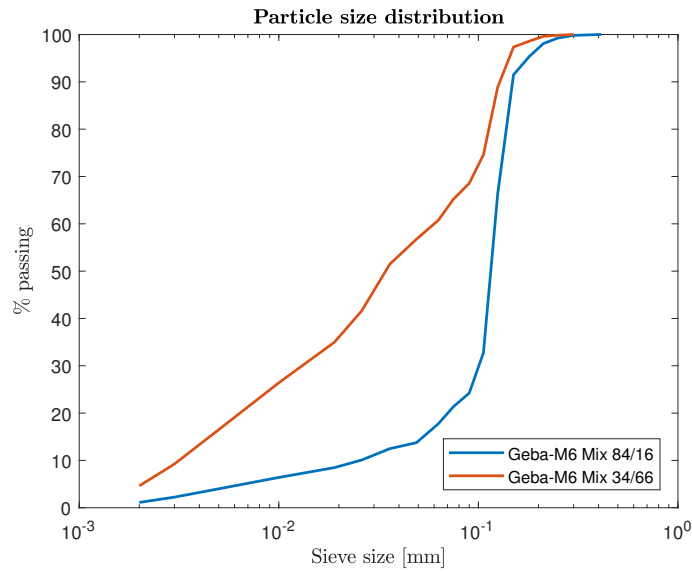


Figure 3.1: Particle Size Distribution for Geba-M6 84-16 (blue) and Geba-M6 34-66 (red) soil

Table 3.1: Particle size analysis. Results in *mm*

Soil	D_{10}	D_{30}	D_{50}	D_{60}	D_{90}	C_U	C_Z
Geba-M6 84-16	0.026	0.101	0.116	0.122	0.149	4.69	3.22
Geba-M6 34-66	0.003	0.012	0.034	0.060	0.128	20	0.8

3.2.2 Minimum and maximum void ratio

The minimum and maximum voids ratios are determined according to the Japanese Standard specified by Mulder and Verwaal (2006). For the Japanese test, a rigid cell (dimensions $\phi=59.9\text{mm}$ and $h=40\text{mm}$) is filled with dried material and weighed to determine minimum and maximum dry densities. For the minimum dry density, the material is carefully placed with a funnel. The maximum dry density is determined through the placement of the material in incremental layers ($\approx 8\text{mm}$ thick) and densifying the material by 100 blows on the side of the cell with a 90° rotation after every 10 consecutive blows. Minimum and maximum packing densities are determined and the voids ratios computed using Equation 3.3. The results are displayed in Table 3.2.

$$e = \frac{G_s}{\rho} \cdot \rho_w - 1 \quad (3.3)$$

Table 3.2: Minimum and maximum void ratios

Soil	ρ_{min} [kg/dm^3]	ρ_{max} [kg/dm^3]	e_{max} [-]	e_{min} [-]
Geba-M6 84-16	1.3000	1.7100	1.0385	0.5497
Geba-M6 34-66	1.1000	1.786*	1.4091	0.4838

*The maximum density is taken from the modified Proctor test as the value obtained from the Japanese standard ($1.62\text{kg}/\text{dm}^3$) is deemed unrepresentative for this material as it is significantly lower than the value achieved in a Modified Proctor

3.2.3 Optimum water content

The relationship between dry density and water content for the soil is determined through the procedures stated in BS 1377: 1990: Part 4. A Standard Proctor (SP) and Modified Proctor (MP) is performed on the Soil Sample with the results presented in Figure 3.2. The compactive effort applied to the sample is $596kJ/m^3$ for the BS light compaction test and $2682kJ/m^3$ for the BS Heavy compaction test. In the case of the Geba-M6 84-16 soil sample, a modified Proctor test was conducted by executing compaction in three layers (instead of the standard five layers), thus only 60% of the energy was applied, corresponding to $1609.2kJ/m^3$.

At least five points are obtained with variable water contents with at least two points after the optimal water content at the specific energy level. Values for water content w and density ρ are recorded for each point. The dry density is consequently calculated through Equation 3.4 for each point and the result plotted on the dry density- water content plane.

$$\rho_d = \frac{\rho}{1 + w} \quad (3.4)$$

Levels of air content are indicated on the same plane with the help of Equation 3.5 by substituting values for air content A into the formula. Similarly, levels of saturation can be indicated on the dry density- water content plane by replacing the value for air content with its relationship to Saturation (Equation 3.6). In this case, porosity is calculated as in Equation 3.7. By combining Equations 3.5, 3.6 and 3.7, the Saturation can be written as in Equation 3.8 and plotted on the dry density - water content plane.

$$\rho_d = \frac{G_s \cdot (1 - A)}{1 + w \cdot G_s} \cdot \rho_w \quad (3.5)$$

$$A = n(1 - S_r) \quad (3.6)$$

$$n = 1 - \frac{\rho_d}{\rho_s} \quad (3.7)$$

$$S_r = \frac{\frac{\rho_d}{\rho_w \cdot G_s} \cdot (1 + w \cdot G_s) - 1}{1 - \frac{\rho_d}{\rho_s}} + 1 \quad (3.8)$$

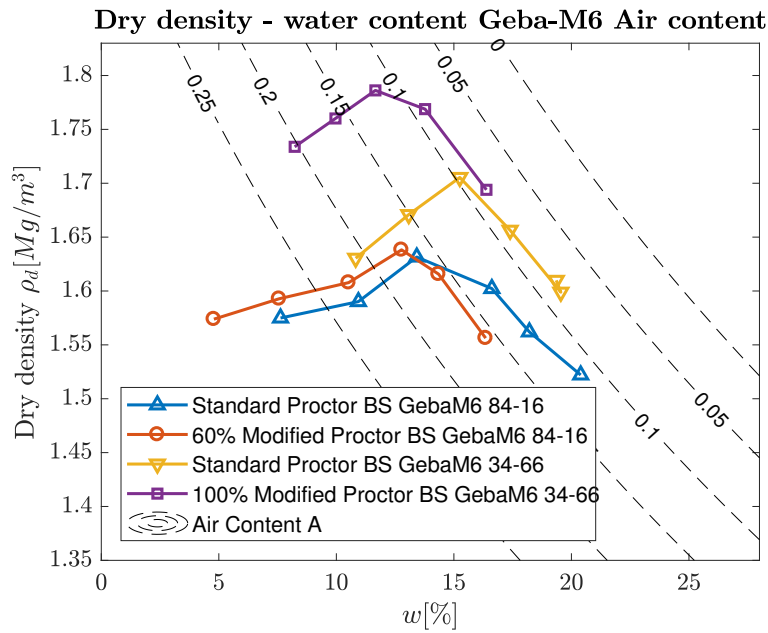


Figure 3.2: Dry density - water content relationship for Geba-M6 soils with air content

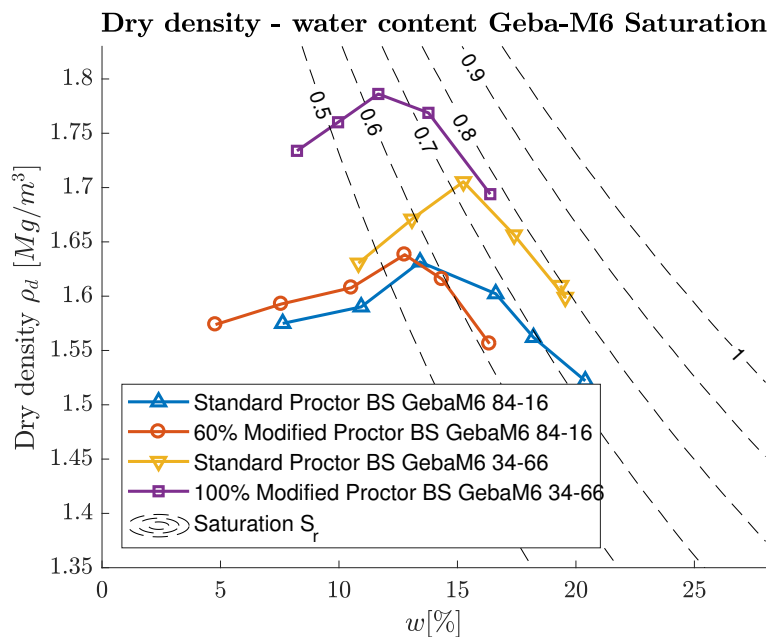


Figure 3.3: Dry density - water content relationship of Geba-M6 soils with saturation

3.3 Bacteria Enrichment

A similar set up to the one used by Pham et al. (2016), was employed to incubate the denitrifying bacteria to be used in further experiments. The substrate solutions for the experiment contained calcium nitrate ($Ca(NO_3)_2$) as nitrate source, together with calcium acetate ($Ca(C_2H_3O_2)_2$) as organic carbon source in the varying concentrations. Additionally, 10 mM ammonium sulphate ($(NH_4)_2SO_4$), 10 mM magnesium sulphate ($MgSO_4$), 10 mM monopotassium phosphate (KH_2PO_4), 10 mM dipotassium phosphate (K_2HPO_4) and 1 mL/L trace element solution SL12B was added to

3.3. BACTERIA ENRICHMENT

the substrate solution (Pham et al., 2016) to avoid nutrient limitation during bacterial growth. The unit molar (M), or molarity, denotes concentration and is equivalent to mole/litre, which is the most common way of expressing the concentration of a solute in a solution.

Batch experiments ranged between 0.4 and 0.5 litres and were conducted at ambient (atmospheric) pressure and a controlled temperature (25 °C). With the use of a gas washing bottle, pictured in Figure 3.4, fluid could be extracted while maintaining the anaerobic environment. The gas washing bottle, open to the gas phase, was connected to an upturned graded cylinder placed in a bucket of water to seal the gas fraction off from the surroundings. Marprene tubing, impermeable to oxygen, nitrogen and nitrogen oxides, was used to ascertain a closed system. All open tubes were clamped tightly with Hoffman tubing clamps when not in use. The two tubes entering the upturned cylinder enabled one to flush the system through and extract the accumulated gas if needed.

After the preparation of the substrate solution, all tubing connections were checked to assure a tight fit and the system was flushed with nitrogen gas to ensure anaerobic conditions. The N_2 gas cylinder was connected to the gas washing bottle connection leading to the liquid phase. This allowed the N_2 gas to break the surface (bubble through) of the substrate solution and flow out into the upturned cylinder, alternating between releasing gas out the bottom of the cylinder and releasing gas through the flushing tube. A slight overpressure is maintained by controlling the flushing tube clamp so that the water level inside the cylinder was slightly below the surrounding water level. When the clamps were closed and the gas flow was shut off, this overpressure prohibited air to enter the system. The cylinder was fixed at a convenient height to ensure formed gas could not escape from the bottom of the cylinder. Atmospheric pressure was ensured by keeping the inside and outside water level the same when measurements were taken. The datum was recorded and the bacteria was allowed time to grow.

The subsequent procedures were followed when extracting liquid to take measurements:

1. The cylinder was readjusted so that the internal water level coincided with the surrounding water level. The water level was recorded and the gas produced since the previous measurement, determined
2. A syringe was connected to the gas washing bottle and the clamp opened
3. Liquid was extracted (a volume larger than the tube entering the liquid) and injected back into the system a number of times to ensure mixing of the substrate
4. Sufficient liquid is extracted to conduct pH, EC and concentration measurements, where after the Hoffman Clamp is closed and the syringe detached
5. The liquid was placed in a tube. 200 μ l was extracted for concentration measurements and cleaned pH and EC electrodes were placed into the liquid to take measurements
6. The same syringe (prevent cross contamination) was used to extract the liquid from the tube and again connected to the gas washing bottle inlet
7. Suction was applied to the syringe to extract any trapped air from the tube when the clamp was opened
8. The liquid was injected back into the system, assuring that no air entered with it
9. The cylinder height was readjusted and the water level recorded to act as reference for ensuing gas production.

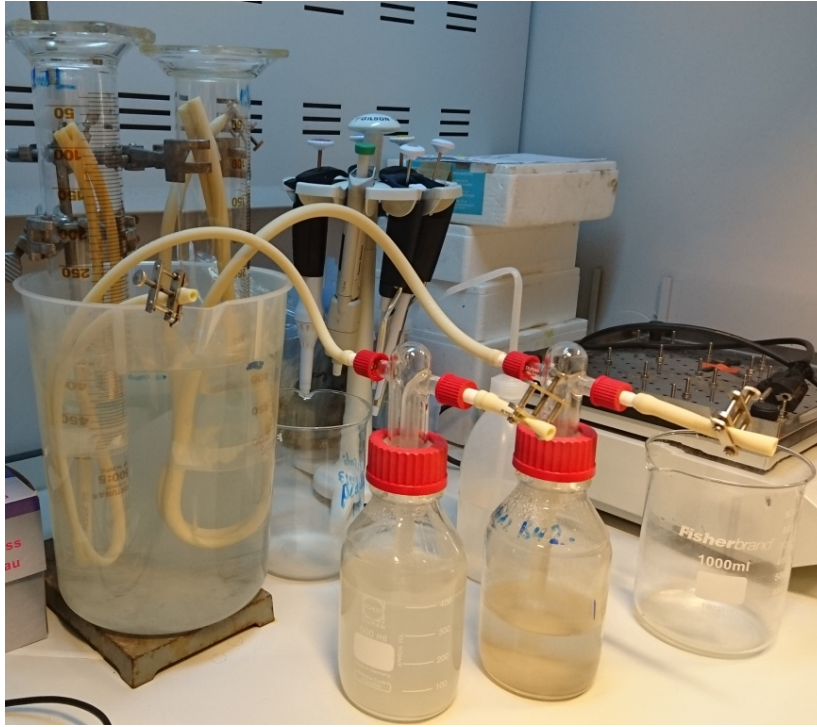


Figure 3.4: Bacteria incubation test measurement set-up with upturned graded cylinders (eudiometer) to measure gas production over time

Once a week the system was flushed with N_2 gas to ensure anaerobic conditions. This was done to eliminate air from the system that could have entered through leakages or during extracting or injecting of liquid.

A standard conductivity cell (WTW TetraCon 325) suitable for groundwater measurements, together with a hand-held conductivity meter (WTW LF320), was used to measure the electrical conductivity (EC) in the extracted liquid. The pH was measured with calibrated pH electrode (WTW SenTix 21 Gel electrode) combined with a hand-held pH measuring instrument (WTW pH 315i). The extracted liquid for concentration measurements was adequately diluted to fall within the measurement range of the various tests. Consequently, concentration $NO_3^- - N$ (Hach Lange LCK 339), $NO_2^- - N$ (Hach Lange LCK 341) and Ca^{2+} (Hach Lange LCK 327) was measured quantitatively using a portable spectrophotometer (Hach Lange DR 1900).

3.3.1 Determination of substrate concentration

The method to determine the gas saturation in the porous medium follows from Pham's (2017) research on microbial induced desaturation. The molar quantity of nitrogen gas ($n_{N_2^g}$) required to achieve 20% gas saturation (S_g) was determined with the ideal gas law (Equation 3.9). Initially the sample was assumed to be fully saturated. The volume of gas to be produced is a function of the target gas saturation, the porosity (n) and the volume to be treated (V_{tot}).

$$n_{N_2^g} = \frac{P \cdot V_g}{R \cdot T} \quad (3.9)$$

Where:

$$V_g = S_g \cdot V_v \quad (3.10)$$

$$V_v = n \cdot V_{tot} \quad (3.11)$$

$$S_g = 1 - S_r \quad (3.12)$$

The concentration nitrogen gas required is the sum of the concentration dissolved nitrogen and the concentration nitrogen in a gaseous state (Equation 3.13). The dissolved fraction was calculated using Henry's law (Equation 3.14) with $k_{HN_2} = 1542.6 \frac{atm \cdot L}{mol}$. The gaseous fraction is a function of Equations 3.9, 3.10 and 3.11.

$$c_{N_{2tot}} = c_{N_2}^g + c_{N_2}^l \quad (3.13)$$

$$c_{N_2}^l = \frac{p_{N_2}}{k_{HN_2}} \quad (3.14)$$

$$c_{N_2}^g = \frac{n_{N_2}^g}{n \cdot V_{tot}} \quad (3.15)$$

$$c_{N_{2tot}} = \frac{S_g \cdot n \cdot V_{tot} \cdot p_{N_2}}{n \cdot V_{tot} \cdot R \cdot T} + \frac{p_{N_2}}{k_{HN_2}} \quad (3.16)$$

The nitrate concentration required to produce the equivalent nitrogen gas concentration was determined from the stoichiometrical coefficients for maximum growth (Equation 3.17). $\frac{0.97}{0.39} = 2.49$ is considered as conservative.

$$c_{NO_3^- \text{ consumed}} = \left[\frac{Y_{NO_3^-}}{Y_{N_2}} \right]_{max-growth} \cdot c_{N_{2tot}} \quad (3.17)$$

Equations 3.16 and 3.17 were combined to calculate the concentration

$$c_{NO_3^- \text{ consumed}} = \frac{Y_{N_2}}{Y_{NO_3^-}} \cdot \left[\frac{S_g \cdot p_{N_2}}{R \cdot T} + \frac{p_{N_2}}{k_{HN_2}} \right] \quad (3.18)$$

An acetate to nitrate ratio of 1.2 was implemented. Subsequently the concentration acetate can be calculated as in Equation 3.19.

$$c_{C_2H_3O_2^- \text{ consumed}} = 1.2 \cdot c_{NO_3^- \text{ consumed}} \quad (3.19)$$

From Figure 3.5 it is determined that the concentration nitrate (NO_3^-) required to desaturate the medium to 80% at 5 metres below the ground water table is calculated as 33.4 mM. From Equation 3.19, the concentration acetate ($C_2H_3O_2^-$) is determined to be 40 mM. 20 mM calcium acetate ($Ca(C_2H_3O_2)_2$) and 16.7 mM calcium nitrate ($Ca(NO_3)_2$) is required to reach the targeted gas saturation.

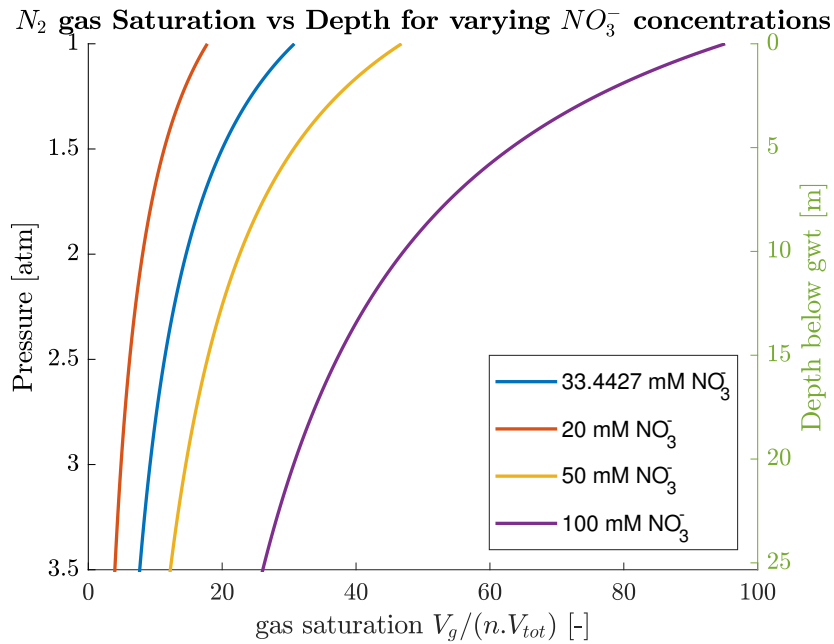


Figure 3.5: Saturation as a function of depth for varying concentrations of nitrate with phreatic level at surface. Ideal gas behaviour at maximum growth stoichiometry is assumed. The porous medium is assumed to have a porosity n of 0.4. The substrate concentration required to desaturate the medium to 80% at 5 metres below the ground water table is calculated as the blue line.

3.4 pH Buffering of soil

Initial tests conducted exhibited a longer than expected lag period prior to significant gas production. A study into the soil pH was launched. It was noticed that the pH of the Geba soil fraction is lower than the pH 7 stated in the technical information sheet (Sibelco). pH measurements were conducted according to ISO 10390 (ISO-NEN, 2005), a test with liquid to solids ratio of 5 (LS5) by volume. About 6 ml of soil was added to 30 ml of demi water or a 10 mM $CaCl_2$ solution. The specimen was placed on a linear actuating shaking table (Heidolph Promax 1020) at 130 actuations per minute (the speed at which the liquid does not fold in on itself) for 60 minutes and was left stationary for another 60 minutes to settle. The pH was measured at 0 and 60 minutes after the settlement period is concluded.

The electrometric method included in the outdated British Standard BS 1377: Part 3: 1990: 9 (Head, 2006) was also referenced due to the implementation of an LS2.5 test by mass. Thirty grams of soil was added to 75 ml of liquid and was left for at least 8 hours before measuring the pH. The lower LS ratio was favourable for the treatment of relatively large quantities of material, as less liquid was required.

An experiment was set up to test different combinations of soil (Geba and Geba-M6 84-16 mix), in different solutions. The different regimes include 10 mM $CaCl_2$ control-, demi water and 10 mM and 100 mM phosphate buffer solutions as indicated in Table 3.3. Only clean Geba sand and the Geba-M6 84-16 soil mixture were tested.

The phosphate buffer used was a solution of dipotassium phosphate (K_2HPO_4) and potassium dihydrogen phosphate (KH_2PO_4) with a pK_a of 7.2. Two concentrations of buffers were tested, one 10 mM- and one 100 mM solution. The concentration to be used in further soil treatment will depend on the required buffering capacity of the system. The regime with sufficient capability to buffer the soil to a pH of 7.2 was then decanted, rinsed with demi water to dilute the phosphate buffer out of the

Table 3.3: Soil pH buffer test regime

	Material	LS ratio by type	Concentration & Solute	Time span
1a	7 ml Geba+M6	5 by volume	10 mM Phosphate buffer	1 day
1b	above material	Decanted, demi water diluted, decanted, air dried		1 day
1c	above material	5 by volume	10 mM $CaCl_2$	5 days
2	7 ml Geba+M6	5 by volume	100 mM Phosphate buffer	7 days
3	7 ml Geba+M6	5 by volume	10 mM $CaCl_2$	7 days
4	7 ml Geba	5 by volume	10 mM $CaCl_2$	7 days
5	30 g Geba+M6	2.5 by mass	10 mM $CaCl_2$	8 days
6	30 g Geba	2.5 by mass	10 mM $CaCl_2$	8 days
7a	30 g Geba	2.5 by mass	demi water	1 day
7b	above material	Decanted, air dried over night at 25 °C		1 day
7c	above material	5 by volume	10 mM $CaCl_2$	6 days

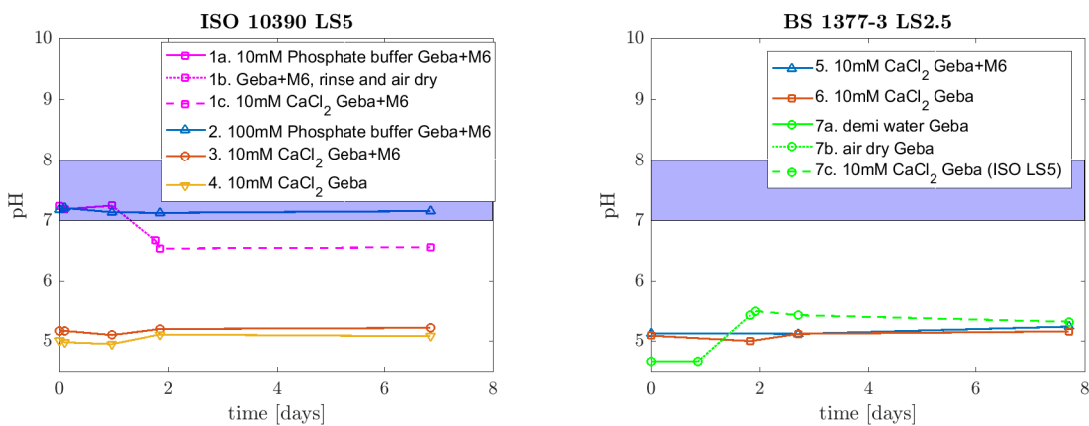


Figure 3.6: pH Measurements on various soil samples with different solutions. The numbers correspond with Table 3.3. The 'Happy band' of the bacteria is displayed in hatched blue to indicate the optimum range as defined by Knowles (1982) for Nitrogen gas production.

system and air dried in a fume hood at 25 °C. The pH was determined in a 10 mM $CaCl_2$ solution according to the method indicated in the ISO standard. Specimen 7 (Table 3.3) was rinsed with demi water to study whether the cause of the low soil pH was a superficial residue as a result of possible treatment during production. A set of control tests on the Geba and Geba-M6 mixture were also performed according to both British and ISO standard. pH Measurements for all tests were repeated after an extended period (5-8 days) to determine whether a change in pH occurred over time.

3.5 Hydraulic (Rowe) Cell Methodology

The hydraulic consolidation cell, or Rowe cell, was used to evaluate the energy absorbed during a one-dimensional compression test. With this set-up, the sample could be maintained at in-situ conditions throughout the gas production phase, while the volume of the sample, pore volume and saturation could be monitored continuously. During the gas production phase, the apparatus could determine if any swelling (inflating) of the sample occurred. The cell also allowed for various drainage scenarios to be implemented, as well as hydraulic conductivity tests and the flush through of a sample. Throughout this experiment only top vertical drainage with a mix-in-place inoculated substrate solution was investigated.

The procedures followed during Rowe cell tests were adapted from the British Standard BS 1377: Part 6: 1990. The procedures for general consolidation and permeability tests were described in depth by Head and Epps (2014). The process was adapted to perform a one dimensional compression test, as opposed to the consolidation test as specified by the standard. Cell preparations and diaphragm calibration were conducted as stated. The set-up is depicted in Figure 3.7.

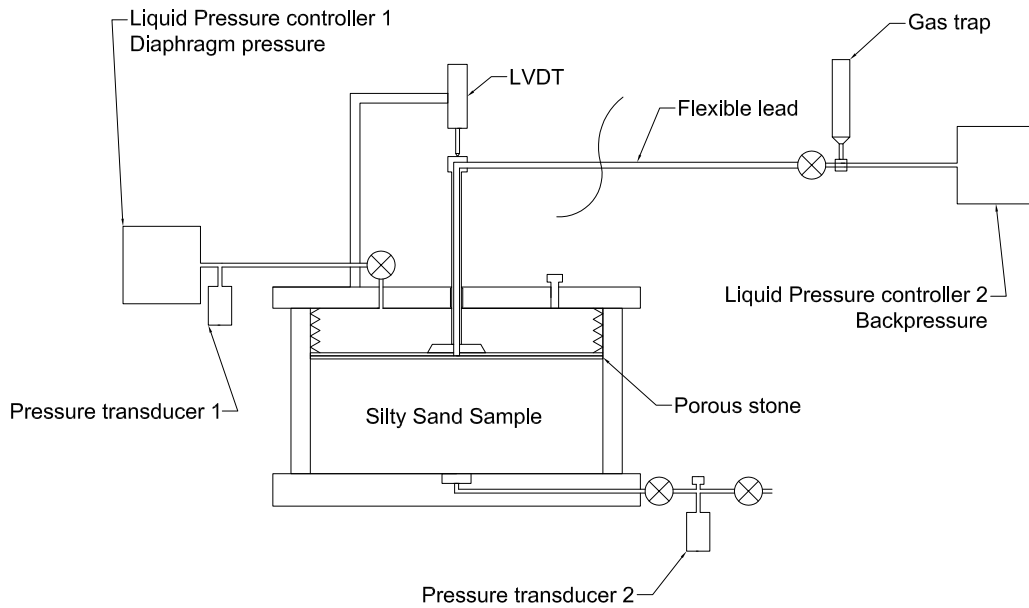


Figure 3.7: Hydraulic cell set-up

The set-up had been altered in several ways. Two automatic hydraulic pressure controllers (VJ Technology 3000 kPa 250cc APC) were used, one to control the diaphragm pressure and the other to control the back-pressure. The pressure controllers were both connected to a data logger (VJ Technology MPX3000) with variable measurement intervals set at the start of the test. One of the main alterations made compared to the standard set-up, was the inclusion of a gas trap in the back-pressure line. This was intended to serve as a qualitative measurement of expelled gas from the cell to assist with saturation calculations throughout the test. Sample displacement was tracked via an LVDT (20 mm travel), with measurement interval of $1\mu\text{m}$, mounted on the cell with displacement of the spindle measured throughout the experiment. Pore pressure was measured at the bottom in the centre of the sample. All pressure transducers (pore-, diaphragm-, and back-pressure transducers) had a measurement interval of 1 kPa. All measurement points, apart from the gas accumulated in the gas trap, were logged at a set time-step over the duration of the test using measurement software on a personal computer.

The gas trap, depicted in Figure 3.8, consisted of an acrylic cylinder sealed at both ends. It had a capacity of approximately 150 ml and could safely maintain the required pressures. The cylinder was calibrated to measure the gas trapped under pressure. Two elbow connections at the base of the cylinder connected the trap to the back-pressure line and allowed for escaped gas to be captured at the top of the gas trap. The cylinder was clamped upright with a circular bubble level positioned on top for accurate measurements.



Figure 3.8: Gas trap connected to the back-pressure line of Rowe cell

3.5.1 Preparation of cell

Prior to sample placement, the pore pressure line and centre porous insert was saturated by flushing 500 mL of demineralised (demi) de-aired water under 500 kPa through the flushing valve until virtually no air rose from the porous insert. Trapped air was bled out through the air bleed. The valve between the pore pressure transducer and cell was closed momentarily for all three pressure transducers to be calibrated to the same pressure. The flushing valve was closed and the pressure controller disconnected while keeping the porous insert covered with demi de-aired water.

3.5.2 Sample placement

To obtain a fully saturated sample, the sample was placed using the wet pluviation method. A known weight of soil was fully saturated by adding an amount of liquid corresponding to a bulk density of 1.55 obtained through practised sample placement. To be certain on how much bacterial solution was required to fully saturate a sample for control purposes, a prediction was made on the pore fluid required. The amount of liquid was calculated from an estimation of bulk density and the estimated volume that the sample will occupy. Porosity n was calculated using Equation 3.20, corresponding to ≈ 0.4 for the tested materials.

$$n = 1 - \frac{\text{Bulkdensity}}{\text{Particledensity}} = 1 - \frac{\rho_b}{\rho_s} \quad (3.20)$$

The pore volume was calculated as the product of porosity and total volume as stated in Equation 3.21.

$$V_v = V_{tot} \cdot n \quad (3.21)$$

The substrate solution was prepared with the required concentrations calculated in Section 3.3.1 (16.7 mM $Ca(NO_3)_2$ and 20 mM $Ca(C_2H_3O_2)_2$) and inoculated with 100 ml/l bacterial solution. Then mixed into the dry soil with an additional 200 ml of substrate solution added to the cell. The sample was placed in a vacuum desiccator at -1.0 bar to let air entrained during mixing escape from the sample. The chamber was agitated to encourage extraction of air. After ± 20 minutes, when no

air was seen boiling from the surface, the sample was removed from the vacuum desiccator, ready to be placed in the cell. The sample was carefully placed with a spoon, spreading the material evenly to ensure that the sample remain below the liquid throughout placement. The sample was trimmed and levelled with a straight edge to ensure an even surface. Excess liquid was removed and measured until the liquid level corresponded to the surface of the specimen. The amount of liquid in the pore space was determined by subtracting the removed excess liquid from the inoculated substrate mixed into the sample and the additional substrate that was poured into the cell. This allowed for the water content to be determined and to calculate whether full saturation had been achieved.

The supernatant (removed liquid) was analysed for pH, Ca^{2+} -, NO_3^- -, and NO_2^- concentrations (quantitatively with the corresponding LCK test kits and DR6000 Hach Lange spectrophotometer) to be compared with the concentrations at test completion. A thin layer of liquid was left on the surface of the sample to ensure no air was trapped between the porous stone and the specimen. The vacuum de-aired sintered brass porous stone was carefully placed and the height of the specimen verified. It was measured from the top of the cell down to the porous stone, thus accounting for the thickness of the porous stone. No pore pressure build-up was expected to occur during placement. The porous stone was covered with demi de-aired water to assure a fully saturated cell after cell cover installation. The rigid disk was lowered into place, without disturbing the sample. The cell was filled to the brim with demi de-aired water. The de-aired porous rim drain was installed underneath the water level to alleviate pressure build up between the diaphragm and cell wall. The same method was followed for the control tests, though in all instances the substrate solution was replaced by demi de-aired water.

3.5.3 Fitting of cell cover

The cell cover was supported over the cell body on spacer blocks while demi de-aired water was let through the back-pressure controller to clear the back-pressure line and gas trap from any trapped air. The diaphragm pressure controller had to be filled with a sufficient volume of de-aired water to allow for expansion and pressure build up within the diaphragm. Conversely, the back-pressure controller should have adequate room for expelled water from around the diaphragm, as well as pore fluid expelled through gas production. For these experiments, a filled diaphragm pressure controller and a back-pressure controller with 220 ml of spare capacity was found to be suitable. Care was taken not to trap any air between the porous stone and the rigid steel plate. The hollow drainage spindle was clamped into place to minimise disturbance of the sample when the cell cover was installed. While lowering the diaphragm into place, displaced water was allowed to overflow from the top of the cell body to ensure that no air was trapped between the diaphragm and the cell wall. The diaphragm was fitted into the cell body with care to ensure that no confined air would be trapped in the folds. The cover was bolted to the cell body.

The diaphragm was filled with de aired water allowing for air to escape through the air bleed. The drainage spindle was released and a small diaphragm seating pressure p_{d0} of 10 kPa was applied. This initial pressure was lower than the allowed p_{d0-max} of 10 kPa due to diaphragm calibration not being considered. The LVDT was fixed into position and zeroed, allowing for a small upwards movement. The initial pore water pressure corresponding to p_{d0} was recorded and the corresponding pressure on the sample, p_0 , related to the seating pressure p_{d0} was determined. The gas trap was flipped from its initial position in order for the back-pressure line to enter the trap at the bottom of the cylinder. The height of the centre spindle was measured to determine whether the sample was disturbed during cell cover installation and to obtain the initial sample height under initial diaphragm pressure, $H_{p_{d0}}$. Both diaphragm- and back-pressure volume controllers were zeroed at this stage. It was assumed that no gas was produced during sample preparation based on the lag period observed in the incubation tests. The time however, between inoculating the substrate solution and installing the cell cover should be kept to a minimum.

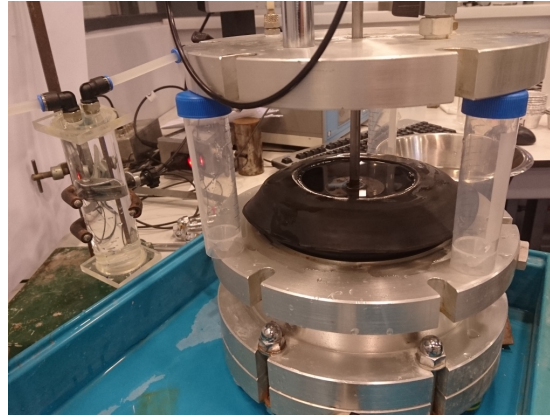


Figure 3.9: Fitting the cell cover

3.5.4 Saturation

Saturation procedures were conducted to ensure that the sample was fully saturated. The saturation was estimated by determining the ratio $\frac{\delta u}{\delta \sigma}$, where δu is the change in pore pressure resulting from an incremental change in vertical stress $\delta \sigma$ when no drainage is allowed. A ratio of $\frac{\delta u}{\delta \sigma} = 0.95$ was accepted as sufficiently saturated, although higher ratios were obtained. Increments of diaphragm pressure and back-pressure were applied alternately. The drainage valves were closed during increments of diaphragm pressure to not allow flow into, or out of the system. This allowed for the pore pressure ratio (Skempton B parameter) to be determined at each stress increment.

Cell pressure increments should be lower than the effective consolidation pressure and a difference of $\pm 10\%$ between diaphragm pressure and pore pressure should be avoided. The pore pressure, u_1 , was recorded when a steady value was reached and $B = \frac{du}{d\sigma} = \frac{u_1 - u_0}{p_1 - p_0}$, could be calculated. The back-pressure was increased to a value of 10% less than the diaphragm pressure and 1 kPa higher than the pore pressure to allow for saturation, if required. The controller volume v_1 was recorded and the valve opened to admit the back-pressure into the cell. When the pore pressure and back-pressure equalised and the volume change stabilised, the valve was closed after the values for the pore pressure u_2 and the back-pressure volume v_2 were recorded. The volume taken up by the specimen ($v_2 - v_1$) was an indication of water taken up into air voids as no swelling was observed in the reconstituted soil. The procedure was repeated until $B > 0.95$ was achieved.

When saturation was reached, the equivalent initial pressure conditions were gradually introduced. The diaphragm pressure was set to 100 kPa, adjusted for diaphragm calibration, and the back-pressure gradually lowered to 50 kPa with two intermediate steps (90 kPa, 65 kPa). This was to bring the sample to in-situ conditions and allow for initial settlement to occur.

The different phases in the Rowe cell test are envisaged in Figure 3.10. The hydraulic cell is pictured with de-aired water filled diaphragm applying a constant overburden pressure to an initially fully saturated sample (a). The rigid plate ensures constant deformation and maintains a constant cross section area (A_ϕ). The Back pressure (σ_{BPC}) is controlled at the specified (hydrostatic) pressure and connected to the sample via the back pressure line. The line connects to a porous stone covering the entire top surface of the sample. During the reaction phase (b), the sample is desaturated. Some gas escapes through the porous stone, into the back-pressure line and is caught in the gas trap where it is quantified ($\Delta V_{gastrap}$). Possible expansion of the sample is monitored at the top of the centre spindle (ΔH). During the loading phase (c), the diaphragm pressure is increased (σ_{DP}). The surface displacement (ΔH), further gas expulsion ($\Delta V_{gastrap}$), and controller volume changes (ΔV_{BPC} and ΔV_{DPC}) are monitored and allow the formulation of volume balances. Note the apparent reduction of the trapped volume between the diaphragm and cell wall.

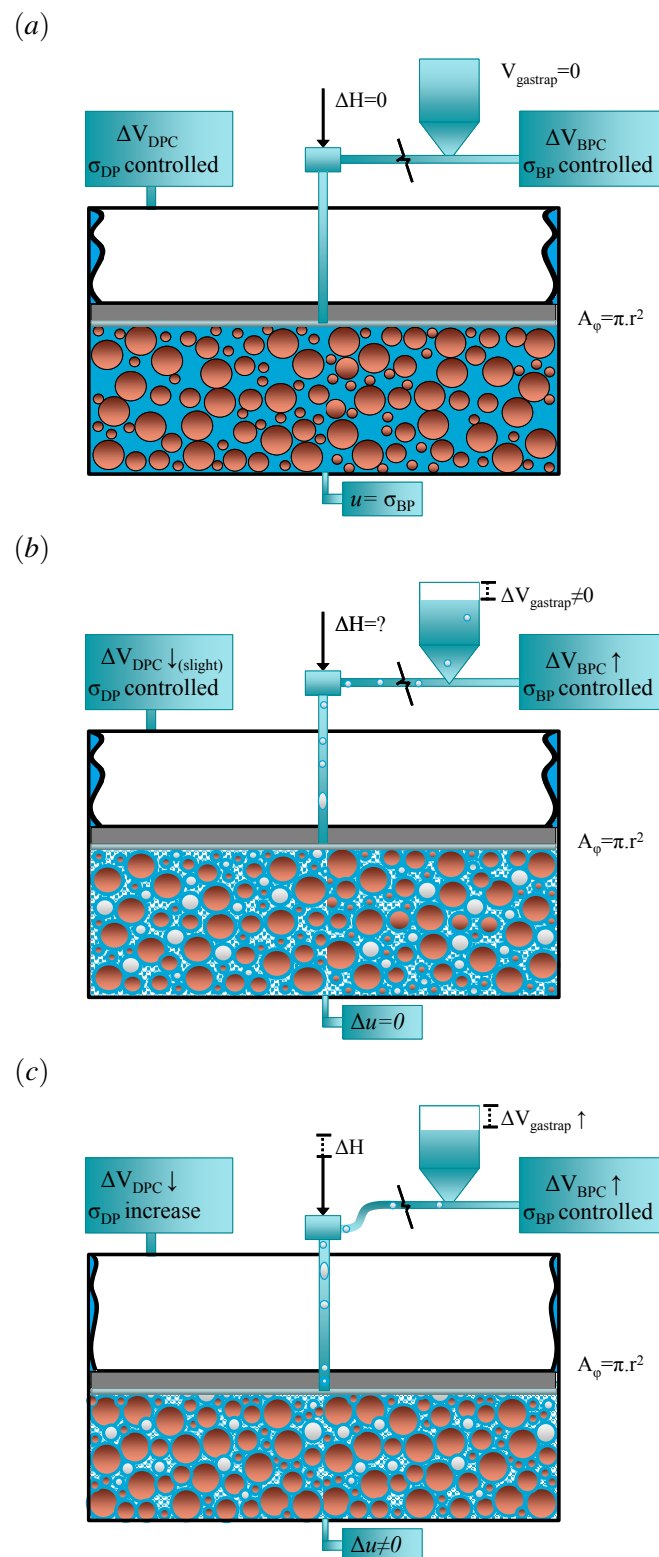


Figure 3.10: Rowe cell phases: (a) end of saturation phase at in-situ conditions and fully saturated, (b) Desaturation phase and (c) Loading phase - note ΔH

3.5.5 Reaction phase (Bacterial solution for pore fluid)

When the in-situ conditions were reached, the bacteria were left to consume the nutrients and produce gas until no increase in expelled pore liquid was observed in the back-pressure controller or until the targeted volume of gas production had been reached, whichever occurred first. The controllers were set to maintain the specified *in-situ* pressure conditions while pore pressure, vertical displacement and volume change was measured over time. The duration of the reaction phase was expected to last half the time of the same concentration of substrate solution in the bacterial incubation tests Pham (2017). The temperature was controlled at 20°C.

The following assumptions were made to calculate the volume of gas produced during the reaction phase, based on a volume balance in the cell:

- Once in-situ conditions were reached, the volume change in the back-pressure controller was caused by gas production inside the cell. All volume changes prior to the adjustment of pressure, was influenced by excess fluid displaced from around the membrane
- The sample was assumed to be fully saturated at the start of reaction phase
- All gas was assumed to be produced inside the sample
- The gradual decrease in diaphragm volume caused by leakage (< 2ml/day, too slight to be located), allowed for the equivalent volume of gas to be removed from the solution and formed in the sample
- The density of the displaced pore fluid was assumed to be that of demi water

Therefore, the saturation of the sample could be computed. A different set of assumptions are valid for the determination of displaced pore fluid during the loading stage due to the influence of excess fluid displacement from around the diaphragm. The standard suggested that the water build up around the diaphragm has to be drained through the rim drainage valves when a low permeable specimen is tested. The tested sample was relatively highly permeable, therefore it was decided to drain this volume to the back-pressure controller.

Based on the volume balance inside the cell, the gas produced was a function of the change in volume in the back-pressure controller (BPC) and diaphragm pressure controller (DPC), as well as the change in the sample volume. The last being a function of the sample surface displacement. Equations 3.22 and 3.23 provided the formulation for calculating the amount of gas produced.

$$\Delta V_{gas} = \Delta V_{BPC} + \Delta V_{DPC} + \Delta V_{sample} \quad (3.22)$$

With:

$$\Delta V_{sample} = A_{\phi} \cdot \Delta H \quad (3.23)$$

The air content A and saturation S_r was computed using Equations 3.24 and 3.25, with both porosity n and sample volume V_{sample} being functions of the sample height H at any given point in time.

$$S_r = 1 - \frac{A}{n} \quad (3.24)$$

With:

$$A = \frac{V_{gas}}{V_{sample}} \quad (3.25)$$

One must account for the gas accumulated in the gas trap. The volume of gas in the gas trap was not continuously monitored. The first signs of expelled gas were manually noted and accounted

for by normalising the amount of gas determined through Equation 3.22, with the volume of gas in the gas trap at the end of the reaction phase. The normalised saturation S_r was determined through Equation 3.24 with air content A replaced with Equation 3.26, accounting for the vented gas fraction.

$$A_{actual} = \frac{V_{gas} - V_{gastrap}}{V_{gas}} \cdot A \quad (3.26)$$

3.5.6 Loading phase

Drained loading was applied to fully saturated control samples and desaturated treated samples. The drainage valve to the back-pressure controller was opened while the diaphragm pressure was increased, taking diaphragm calibration into account.

Pressure was transferred to the soil skeleton while pore pressure, pressure controller volumes and sample displacement changes were monitored. Due to a relatively high permeability in the silty sand samples, pore pressure stabilisation towards the back-pressure occurred relatively quickly compared to that in the sandy silt samples.

Continuation to the following pressure increment occurred after a negligible controller volume change ($< 10\mu l$ in 60 consecutive seconds) was recorded. Pore pressure had dissipated and again equalised to the back-pressure and all pressure sensors record the controlled pressure conditions.

The standard (BS 1377-6) specifies that a constant pressure increment ratio should be maintained (i.e. 100, 200, 400, 800 kPa for consolidation tests, an increment ratio of 1) and that no less than four steps should be conducted to plot the $e - \log \sigma'$ curve over a range. These steps continued out of the diaphragm calibration range, thus the incremental steps were carried out to 500 kPa only as indicated in Table 3.4.

This corresponded to a stress increment ratio of $\frac{2}{3}$ (50%/step). Once the maximum pressure was reached and the pore pressure and volume change stabilised, unloading was initiated. The standard advised a minimum of two unloading steps (half the number of loading steps) with a constant unloading stress ratio. A ratio of $\frac{2}{3}$ was chosen for convenience.

The decremental loading steps, as in Table 3.5, were applied when the volume change was stable and no change in pore pressure was observed, after the final incremental step. The next decremental loading step was initiated as soon as no change in volume and pore pressure were observed. Similar to the conditions for the incremental steps.

Table 3.4: Hydraulic cell incremental loading regime

Step	Total pressure [kPa]	Diaphragm pressure [kPa]	Back pressure [kPa]	Effective pressure [kPa]
-	100	113	50	50
1	150	167	50	100
2	225	246	50	175
3	338	363	50	288
4	500	528	50	450

Table 3.5: Hydraulic cell unloading regime

Step	Total pressure [kPa]	Diaphragm pressure [kPa]	Back pressure [kPa]	Effective pressure [kPa]
-	500	528	50	450
1	333	352	50	283
2	111	124	50	61
3	55	61	50	5
4	P_{d0}	10	0	P_{d0}

3.5.7 Dismantling of test

The back- and diaphragm pressures were opened to the atmosphere and the cell cover removed. The porous stone and excess water from the sample surface was removed and the final dimensions were accurately determined to the nearest 0.1 mm. Representative samples (two or more points) were taken to determine the final moisture content.

A sample of the pore fluid was taken for chemical analysis. The pore fluid was extracted from the sample by liquefying the soil removed from the cell on a vibrating table. Pore fluid was effectively separated from the soil and analysed for post pH, nitrate, nitrite and calcium content with the relevant LCK tests (Hach Lange-Germany).

3.5.8 Water content during loading phase

The use of the volume balance as in section 3.5.5 did not hold for the determination of the water content during loading, as the excess volume change recorded in the back-pressure controller was influenced by the excess water displaced from around the diaphragm. An additional set of assumptions needed to be introduced to quantify the water content in the sample during loading:

- During the control tests, the sample was assumed to remain fully saturated
- It was assumed that only liquid was displaced from between the diaphragm and the cell wall into the back-pressure line
- All gas that was displaced from the sample was assumed to accumulate in the gas trap
- The soil particles behaved stiff, thus the sample volume change was attributed to the sample pore volume change
- The displaced liquid fraction is assumed to have the same density as that of water ($\rho_w = 1.0$)

Implementing the above assumptions, Equation 3.27 was formulated for the liquid displaced from between the diaphragm and cell wall ($\Delta V_{diaph_{disp}}$). A volume balance was devised in Equation 3.28, stating that the volume displaced into the back-pressure controller (BPC) was the sum of the pore fluid displaced from the sample (ΔV_v) and the liquid displaced from around the diaphragm. By combining Equations 3.27 and 3.28, Equation 3.29 was formulated to describe the change in the sample pore fluid volume change ($V_{p_{fv}}$) during loading. However, as the sample is not fully saturated when gas was produced, the pore volume change was the sum of gas volume change (V_g) and the water volume change (V_w) within the sample pore space. The volume of gas in the gas trap was not continuously monitored. It was accounted for by normalising the recorded displaced fluid and taking the accumulated gas in the gas trap into account (Equation 3.31). The volume of liquid expelled from the sample at any point during the loading stage could subsequently be determined.

$$V_{diaph_{disp}} = \Delta V_{DPC} - \Delta H \cdot A_\phi \quad (3.27)$$

$$\Delta V_{BPC} = \Delta V_{pfv} + \Delta V_{diaph_{disp}} \quad (3.28)$$

$$\Delta V_{pfv} = \Delta V_{BPC} - (\Delta V_{DPC} - \Delta H \cdot A_{\phi}) \quad (3.29)$$

$$\Delta V_{pfv} = \Delta V_g + \Delta V_w \quad (3.30)$$

$$\Delta V_{w_{normalised}} = \frac{\Delta V_{pfv} - V_{gastrap_{end}}}{\Delta V_{pfv}} \cdot V_{pfv} \quad (3.31)$$

Since the expelled liquid volume at any point during loading was known, the saturation throughout loading could be calculated through Equation 3.32. The pore fluid volume at the end of reaction phase (product of the saturation and volume of voids at the end of reaction phase) acted as initial point. The expelled pore fluid volume at any given point (ΔV_{pfv}) was added, and the sum divided by the volume of voids (V_v) at a certain state.

$$S_{r;l} = \frac{S_{r;eorf} \cdot V_{v;eorf} + V_{pfv}}{V_v} \quad (3.32)$$

With:

$$V_v = n \cdot V_{sample} \quad (3.33)$$

To plot the loading-unloading path on a dry density-water content plane, the water content w was calculated through Equation 3.34. The density was computed with the help of Equation 3.35 and the dry density calculated through Equation 3.4.

$$w = \frac{S_r \cdot e}{G_s} \quad (3.34)$$

$$\rho = \frac{G_s \cdot (1 + w)}{1 + e} \cdot \rho_w \quad (3.35)$$

3.5.9 Compaction energy

The work of compaction was determined through integration of the force-displacement curve to obtain the energy absorbed by the sample which resulted in the higher density. The method was followed by Hafez et al. (2010). The applied force was obtained from the product of the acting total stress (σ) and the sample cross-section area (A_{ϕ}). The total stress is calculated as the product of the diaphragm calibration factor (μ) and the applied diaphragm pressure (σ_{DP}) as per Equation 3.37. The total stress is also defined as the sum of the stress on the soil skeleton (effective stress - σ') and the pore pressure (u) (Equation 3.38). Work, as calculated in Equation 3.39, is the integral of the force (Equation 3.36) with respect to the axial displacement (s_a). The work was divided by the sample volume at in-situ conditions during unloading to obtain the work per unit volume (Equation 3.40). This corresponds to the unit of energy input in a Proctor compaction test. The Rowe cell set-up is a stress controlled test. The necessary measurements to determine the rate of strain required, as per Houslyby's (1997) specification for the power input to an unsaturated soil, is not possible.

$$F = \sigma \cdot A_{\phi} \quad (3.36)$$

$$\sigma = \mu \cdot \sigma_{DP} \quad (3.37)$$

$$\sigma = \sigma' + u \quad (3.38)$$

$$W = \int F \cdot ds_a = [N \cdot m] = [J] \quad (3.39)$$

$$\frac{W}{V} = \left[\frac{J}{m^3} \right] \quad (3.40)$$

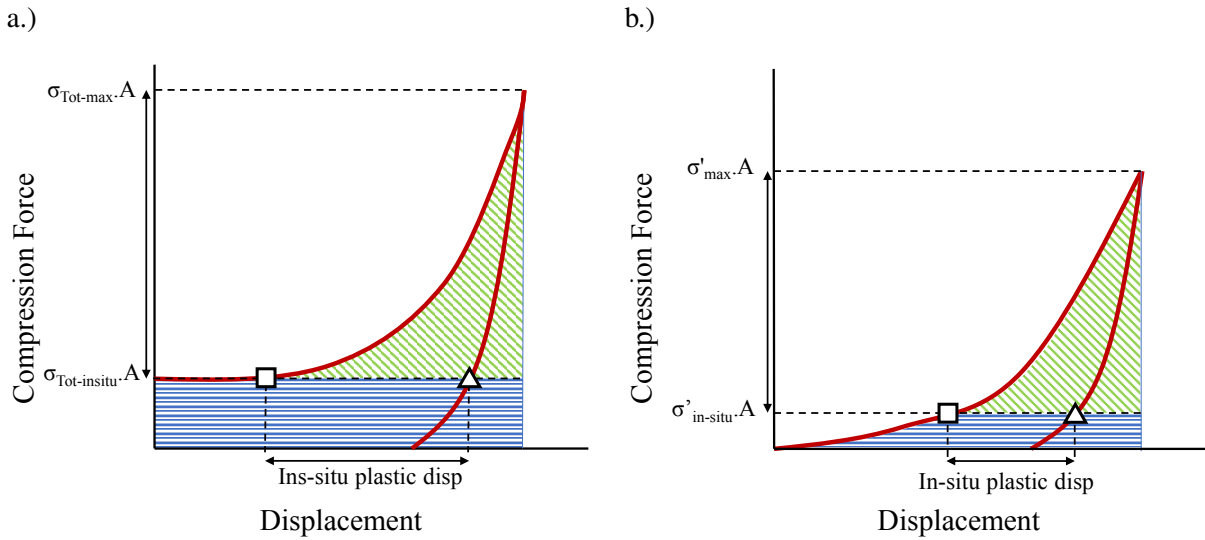


Figure 3.11: Analysis of work input for a.) undrained loading and b.) drained loading. The force-displacement plot (solid red line) is indicated. For a.) the compression force is calculated from the total stress (σ_{tot}) and for b.) the compression force is calculated from the effective stress (σ'). The horizontally hatched blue area indicates the total work absorbed by the sample to bring it to in-situ conditions. The diagonally hatched green area signify the total energy provided during incremental loading. It indicates the total work required to increase the sample from its initial in-situ condition (\square) to the higher residual displacement after compaction (\triangle).

Figure 3.11 depicts the calculation of work input W . If pore pressure accumulates during loading, undrained behaviour is used to calculate the compression force F . If the specimen is sufficiently permeable to allow no pore pressure accumulation, the drained loading case would be considered (b.). Only the incremental loading responsible for additional displacement is used in work input calculations. Relative density increase and strain increase is evaluated from the initial in-situ condition (\square) to the at in-situ condition after the loading regime (\triangle). The plastic deformation due to the incremental

Chapter 4

Results and Discussion

4.1 Dry density - water content curves

The standard Proctor curves are compared to the curves from Figure 2.11 to give an indication of the dry density - water content relationship of similar soils in Figure 4.1.

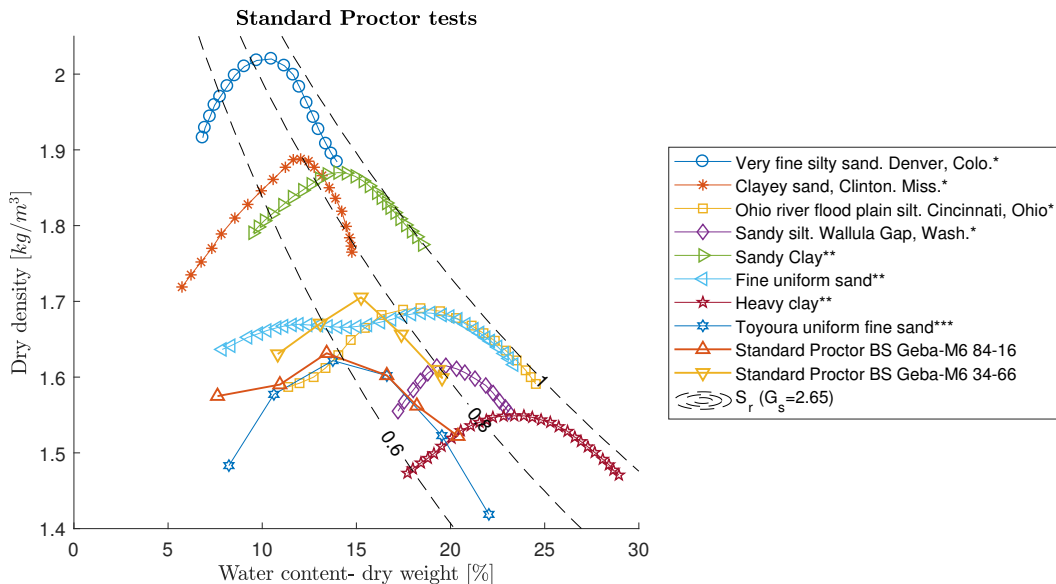


Figure 4.1: Dry density - water content Standard Proctor (light 2.5 kg hammer) test results for Geba-M6 specimens compared to various types of soils from literature. The saturation contours are indicated for $G_s = 2.65$.

*From Terzaghi et al. (1996)

**From Head (2006)

***From Gallage et al. (2016)

The standard Proctor on the Geba-M6 84-16 silty sand has a similar form to that of Ohio river flood plain silt, albeit a maximum dry density similar to that of sandy silt. The optimum water content is lower and located at a lower saturation. As the majority of the material consists of uniformly graded fine sand, a similar curve to Fine uniform sand (Head, 2006) is expected. A similar sensitivity to water content ('spread') is observed. It is possible that the fines fraction due to the added silt accentuates the peak and that a second peak at a lower water content is not measured in this range. The relatively low density is attributed to the lattice structure of a uniform material not being able to fill all the voids.

The sand fraction particles are described as rounded/slightly angular. The voids between particles in a cubic or tetrahedral structure are at a maximum when the soil is very uniformly graded, as is the case. The silt fraction is not high enough to arrange itself between the sand particles and occupy the entirety of the voids.

This is the reason for the higher dry densities achieved with a larger fines content in the Geba-M6 34-66 mixture. The material has a sensitivity similar to that of Sandy Clay (Head, 2006), with maximum dry densities alike Fine uniform sand and Ohio river flood plain silt. A significant difference remains between the maximum dry density achieved for the Very Fine Silty Sand (Denver Colo.) and both reconstituted soils.

The dry density peaks for the Geba-M6 soils are located at significantly lower saturation levels for the indicated specific gravity ($G_s = 2.65$). Higher specific gravities for the curves from literature does not make a substantial difference ($G_s = 2.67$ for the Terzaghi et al. (1996) tests).

4.2 Hydraulic Cell processed results

Three substrate treated tests and three untreated test with similar placement densities corresponding to that of the treated tests, were conducted. Sample Bac1 is conducted on the material with 18% fines with no pretreatment to increase the initial pH. Sample Bac2 is carried out on the same material, but underwent a 10 mM phosphate buffer pretreatment to bring the initial pH closer to neutral. Sample Bac3 is performed on the material with 61% fines. Only the Geba fine sand fraction was treated with a 10 mM phosphate buffer prior to testing.

The properties for the various hydraulic cell samples are indicated in Tables 4.1 and 4.2. The relative density (RD) for each test at different stages during the tests are calculated and displayed together with the compression index (C_c), expansion index (C_c) and compression ratio (CR). RD_{ini} is evaluated at the end of the saturation phase (in-situ effective stress), $RD_{max-load}$ at the the maximum overburden pressure before initiating unloading and RD_{end} is defined as the relative density at in-situ effective stress after unloading. The work per unit volume (W/V) is calculated as per Equation 3.40 with the volume parameter taken as the sample volume when in-situ conditions are reached during unloading (V_{unload}). Based on these parameters, the various tests are compared and contrasted.

Table 4.1: Properties for the range of Hydraulic cell samples (1/2)

Sample	Material (Geba:M6)	M_s [kg]	Vol_{ini} [L]	Vol_{end} [L]	RD_{ini} [-]	$RD_{max-load}$ [-]	RD_{end} [-]
Control 1	84:16	1.3043	0.8249	0.8038	0.7640	0.8022	0.7918
Control 2	84:16	1.3637	0.8749	0.8577	0.7178	0.7688	0.7568
Control 3	34:66	1.2883	0.7453	0.7125	0.9561	0.9814	0.9715
Bac 1	84:16	1.3030	0.8173	0.8038	0.7899	0.8263	0.8157
Bac 2	84:16	1.2810	0.8299	0.8087	0.7022	0.7488	0.7369
Bac 3	34:66	1.2883	0.7417	0.7273	0.9662	0.9941	0.9881

A significantly lower placement density is achieved with the uniform silty sand (Control 1, Control 2, Bac 1, Bac 2) compared to the sandy silt (Control 3, Bac 3). One suggestion for this occurrence is that residual suction does not fully dissipate between being removed from the vacuum desiccator and being placed in 200 ml of solute. The material does not separate properly in the 1.1 cm pluviation height and cause additional densification on impact.

It is evident from the relative density and material that test Control 1 serves as the untreated counterpart for test Bac 1, Control 2 for Bac 2 and Control 3 for Bac 3.

The initial water content w_{ini} may be over estimated due to the separation of the liquid from the soil skeleton due to installation effects. This would result in an overestimation of the calculated

Table 4.2: Properties for the range of Hydraulic cell samples (2/2)

Sample	w_{ini} (gravimetric)	w_{end}	w_{end} (gravimetric)	V_{unload} [L]	W/Vol [kJ/m ³]	C_c [-]	C_e [-]	CR [-]
Control 1	0.2551	0.2470	0.2101	0.8128	1.9868	0.0081	0.0026	0.0048
Control 2	0.2642	0.2531	0.2300	0.8586	2.4057	0.0111	0.0025	0.0065
Control 3	0.2012	0.1942	0.1675	0.7342	2.6724	0.0108	0.0042	0.0070
Bac 1	0.2499	0.2049	0.2101	0.8063	1.7400	0.0085	0.0026	0.0051
Bac 2	0.2705	0.2143	0.2371	0.8113	2.1329	0.0106	0.0024	0.0062
Bac 3	0.1984	0.1692	0.2056	0.7267	3.1778	0.0117	0.0020	0.0077

water content. It is observed that in the untreated samples, the calculated final water content from the saturation calculation (Section 3.5.8) is overestimated when compared to the gravimetric water content measurements and the treated samples' water content is under estimated. A reason for this can be as a result of normalising the expelled water to the gas trap. A suggested solution to obtain more accurate water content estimations during the test is to reverse the formulation and back calculate from the water content determined gravimetrically at the end of the test.

In Table 4.3, results are provided on the bacterially treated samples. Information is given on the soil fraction which has been treated with a phosphate buffer, the reaction time in which the bacteria was left to consume the solute, measurements for pre and post nitrate, nitrite and calcium concentrations, together with pH measurements. The treatment concentration is indicated and change as a result of being combined with a 100 mL/L bacteria inoculum produced from the incubation tests. Test Bac2 shows a significant reduction in reaction time when compared with test Bac1 as

Table 4.3: Measurements for treated specimens. All treatment regimes have a Ca-Ac-N composition of 36.5-39.9-33.2 mM

Sample	bac1	bac2	bac3
Fraction pH treated	none	Geba-M6	Geba
Reaction time [days]	14.2	10.0	6.9
$NO_3 - N_{pre}$ [mM]	32.8	32.3	31.7
$NO_3 - N_{post}$ [mM]	1.4	0.1	0.6
$NO_2 - N_{pre}$ [mM]	0.0	0.1	0.1
$NO_2 - N_{post}$ [mM]	0.4	0.0	0.1
$(NO_3 + NO_2) - N_{pre}$ [mM]	32.8	32.4	31.8
$(NO_3 + NO_2) - N_{post}$ [mM]	1.8	0.2	0.8
Ca_{pre}^{2+} [mM]	31.5	34.3	39.4
Ca_{post}^{2+} [mM]	13.1	11.4	13.1
pH_{pre}	6.4	5.3	6.9
pH_{post}	7.6	7.9	7.8

a result of the pH buffer treatment of the soil. The pH buffering also result in less intermediate nitrite accumulating in the sample. The reaction of sample Bac1 has been stopped prematurely as not all nitrate has been consumed. The cause of the low reaction time for the Bac3 test is not entirely clear. The increased fraction of fines may have resulted in more surface area for the bacteria to attach itself to. The nitrate is also virtually entirely reduced. The low reaction time has to be observed in conjunction with the relatively low gas volume measured during the reaction stage. Even though the initial concentrations of calcium is constant across all the tests (36.5 mM), measurements indicate a significant variation. The residual calcium is in the same range for all three tests, despite the fact that there is a difference in the material, reaction time and pH buffer treatments of the three tests. For test

4.2. HYDRAULIC CELL PROCESSED RESULTS

Bac3, only the Geba fine sand fraction is treated with phosphate buffer to prohibit the loss of fines that could occur due to decanting of the buffer liquid and demi water rinsing process. The initial pH of sample Bac2 is considerably lower than expected despite phosphate buffer treatment. Based on the increase in reaction time and reduction in intermediate nitrite, pH buffering is successful and the cause of the lower initial pH is unknown. From the pH measurements after disassembly, it is evident that denitrification is responsible for the increased pH. In the absence of calcium precipitation, the pH at the end will be significantly higher.

The properties of the incubated test specimen are presented in Table 4.4 with additional interpretation of the gas volume displayed in Table 4.5. The gas production rate \dot{V}_g is determined from the slope of the gas production over time plot in Figures D.4, D.5 and D.6 (c. right). $\dot{V}_{g_{max}}$ corresponds to the maximum gas production rate. A significant difference in the maximum rate of

Table 4.4: Gas measurements for treated specimens. All treatment regimes had a Ca-Ac-N composition of 36.5-39.9-33.2 mM

Sample	bac1	bac2	bac3
$V_{L_{pre}}$ [mL]	331	355	317.5
V_g for NO_3 entirely consumed [mL]	88.6	95.0	85.0
V_g for $(NO_3 + NO_2) - N$ consumed [mL]	82.8	92.0	79.3
V_g measured [mL]	77.1	76.3	56.5
Gas Trap [mL]	20.0	18.0	25.0
Gas in sample [mL]	57.1	58.3	31.5
S_r before loading [%]	82.2	82.6	87.4
M_s [kg]	1.303	1.281	1.288
$w_{end_{gravimetric}}$ [%]	21.01	23.71	20.56
$V_{L_{post}}$ [mL]	273.7	303.7	264.9
$\dot{V}_{g_{max}}$ [mL/day]	14.0	21.5	25.4

gas production is observed among the three treated tests. The biggest difference is noted between the pH buffered and unbuffered specimens with a slightly increased maximum rate when a larger fraction of fines is present.

Table 4.5: Gas measurements versus prediction based on concentrations of treated specimens. All treatment regimes have a Ca-Ac-N composition of 36.5-39.9-33.2 mM

Sample	Bac1	Bac2	Bac3
V_g actual vs predicted NO_3 entirely consumed [%]	87	80	66
V_g actual vs $(NO_3 + NO_2) - N$ consumed [%]	93	83	71
V_g in Gas Trap [%]	26	24	44

If the measured gas production is compared to the predicted gas production according to metabolic stoichiometry (Equation 2.3 - deemed conservative), between 80% and 87% of the original predicted amount is recorded if nitrate is fully converted to nitrogen gas. This fraction drops to 66% in the finer material. If a nitrogen balance is conducted on the conversion from initial measured nitrate and nitrite fully to nitrogen gas, the converted fraction gives a better indication of what is possible within this time frame, between 83 and 93 % of the nitrogen compounds are converted for the coarse material and 71% for the finer material. This fraction is expected to increase with longer periods of reaction time. An interesting phenomena to note is that a shorter reaction period until gas production flats out and a larger maximum gas production rate is coupled with a lower measured gas volume compared to the nitrogen produced according to the nitrogen balance on nitrate and nitrite consumed. This could simply be due to the longer reaction period allowed in Bac1, resulting in more nitrate consumed

Table 4.6: Nitrogen balance for the treated Rowe cell tests

	Bac1	Bac2	Bac3
Nitrate initial pore fluid [mmol $NO_3 - N$]	10.85	11.47	10.07
Nitrite initial pore fluid [mmol $NO_2 - N$]	0.01	0.02	0.02
Nitrate end pore fluid [mmol $NO_3 - N$]	(0.37)	(0.05)	(0.04)
Nitrite end pore fluid [mmol $NO_2 - N$]	(0.12)	(0.01)	(0.01)
Dissolved N_2 gas [mmol $N_2 - N$]	(0.27)	(0.29)	(0.26)
N_2 gas end [mmol $N_2 - N$]	(9.58)	(9.48)	(7.02)
Supernatant [mmol N]	n.d.	0	n.d.
N-gap [mmol]	0.54	1.66	2.76
N-gap [%]	5%	14%	27%

to form gas. The fraction of produced gas ending up in the gas trap is almost double for the finer material. With a much higher placement relative density, the gas is thought to form near the surface of the sample from where it can easily escape. The gas trapped in the lead between the surface of the sample and the gas trap is unaccounted for, which may cause an overestimation of the gas inside the sample.

Table D.2 represents a nitrogen balance conducted on the treated samples. A balance is also conducted on samples Bac1 and Bac3, even though the volume of overlying fluid (supernatant) could not be determined accurately.

The 2 mmol shortcoming may be due to measurement and dilution. Similar deficiency in the nitrogen balance was obtained in Pham's (2017) work.

The above trends are represented in plots for the nitrate, nitrite, calcium and the calculated concentration of nitrogen gas in Figure 4.2, together with the pH of the pore fluid before and after test execution.

Results shown in Figures 4.3, 4.4 and 4.5 present the Force-displacement plots, the sample saturation vs. time plots, and the dry density-water content plots in the first-, second- and third column, respectively.

From the force displacement graphs it is evident that the majority of the settlement occur at low effective stresses, prior to the set *in-situ* condition of 50 kPa effective stress is reached. The force displacement curve can be divided into an elastic and plastic work sections. Elastic energy is recovered during the expansion of the sample during unloading. A lasting effect is nevertheless maintained to result in a denser structure after loading. The total work input to achieve this higher density is the sum of the elastic a plastic work, as the energy is not recovered by the compaction process. *In-situ* stress levels without surcharge corresponds to 0.9 kN compression force. This needs to be taken into account when evaluating compaction.

The mass balance to calculate the sample saturation throughout the reaction phase is implemented in combination with the volume recorded in the gas trap to estimate the saturation at the end of the reaction phase. If the initial water content is overestimated as mentioned earlier, so too is the saturation. It has to be considered that gas present in the back pressure lead between the sample and the gas trap is not taken into account and will result in an overestimation of the calculated saturation, which counters the higher water content measured gravimetrically in the treated samples , Bac1, Bac2 and Bac3, compared to the calculated water content.

The dry density - water content curves for the control tests, the water content is calculated based on the assumption that the sample remains fully saturated. Based on the lower gravimetric water content measurements, this assumption is to be questioned. No decrease in dry density is measured during the reaction phase. In fact, a slight increase is noted in the samples that were tested for a prolonged time due to consolidation. This leads to the conclusion that the soil body does not

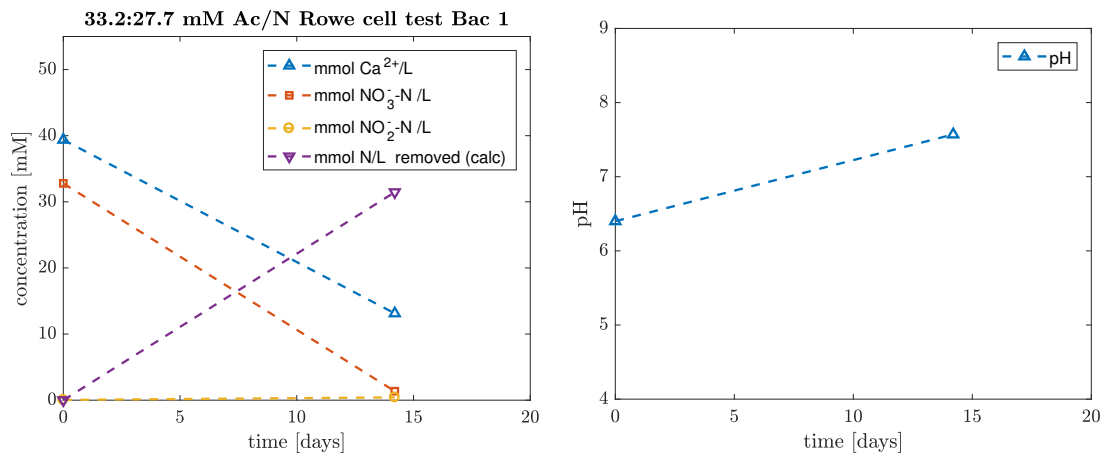
4.2. HYDRAULIC CELL PROCESSED RESULTS

expand when gas is produced in-situ. The unusual path during loading and unloading is attributed to the relatively large time-step between measurements (30 seconds) and dissipation of generated pore pressures.

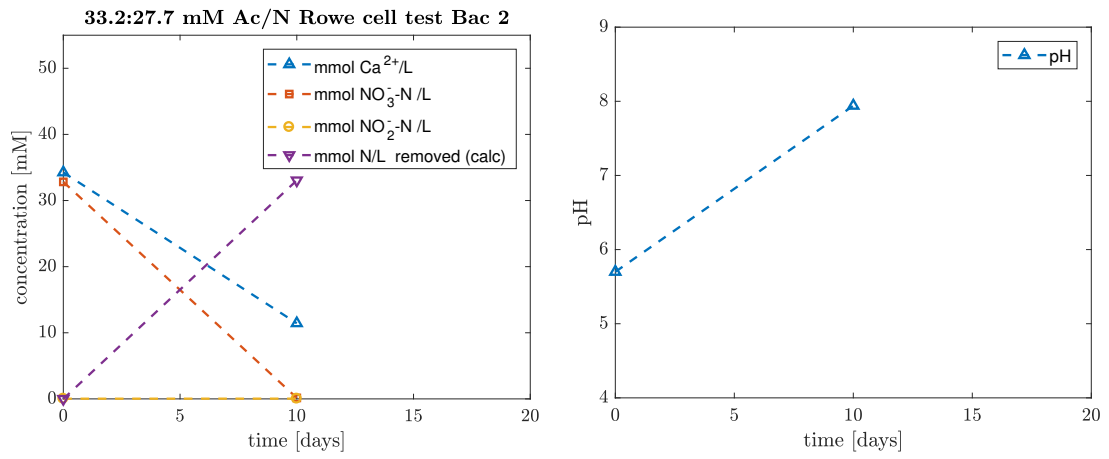
The results of the dry density - water content curves for all three comparisons do not deliver conclusive results to indicate that less energy is required to compact a treated specimen as opposed to the control specimen. It can be observed that the placement density plays a substantial part in the maximum density that can be achieved during static compaction in the Rowe cell.

The combined results for the Proctor tests and hydraulic cell test can be observed for the silty sand and sandy silt in Figures 4.6 and 4.7, respectively. It is evident that the target desaturation corresponding to the optimal water content is not reached. In the GebaM6 34-66 mixture the high placement density, comparable to densities achieved in a modified Proctor, is clearly noticed.

a.)



b.)



c.)

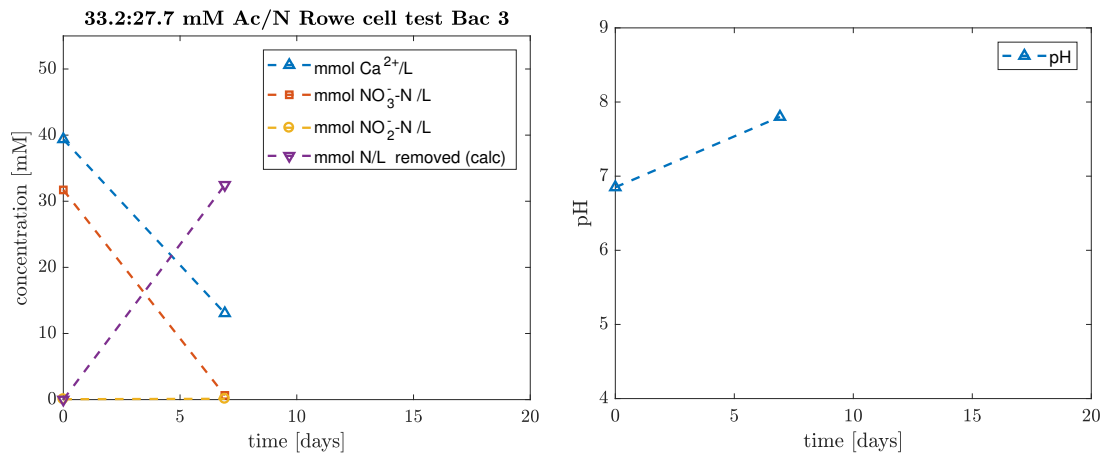


Figure 4.2: Comparison of changes in chemical composition of treated Rowe cell tests over time with constant Ac/N = 1.2 and 100 mL/L bacteria inoculum: a.) bac1; b.) bac2; c.) bac3

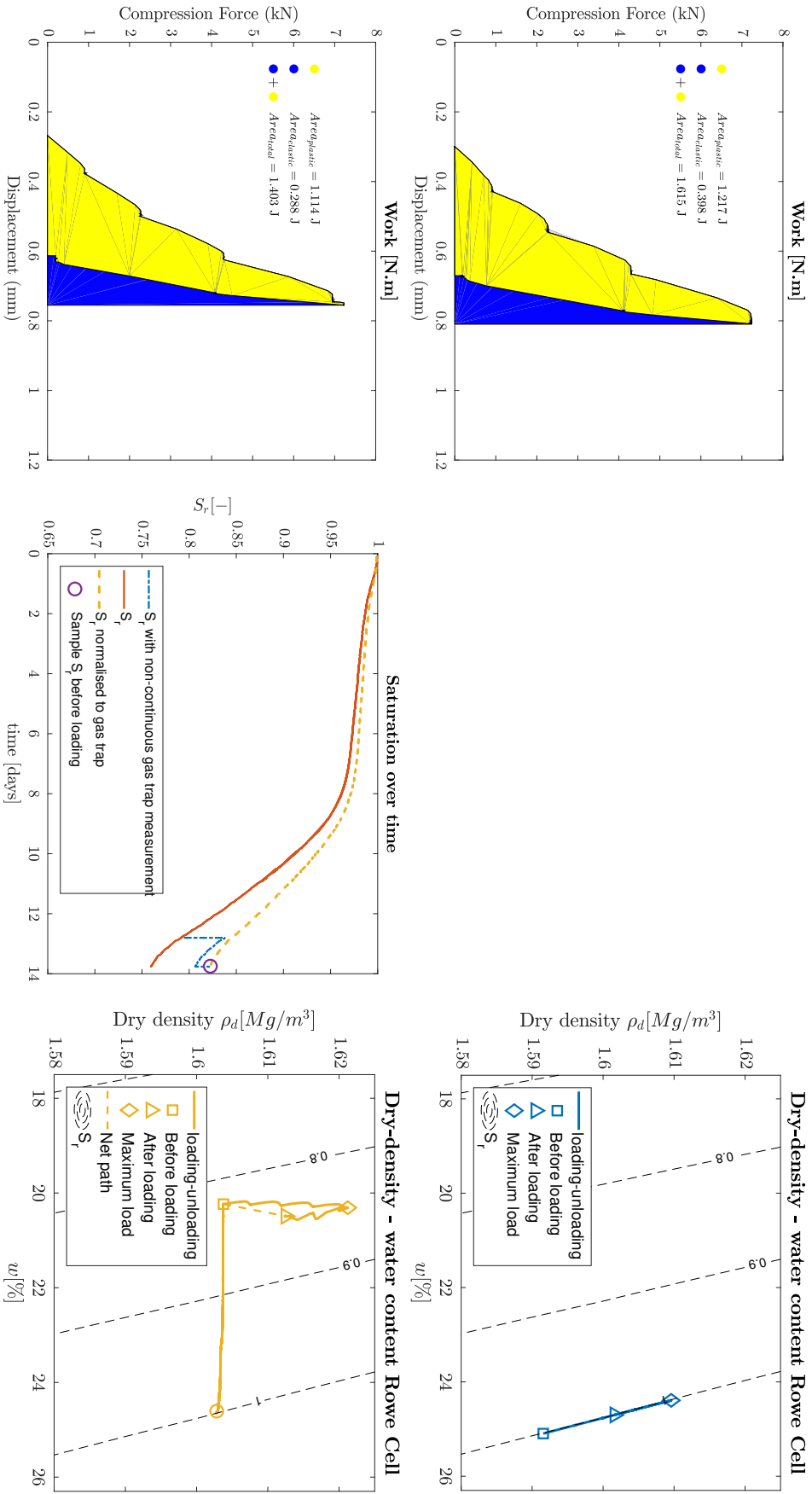


Figure 4.3: Results for Rowe cell tests. Top row: Control I - zero gas production, Bottom row: Bacl Treated. The plastic work input is indicated in yellow and the elastic work, indicated in blue. The total work (sum of elastic and plastic work) is responsible for the higher density after loading

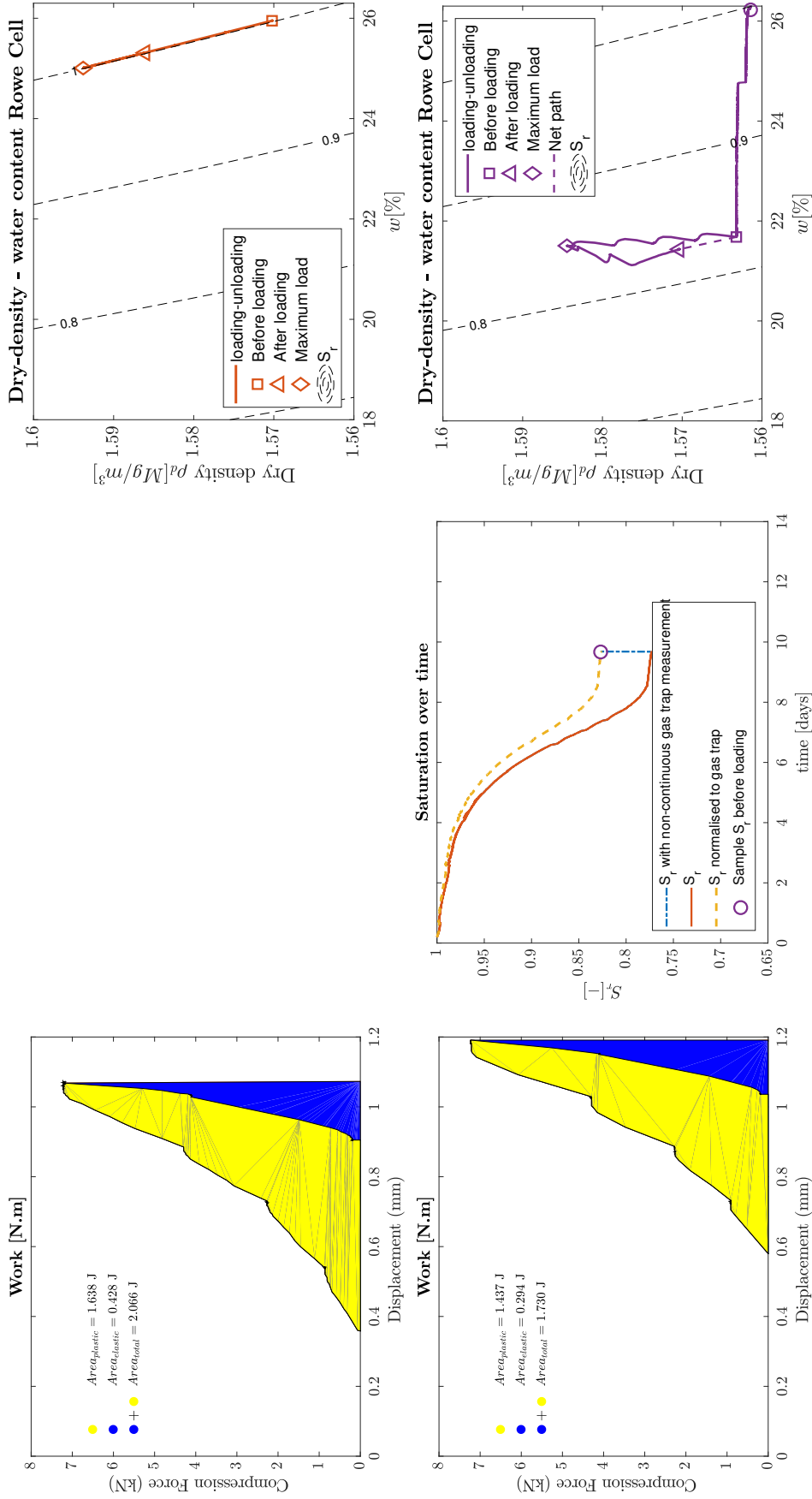


Figure 4.4: Results for Rowe cell tests. Top row: Control2- zero gas production, Bottom row: Bac2 Treated and pH buffered. The plastic work input is indicated in yellow and the elastic work, indicated in blue. The total work (sum of elastic and plastic work) is responsible for the higher density after loading

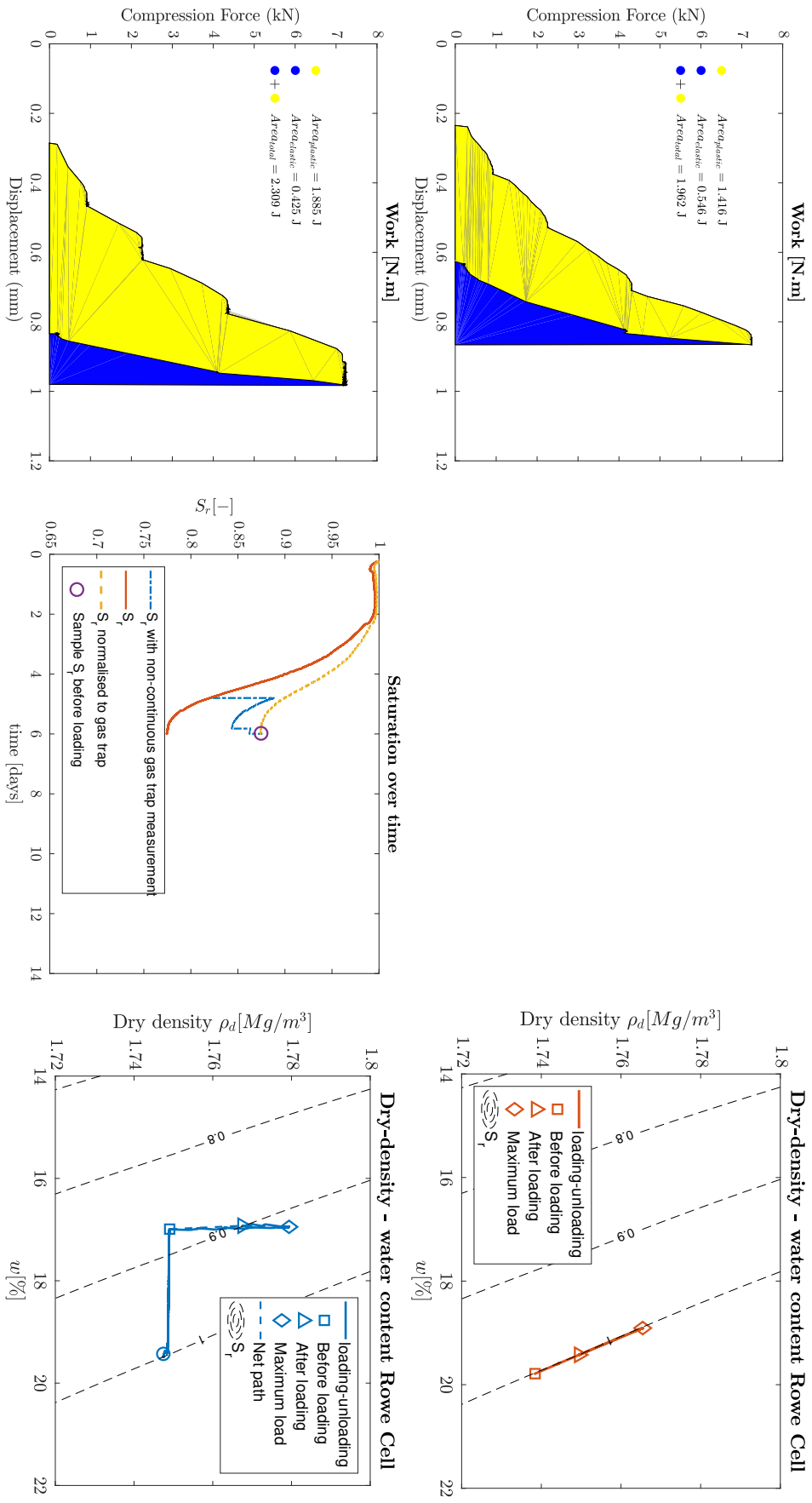


Figure 4.5: Results for Rowe cell tests. Top row: Control3- zero gas production, Bottom row: Bac3 Treated and pH buffered. The plastic work input is indicated in yellow and the elastic work, indicated in blue. The total work (sum of elastic and plastic work) is responsible for the higher density after loading

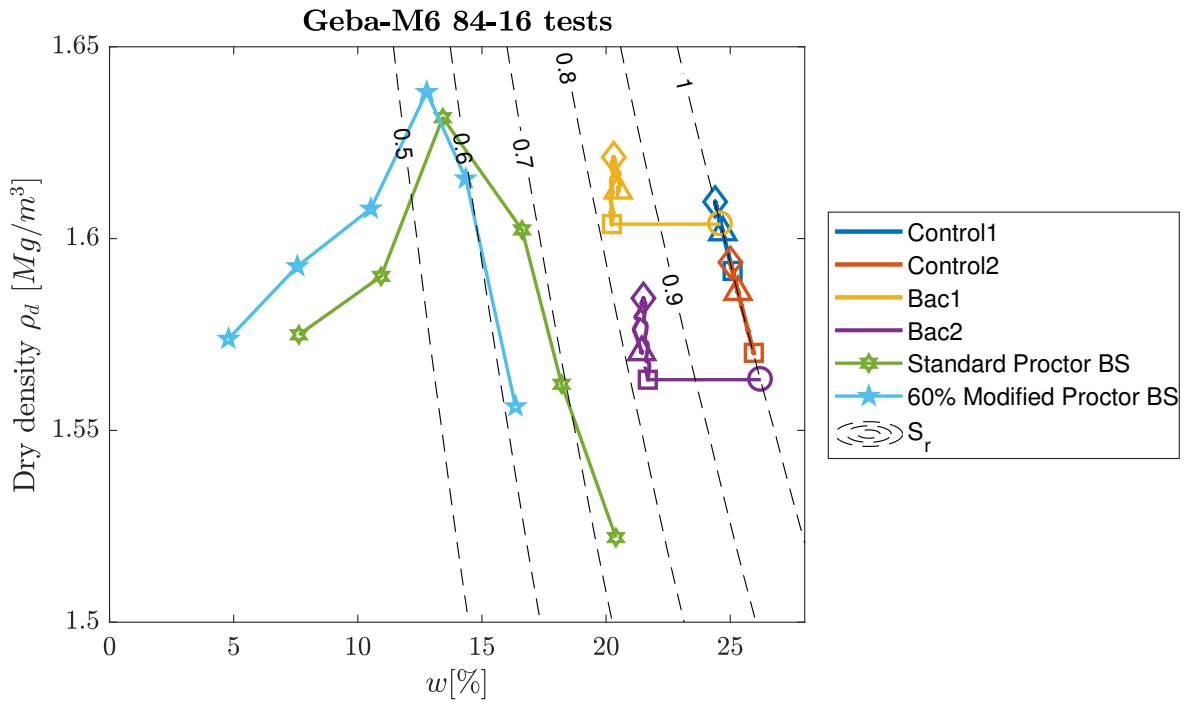


Figure 4.6: Dry density-water content of Geba M6 84-16 Hydraulic cell and Proctor tests. The sequence for the hydraulic cell test is as follows: \circ sample at the start of reaction phase; $\circ - \square$ gas desaturation phase; \square state of sample at the start of loading phase; $\square - \diamond$ loading; \diamond maximum dry density reached; $\diamond - \triangle$ unloading; \triangle state of sample after unloading

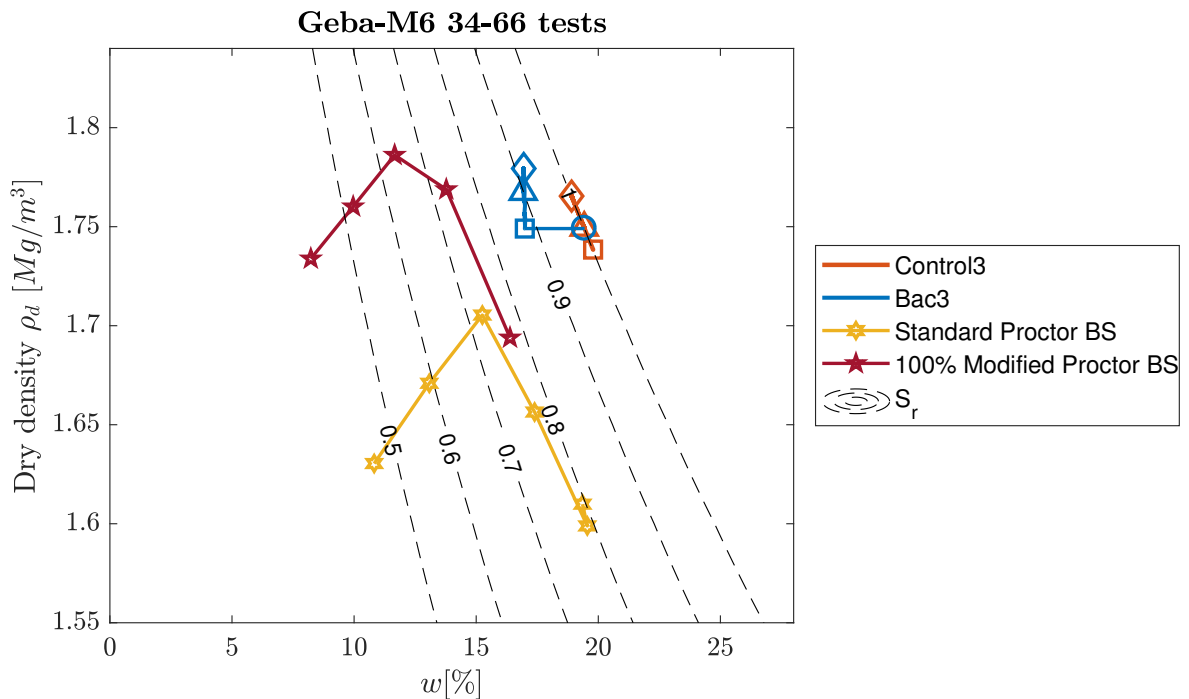


Figure 4.7: Dry density-water content of Geba M6 34-66 Hydraulic cell and Proctor tests. The sequence for the hydraulic cell test is as follows: \circ sample at the start of reaction phase; $\circ - \square$ gas desaturation phase; \square state of sample at the start of loading phase; $\square - \diamond$ loading; \diamond maximum dry density reached; $\diamond - \triangle$ unloading; \triangle state of sample after unloading

4.2.1 Evaluation in terms of work input

In Table 4.7, the Rowe cell work input per unit volume is evaluated in terms of the percentage increase in relative density and axial strain for each sample. The increase in relative density is calculated from RD_{ini} to RD_{end} with the increase in axial strain calculated from the difference between the axial strain of the sample at 50 kPa effective stress just before loading is initiated and at the same effective stress during unloading.

Table 4.7: Evaluation of Rowe cell samples in terms of RD and axial strain increase for the measured amount of work input - smaller is better

Sample	$RD_{increase}$ [%]	$\varepsilon_{a_{increase}}$ [%]	W/V per $RD_{increase}$ [kJ/m ³ per RD increase]	W/V per $\varepsilon_{a_{increase}}$ [kJ/m ³ per ε_a increase]
Control1	2.78	0.81	0.715	2.453
Bac1	2.58	0.76	0.674	2.292
Control2	3.91	1.12	0.616	2.141
Bac2	3.47	0.99	0.614	2.156
Control3	1.54	0.93	1.734	2.874
Bac3	2.19	1.33	1.449	2.389

In terms of W/V per RD increase, a marginal improvement is measured in the treated material as opposed to the untreated counterpart. This is reflected in the W/V per axial strain increase, apart from the Control2-Bac2 specimen comparison where marginally fewer energy is absorbed to compact the untreated sample. The results seem to depend greatly on sample placement density. However, when the RDs from Table 4.10 are compared, it is noted that the treated specimen, apart from the Bac2 specimen, are placed at higher densities compared to the untreated counterpart. The behaviour of the samples are highly non-linear, which entails that care should be taken in extrapolation of the results.

4.3 Discussion

4.3.1 Description of scenario

The Rowe cell is initially suggested as a controlled alternative to compare drained loading to that of the Proctor test. One has to scrutinise the method of loading, as well as the loading conditions. The drainage conditions are thought to be similar, with the Rowe cell set up to drain from the top surface. The type of porous disc employed in the test consist of sintered bronze, a low permeable material suitable for consolidation, but not for drained loading experiments. The porous disk was chosen to prohibit the production of significant amounts of gas inside the porous stone which result in inaccurate sample saturation calculation. In Appendix D, the pore pressure build-up during each loading increment is clearly noticed. The slow dissipation is thought to be as a result of the low permeable porous stone. The effect is exaggerated in the finer material (Control3, Bac3), which has a lower permeability due to an increased fines content.

This is analogues to the situation indicated in Figure 4.8 (left), with a low permeable material covering the targeted soil. The energy delivered to a unit volume, as calculated for both instances in Equation 4.1 in J/m^3 or N/m^2 holds true, but different mechanisms are at work. These mechanisms are conveyed in Figure 4.8. The radial constraint and rigid plate transferring the constant stress to the specimen, which is the case in the hydraulic cell (left), prohibits shearing effects to contribute to compaction. Bulging is common when the load is transferred through the Proctor hammer. As the head of the hammer is smaller than the area of the mould, boundary and constraint effects have a smaller influence, allowing for the sample to contract and air voids to be minimised.

$$\frac{W}{V} \equiv \frac{\int F ds}{Vol} \equiv \frac{M_{proc} g H_{proc} N_{blows}}{Vol} \equiv \int \sigma d\varepsilon = \frac{[N \cdot m]}{[m^3]} \quad (4.1)$$

To obtain a higher density after compaction, the voids must be compressed or removed from the sample. However, only the gas phase is compressible. The shearing effect resulted by the impact of the Proctor hammer assist in the destabilising of the bubbles, creating a flux of gas from the sample. The work input per unit volume for the Standard - and Modified Proctor is $569kJ/m^3$ and $2682kJ/m^3$ respectively. This is orders of magnitude larger than what is achieved in the Rowe cell. The comparison in loading method cannot be made directly.

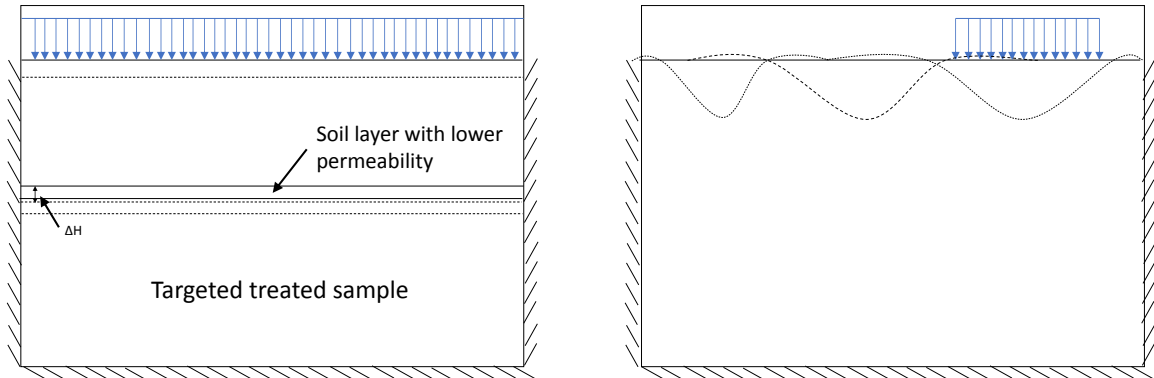


Figure 4.8: [left] Scenario in hydraulic cell, a 1D radially constrained test with a constant stress applied over the entire rigid surface [right] Scenario in Proctor cell, a localised impact allowing for shear to occur

4.3.2 Diaphragm calibration

The calibration data used to calculate the actual force acting across the surface may be influenced by the change of diaphragm characteristics. After several tests it is apparent that blisters formed in the folds of the diaphragm, with a slight increase in diameter recorded. This is thought to not have a influence at operating and loading pressures, as the displacements recorded are relatively small. Jolting and sudden shifting of the diaphragm during the increase of effective stress from zero to the *in-situ* pressures may cause premature compaction.

4.3.3 Gas production assumptions

The mass balance in Equation 3.22 has to be queried: The inclusion of the term for diaphragm pressure controller (DPC) volume change is unusual. When the difference in volume change over time is analysed between sample Ba1 (Figure D.4 c.) and the extended control test Control1 (Figure D.1 c.), it is seen that the volume change in the DPC is mirrored by the back pressure controller (BPC). As no gas is produced during the control test, this term needs to be included in the volume balance to result in zero gas production being calculated. This volume change in the DPC may be due to possible leakage or relaxation of the leads. It should be scrutinised if this fraction of gas due to relaxation could be taken into account for gas produced inside the sample, or merely on the surface or around the diaphragm.

The assumption is made that all gas production occurs homogeneously throughout the sample. In Figure 4.9 it is seen that pockets of gas form between the sample and the porous stone. This gas

may have escaped if a more permeable porous stone is used. The voids visible in the bulged material around the edge (interface flow) could mean that gas surpassed the porous stone and accumulated around the rigid plate and diaphragm, resulting in a further error in calculated sample saturation. This effect may be exacerbated in the finer Geba-M6 34-66 specimen.

The implementation of mixed in place bacterial solution should result in optimal distribution of bacteria and substrate, maximising the probability of homogeneous gas distribution. This cannot be verified in the sealed, pressurised cell.

The validity of a post analysis should be questioned. Due to the pressure relief at disassembly, gas pockets expand and may alter the soil structure further. This leads to aggravated voids visible on the surface. The results of post gravimetric water content measurements may be influenced by this. If this is taken into account, the post water content of the treated samples are further underestimated.



Figure 4.9: Visible gas pockets on surface of a treated Geba-M6 84-16 sample and bulging of the soil around the edge of the cell - after disassembly

4.3.4 Nitrogen Balance

The results of the nitrogen balance in Table 4.6 is depicted in Figure 4.10. It is clearly indicated that the largest fraction of nitrogen is converted into gas, with an insignificant fraction of nitrite at disassembly. It is interesting to note that the shortcoming of nitrogen (N-gap) increases as the reaction time and rate increases. A prolonged reaction time possibly allows for a more stable gas phase. The deficiency is largest in the material with 66% fines content. A possible reason for this is the smaller and more confined pore space. Due to the confinement, the gas bubbles are limited in size. The pressure inside the smaller bubbles are significantly higher than its larger counterparts due to surface tension. Consequently, a higher molar quantity of nitrogen gas can occupy a smaller volume. This may explain the Between 70% and 93% of the consumed nitrate and nitrite is converted to nitrogen gas during the first 14 days after treatment, corresponding to between 66% and 87% of the initial theoretical available nitrate and nitrite.

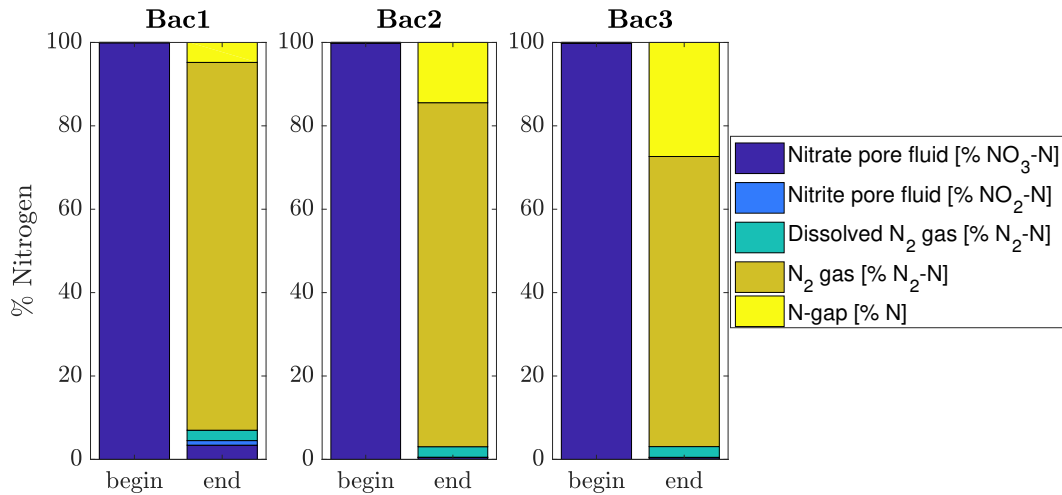


Figure 4.10: Nitrogen balance between the start and end of the treated Rowe cell tests

4.3.5 Diffusion of substrate

Diffusion of substrate to the overlying demi water is not taken into account during the tests. The initially demi water filled porous stone is placed on a inoculated substrate saturated soil sample, which is covered in demi water to reduce the chance of trapped air during instillation. The majority of overlying demi water is expelled during cell cover installation, but may have caused dilution of the substrate on the surface of the sample. Throughout the reaction phase, the sample is in direct contact with demi water in the leads, the gas trap and the back pressure controller. Measurements of nitrate, nitrite and calcium have been conducted and detected significant concentrations in the gas trap water and BPC reservoir. It is inconclusive whether this is due to diffusion. In all likelihood this is due to pore water expelled during loading steps.

4.3.6 $CaCO_3$ precipitation

It is assumed that the concentration of calcium is not enough to cause any significant increase in small strain stiffness due to cementation. This assumption is confirmed for the implemented concentrations. Sampling was done on the specimen after disassembly; three samples were taken in the height per treated specimen, dried and analysed through acid dissolution tests conducted according to NEN-EN-ISO 10693 (2014). The results are presented in Table 4.8. It is evident that less than 0.1% of the specimens consist of $CaCO_3$. The calcium in solution that remains after disassembly is not factored in. No trend exists in the distribution of the calcite in the height of the sample. The finer material of Bac3 contains slightly more calcite. The blank test on the M6-MILLISIL reference material was repeated once and delivered an average calcite content of 0.05% for the two tests. The accuracy of the concentration calcite is questionable as the low calcite content may fall within measurement error. It is thus reasonable to assume that cementation effects can be neglected at low concentration solutions. Multiple treatments at low concentration regimes are required for the precipitate to have an influence on strength, as found by Pham (2017).

The calcium balance is depicted in Figure 4.11, where it is seen that a large fraction of calcium is unaccounted for. The accuracy of the calcium carbonate content tests does not allow for sufficiently accurate measurements. Rounding and averaging of the results create imbalances.

Table 4.8: $CaCO_3$ content for treated tests [g/kg dissolved solids]

Position	Unit	Bac1	Bac2	Bac3
Top	g/kg. d s	0	0	1
Middle	g/kg. d s	0	1	1
Bottom	g/kg. d s	1	0	n.d.
Average	g/kg. d s	0.33	0.33	1

Table 4.9: Ca^{2+} balance for the treated tests

	Bac1	Bac2	Bac3
Calcium initial pore fluid [mmol-Ca]	10.43	12.16	12.50
Calcium end pore fluid [mmol-Ca]	(3.59)	(3.47)	(3.46)
precipitate $CaCO_3$ -Ca [mmol-Ca]	(4.30)	(4.22)	(12.87)
Ca-gap [mmol]	2.54	4.46	-3.83
Ca-gap [%]	24%	37%	-31%

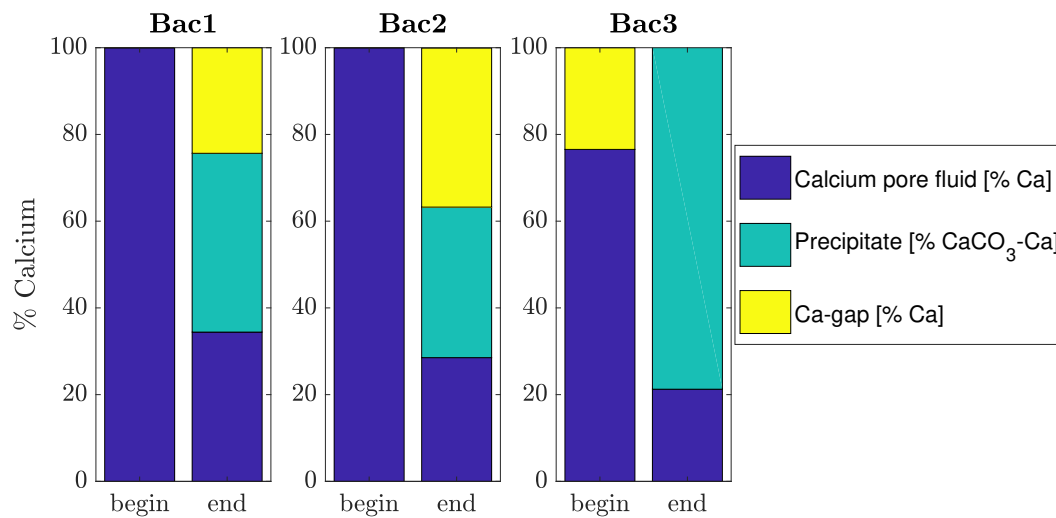


Figure 4.11: Calcium balance between start and end of treated Rowe cell tests

4.3.7 Microbial Desaturation

The process is influenced by substrate concentration, acetate-to-nitrate ratio, temperature, effective stress and total stress, particle size distribution, pH and the presence of oxygen and other substances.

The lag period of 2 to 3 days before significant gas production allows for the bacterial inoculum to be mixed with the substrate at injection. The inoculum can be produced from the enrichment of existing bacteria in an organic rich soil sample. It is also possible to stimulate existing *in-situ* bacteria with substrate injections, albeit at lower gas production rates to account for anabolic bacterial growth.

A lower initial soil pH result in a longer lag period and increased accumulated intermediates. The treatment system, however, has the ability to increase the pH to above 7 which is subsequently limited to pH 8 due to calcite precipitation if calcium is present in the substrate.

Low concentration substrate treatment regimes and an acetate to nitrate ratio of 1.2 are successful at limiting the accumulation of significant concentrations of harmful intermediates.

4.3.8 Initial Relative Density

It is noted that from in Table 4.1 that the initial placement relative density far exceeds that of a fill that one would consider to compact (RDs of $\approx 40\%$ common to compact in practice). Figure 4.12 provides a representation of the envisioned case versus the actual case. The already high relative density at placement may explain why the increase in density is limited.

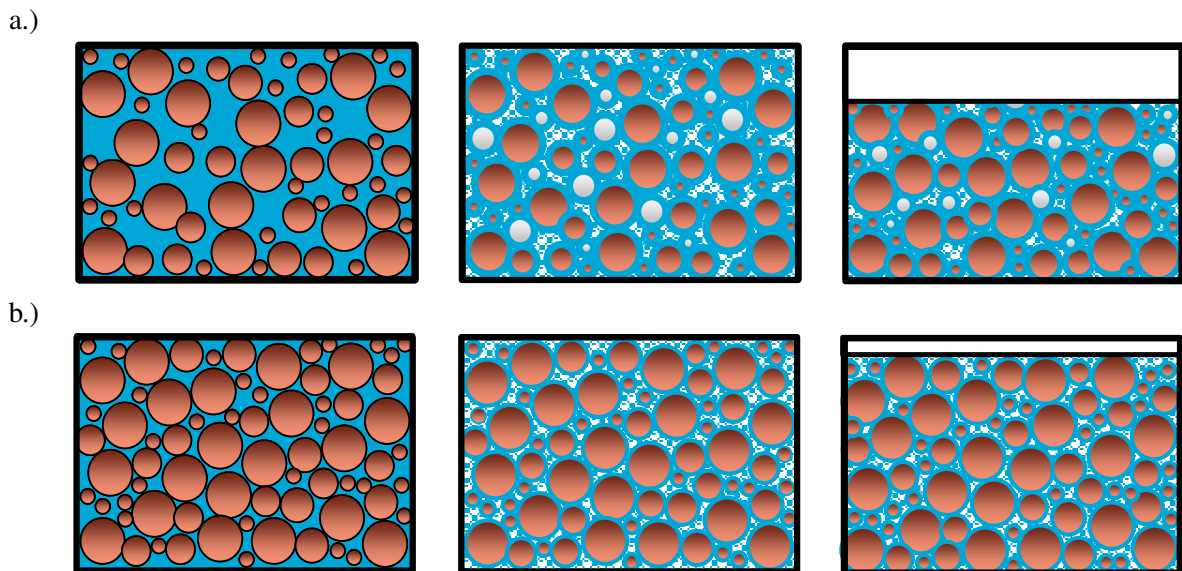


Figure 4.12: Effect of placement density on axial displacement - (a.) Envisioned soil placement condition vs (b.) actual placement condition. The first column represent the fully saturated sample at placement, the gas desaturated soil is represented in the centre column and the compacted sample is envisaged in the rightmost column.

4.3.9 Reduction in work input

Table 4.10 display the results of the Rowe cell tests in Table 4.7 in terms of percentage difference in work per unit volume used per relative density and axial strain increase.

A 5.7% decrease in work per unit volume is measured in the treated sample Bac1. The treated sample Bac3 indicates a 16.4% reduction in energy per unit volume used compared to the untreated counterpart. For both these comparisons, the treated samples had a higher relative density before

4.3. DISCUSSION

Table 4.10: Evaluation of Rowe cell results in terms of initial relative densities prior to loading and percentage difference between treated and untreated samples

Sample	RD_{ini} [%]	% difference W/V per $RD_{increase}$ [%]	% difference W/V per $\epsilon_{d_{increase}}$ [%]
Control1	76.4		
Bac1	79.0	5.7	6.6
Control2	71.8		
Bac2	70.2	0.3	-0.7
Control3	95.6		
Bac3	96.6	16.4	16.9

loading. The percentage decrease in work per unit volume per axial strain is slightly higher. Treated sample Bac2 showed virtually no difference compared to the untreated sample, even though the treated sample has a lower initial relative density. It should be taken into account that the measured displacements are small and may seem overinflated in Table 4.10. Any measurement error will have a large influence on the results. The low number of tests, varying placement densities and mixed outcome do not allow for a definitive conclusion to be drawn.

Even though the saturation corresponding to the optimum water content is not reached, the standard Proctor dry density - water content prescribes that even a small reduction in saturation should lead to an increase in dry density. This may explain the lower energy input per unit volume for the treated specimen.

Chapter 5

Conclusion

During this study into the two-step process of biogenic gas desaturation and subsequent compaction, denitrifying bacteria is successfully enriched and their consumption rates studied. The nutrient concentration and substrate treatment regimes, the main factors which are to be controlled in full scale application, are engineered to produce the targeted gas volume at the chosen pressure conditions. A test set-up was developed and successfully implemented to measure the gas produced and consequent desaturation of the sample. The treated samples are subsequently loaded and compared to untreated samples. Two variations in treated tests are studied, including the influence of soil pH on the reaction rate and consumption time, and the influence of the pore size by an increase in the fines content.

The target saturation of 80%, nearly corresponding to the optimal water content of most materials, was virtually achieved. However, the uniformly graded fine sand with 18% fines content had an optimal water content corresponding to around 60% saturation. The target is out of reach for this method due to the sample's lack of ability to contain the produced gas. The fines content was increased to 61% and the optimum water content increased to a corresponding saturation of 75%. The material, however, could not contain a sufficient volume of gas to reach this saturation. This emphasises the importance of pressure conditions and material factors such as the gas capacity threshold (gas entry value) on the biogenic gas desaturation process. More gas should be produced to reach the optimum water content. One can also not depend on all soils to have an optimum water content around 80% saturation.

From this study, it is evident that the gas production is not only a function of Henry's law, the ideal gas law, the metabolic stoichiometry and the initial substrate concentration. Other factors also influence the chemical balance. The effect of initial soil pH and particle size distribution has been verified in this investigation; a soil with initial pH between pH 6.5 and 7 increases the rate of gas production significantly and an additional increase in gas production is observed in a specimen with increased fines content. A lower initial soil pH result in a longer lag period and can be treated with a phosphate buffer, with concentration depending on the buffering capacity of the soil. It is observed that the biochemical reaction has the ability to increase the pH of a sample with pH 5 to above pH 7 which is subsequently limited to pH 8 due to calcite precipitation if calcium. The presence of calcium in the substrate is therefore important, despite it having a negligible effect on particle cohesion.

In this study, the bacterial inoculum was produced from the enrichment of an existing inoculum. The lag period of 2 to 3 days before significant gas production allows for the bacterial inoculum to be mixed with the substrate at injection. The denitrifying bacteria is successfully stimulated inside a Rowe cell generating gas, measured both inside and outside of the cell. However, based on the measured volume changes, the effect of biogenic gas formation on the compressibility of the silty sand is limited. Some factors did not allow for optimum conditions to be achieved. The small displacements are attributed to the high relative density at sample placement and the static loading method implemented in the Rowe cell is only a partial approximation of compaction techniques in

practice.

The suggested Rowe cell set-up is suited for the evaluation of reduction in compaction energy in a microbially desaturated specimen. The work input can be accurately determined. Axial displacements are measured, even though significant sample contraction is prohibited by the radially constrained condition, uniform stress increments and high initial sample placement densities. The hydraulic cell test set-up is suitable to investigate the gas production in a poroelastic medium under pressure and the volume balance during the reaction phase allows for an accurate measurement of the produced gas. The set-up allows for monitoring of the work input into a soil sample that exhibits highly non linear behaviour. Work input is successfully monitored in terms of total work, i.e. the entire force-displacement behaviour. The generation of excess pore water pressures during loading determined that the undrained loading scenario is considered. It is suggested that the low permeable porous stone may have an influence on this.

The research questions asked in Section 1.4 are reiterated:

- Can the gas created by denitrification reduce the amount of energy required to increase the density of a silty sand layer to a given target density through compaction? And,
- Can *in-situ* gas formation be accomplished without inducing any expansion of the saturated soil skeleton?

Two out of three comparative tests indicate a significant reduction in energy required to bring a biogenic desaturated sample to a higher dry density when compared to the saturated counterpart with similar initial *in-situ* relative density. Due to the low number of tests and mixed results, the effect is inconclusive. It is also measured that no expansion of the saturated soil skeleton is induced through *in-situ* biogenic gas formation, provided that the soil is free to drain.

The designed set-up has the potential to make a valuable contribution to the goal of reasonable predictability of the process of biogenic gas desaturation in practice to remediate pore pressure build up during loading. The remedial method is envisioned as targeted treatment of saturated soil layers or entire soil bodies as an alternative drainage method prior to compaction. The ability to control pressure and drainage conditions in the adapted Rowe cell set-up allows the effect of the pressure gradient and permeability to be investigated.

In conclusion, the premises does not allow to prove or fail the hypothesis whether biogenic gas formation can improve the efficiency of compaction, despite promising results. The low number of tests, high sample placement densities, the material and achieved saturation levels did not allow for optimal conditions.

Chapter 6

Recommendations

It is recommended that the following factors are investigated in future research:

- A similar test with variation of material with an achievable saturation in range of or corresponding to the optimum water content
- A sample placement method that provides control over the substrate solution, the initial saturation and the placement relative density must be developed.
- Adaptations to the test set-up and protocol to increase accuracy of measurements and to make the tests more representative to compaction in practice.

The material that is investigated during this study did not have the ability to contain enough gas to desaturate it to close to the optimum water content. A change of material is advised to one where this threshold is within reach. It is recommended that the Proctor test is conducted on the soil prior to treatment to verify the saturation at the optimum water content. The gas entry value of the soil at different pressure conditions should also be determined to verify if a sufficient volume of gas can be contained.

To remediate the high initial sample relative density in the Rowe cell, it is recommended that the sample placement method is altered. The current placement method provides good control on the initial substrate volume. To remediate the risk of dilution of the inoculated substrate, it is advised that the substrate providing an initial pluviation depth is also inoculated. A greater pluviation depth will facilitate break-up and prevent compaction on impact of larger lumps. The more controlled method of pumping with a pluviation head is advised for loose sample placement. A difficulty in determining the volume of substrate is foreseen when opting for this method. Although a lag period of ± 2 days is observed, it is advised that the placement time of samples is kept to a minimum to prevent exposure to aerobic conditions.

One can also experiment with different loading techniques. External agitation through tapping or vibration can induce contraction while the sample is maintained at the desired pressure conditions and constantly monitored. A cyclic loading regime may be introduced into the diaphragm pressure controller.

Some adaptations to the Rowe cell tests and method are suggested. Flushing, vertically or radially, can be implemented to investigate the suitability of injection strategies. A change of porous disk to one with a higher permeability is proposed to investigate if excess pore water pressure is generated. The influence of the diaphragm, particularly during loading steps, has been accounted for. However, the volume balance remains unverified but seem to produce consistent results. The accuracy of the measured expelled gas can be improved by installing the gas trap closer to the centre spindle and decreasing the diameter of the back pressure line lead. This will reduce the volume of gas trapped in the line and improve the estimation of saturation. It is recommended to devise a method to implement

constant monitoring of the volume of gas in the gas trap. The gas entry value can then be determined. A loading regime where the pore pressure is reduced after treatment may also be implemented. This links to the lowering of the water table after treatment due to pumping. As a result, the same concentration of gas in pore space will expand and occupy a larger volume.

For an alternative evaluation of the reduction of absorbed energy, Pham's (2017) triaxial set-up is suggested with a calibrated double walled cell to monitor volumetric strain and an additional monitored gas trap to detect the point at which gas starts to vent from the sample. The saturation at a given point can be more accurately calculated, as no enclosures exist where gas can be trapped before escaping through the porous stone into the back pressure line. In a strain controlled test, Houlsby's (1997) formulation which includes the power absorbed for all three phases and the flux of liquid and gas from the sample, can be implemented for a more accurate calculation of the compaction power per unit volume. Strain controlled cyclic behaviour can be introduced to evaluate the response of the treated soil samples.

Alternately, the set-up based on the Proctor cell and dynamic loading can be revisited as proof of concept. The experiment is more comparable to dynamic loading, but is performed at atmospheric pressure which does not allow for simulated pressure conditions. The pressure conditions have a prominent influence on the gas phase.

A vast number of factors have an influence on the process, of which only the effect of initial soil pH and particle size distribution have been verified under static loading. For future tests it is recommended that emphasis is placed on the application of dynamic loading. Due to the gas bubble's ability to compress and dampen compression waves, the use of this method could be limited in compaction.

Bibliography

- Bonett, A. and Praftis, D. (1996), 'Getting to the Root of Gas Migration', *Oilfield Review* **8**(1), 36–49.
URL: http://www.slb.com/%5C/media/Files/resources/oilfield_review/ors96/spr96/ors96_gas_p36_49.pdf
- Chu, J., Wardani, S. P. R. and Iizuka, A. (2013), 'Geotechnical Predictions and Practice in Dealing with Geohazards', **25**, 375–384.
URL: <http://link.springer.com/10.1007/978-94-007-5675-5>
- Craig, R. F. (2004), *Craig's Soil Mechanics, Seventh Edition*, 7, illustr edn, CRC Press.
- DeJong, J. T., Fritzges, M. B. and Nüsslein, K. (2006), 'Microbially induced cementation to control sand response to undrained shear', *Journal of Geotechnical and Geoenvironmental Engineering* **132**(11), 1381–1392.
- DeJong, J. T., Mortensen, B. M., Martinez, B. C. and Nelson, D. C. (2010), 'Bio-mediated soil improvement', *Ecological Engineering* **36**(2), 197–210.
- DeJong, J. T., Soga, K., Kavazanjian, E., Burns, S., Van Paassen, L. A., Al Qaban, A., Aydilek, A., Bang, S. S., Burbank, M., Caslake, L. F. and Chen, C. Y. (2013), 'Biogeochemical processes and geotechnical applications: progress, opportunities and challenges', *Géotechnique* **63**(4), 287–301.
URL: <http://www.icvirtuallibrary.com/content/article/10.1680/geot.SIP13.P.017>
- Fredlund, D. G. and Rahardjo, H. (1993), *Soil Mechanics for Unsaturated Soils*, John Wiley & Sons, Inc., New York.
- Gallage, C., Dareeju, B., Dhanasekar, M. and Ishikawa, T. (2016), 'Effects of Principal Stress Axis Rotation on Unsaturated Rail Track Foundation Deterioration Effects of Principal Stress Axis Rotation on Unsaturated Rail Track Foundation Deterioration', *Procedia Engineering* **143**(December), 252–259.
- Hafez, M. A., Doris Asmani, M. and Nurbaya, S. (2010), 'Comparison between Static and Dynamic Laboratory Compaction Methods', *The Electronic Journal of Geotechnical Engineering* **15**(1), 1641–1650.
URL: <http://www.ejge.com/2010/Ppr10.118.pdf>
- Head, K. (2006), *Manual of Soil Laboratory Testing. Volume 1: Chemical tests*, third edn, Whittles Publishing, Dunbeath.
- Head, K. and Epps, R. (2014), *Manual of soil laboratory testing. Volume 3: Effective stress tests*, third edn, Whittles Publishing, Dunbeath.
- Houlsby, G. T. (1979), 'The work input to a granular material', *Géotechnique* **29**(3), 354–358.
- Houlsby, G. T. (1981), Study of plasticity theories and their applicability to soils, Phd dissertation, University of Cambridge.

- Houlsby, G. T. (1997), 'The work input to an unsaturated granular material', *Geotechnique* **47**(1), 1–7.
URL: http://www.eng.ox.ac.uk/civil/publications/reports-1/ouel_2084_96.pdf
- Huang, Y. and Wen, Z. (2015), 'Recent developments of soil improvement methods for seismic liquefaction mitigation', *Natural Hazards* **76**(3), 1927–1938.
- Hyodo, M., Yoneda, J., Yoshimoto, N. and Nakata, Y. (2013), 'Mechanical and dissociation properties of methane hydrate-bearing sand in deep seabed', *Soils and Foundations* **53**(2), 299–314.
URL: <http://dx.doi.org/10.1016/j.sandf.2013.02.010>
- ISO-NEN (2005), *ISO 10390:2005 Soil quality - Determination of pH*, second edn, Nederlands Normalisatie-instituut, Geneva.
- Jones, S. F., Evans, G. M. and Galvin, K. P. U. (1999), 'Bubble nucleation from gas cavities - a review', *Advances in colloid and interfaces science* **80.1**((1990)), 27–50.
- Keller (n.d.a), 'Compaction Grouting 66.01E Brochure'.
URL: <http://www.kellerholding.com/download-keller-publications.html>
- Keller (n.d.b), 'Deep Vibro Techniques 10.02E Brochure'.
URL: <http://www.kellerholding.com/download-keller-publications.html>
- Knowles, R. (1982), 'Denitrification', *Microbiological reviews* **46**(1), 43.
- Krapfenbauer, C. (2016), Experimental Investigation of Static Liquefaction in Submarine Slopes, Master thesis, ETH Zurich/TU Delft.
- Maggi, F. and Riley, W. J. (2015), 'The effect of temperature on the rate, affinity, and ^{15}N fractionation of NO_3^- during biological denitrification in soils', *Biogeochemistry* (3), 235–253.
URL: <http://dx.doi.org/10.1007/s10533-015-0095-2>
- Monahan, E. J. (1994), *Construction of Fills*, second edn, John Wiley & Sons, Inc., New York.
- Nageswaran, S. (1983), Effect of gas bubbles on the sea bed behaviour., PhD thesis, St. Catherines's College, Oxford.
URL: <http://ethos.bl.uk/OrderDetails.do?uin=uk.bl.ethos.348153>
- NEN-EN-ISO 10693 (2014), *NEN-EN-ISO 10693 Soil quality - Determination of carbonate content - Volumetric method*, number april 2014, International Organization for Standardization, Geneva, Switzerland.
- NEN-EN-ISO 17892-4 (2016), *NEN-EN-ISO 17892-4 Geotechnical investigation and testing - Laboratory testing of soil - Part 4: Determination of particle size distribution*, number december 2016, 1 edn, International Organization for Standardization, Geneva, Switzerland.
- Okamura, M., Takebayashi, M., Nishida, K., Fujii, N., Jinguji, M., Imasato, T., Yasuhara, H. and Nakagawa, E. (2011), 'In-Situ Desaturation Test by Air Injection and Its Evaluation through Field Monitoring and Multiphase Flow Simulation', *Journal of Geotechnical and Geoenvironmental Engineering* **137**(7), 643–652.
- Pham, V. P. (2017), Bio-based Ground Improvement through Microbial Induced Desaturation and Precipitation (MIDP), Phd thesis, Technical University Delft.
- Pham, V. P., Nakano, A., Van Der Star, W. R. L., Heimovaara, T. J. and Van Paassen, L. A. (2016), 'Applying MICP by denitrification in soils: a process analysis', *Environmental Geotechnics* pp. 1–15.

- Rebata-Landa, V. and Santamarina, J. C. (2012), 'Mechanical Effects of Biogenic Nitrogen Gas Bubbles in Soils', *Journal of Geotechnical and Geoenvironmental Engineering* **138**(2), 128–137.
- Stabnikov, V., Ivanov, V. and Chu, J. (2015), 'Construction Biotechnology: a new area of biotechnological research and applications', *World Journal of Microbiology and Biotechnology* **31**(9), 1303–1314.
- Terzaghi, K., Peck, R. B. and Mesri, G. (1996), *Soil Mechanics in Engineering Practice*, third edn, John Wiley & Sons, Inc., New York.
- Van Paassen, L. A., Daza, C. M., Staal, M., Sorokin, D. Y., Van Der Zon, W. H. and Van Loosdrecht, M. C. M. (2010), 'Potential soil reinforcement by biological denitrification', *Ecological Engineering* **36**(2), 168–175.
- Van Paassen, L. A., Harkes, M. P., Van Zwieten, G. A., Van Der Zon, W. H., Van Der Star, W. R. L. and Van Loosdrecht, M. C. M. (2009), 'Scale up of BioGrout: A biological ground reinforcement method', *Proceedings of the 17th International Conference on Soil Mechanics and Geotechnical Engineering: The Academia and Practice of Geotechnical Engineering* **3**(August 2015), 2328–2333.
- van Paassen, L. A., Pham, V. P., Mahabadi, N., Hall, C., Stallings, E. and Kavazanjian, E. (2017), Desaturation via Biogenic Gas Formation as a Ground Improvement Technique, in 'PanAm-UNSAT', Dallas.
- van Spanning, R. J. M., Richards, D. J. and Ferguson, S. J. (2006), Introduction to the Biochemistry and Molecular Biology of Denitrification, in H. Bothe, S. Ferguson and W. Newton, eds, 'Biology of the Nitrogen Cycle', first edn, Elsevier, Amsterdam, chapter 0, 1, pp. xiii–20.
- Yamamoto, Y., Hyodo, M. and Orense, R. P. (2009), 'Liquefaction Resistance of Sandy Soils under Partially Drained Condition', *Journal of Geotechnical and Geoenvironmental Engineering* **135**(8), 1032–1043.
- Yegian, M. K. (2007), 'Induced-partial saturation for liquefaction mitigation: experimental investigation', *Journal of Geotechnical and Geoenvironmental Engineering* **133**(4), 372–380.
- Zeybek, A. and Madabhushi, S. P. G. (2016), 'Centrifuge testing to evaluate the liquefaction response of air-injected partially saturated soils beneath shallow foundations', *Bulletin of Earthquake Engineering* **15**(1), 1–18.

Appendix A

Incubation tests

A.1 Incubation test results

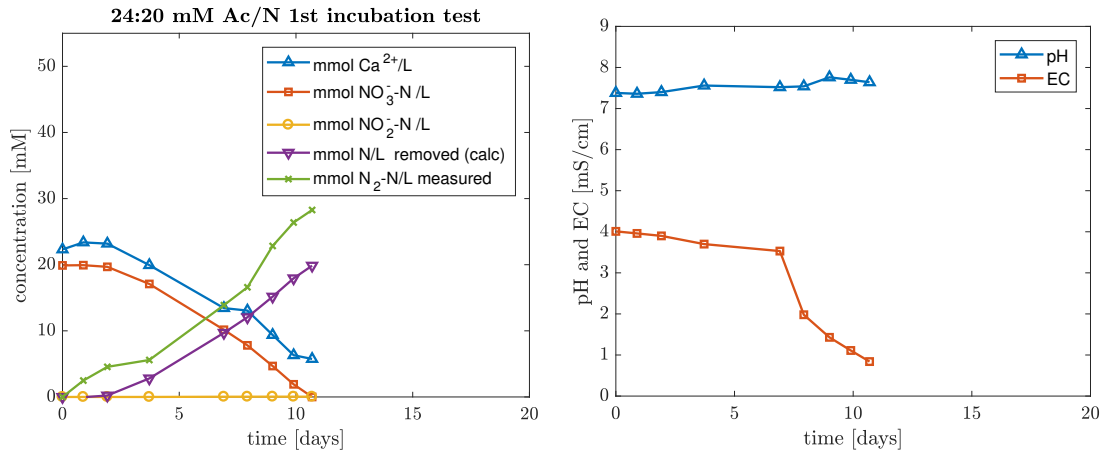
Results for the incubation tests are depicted in Figure A.1. The inoculum for the 1st incubation tests was obtained from the 6th incubation following from Pham et al.'s (2016) work. The subsequent tests were inoculated from the prior tests. After the completion of the incubation experiments, the inoculum were combined to be used in future experiments. The inoculum originated from the Delft University of Technology's botanical garden, where an organically rich soil from two metres below ground level (anaerobic conditions) were collected. It is noted that the inoculum has been kept at 4 °C for six months prior to use. From Figure A.1 (a.) and (b.), it can be seen that the inoculum responded well with repeatable results, thus deemed suitable for further experiments.

The reaction is stagnant for the first 2 to 3 days, whereafter the nitrate reduce at a near-constant rate. Calcium ions in solution reduce over time due to the reaction with bicarbonate and precipitate as calcium carbonate. It is noticed that not all calcium ions are consumed. The levels of nitrite is negligibly low, possibly as a result of the low concentrations of initial nitrate (Pham, 2017). For the 1st and 2nd incubation tests, the produced gas volume is successfully measured and corresponds well with the calculated gas volume through nitrogen balance (assumed to be N_2 only). A potential cause for the deviation of the measured gas concentration from the calculated concentration could be that carbon dioxide is out of solution at atmospheric pressure. At higher pressures, the CO_2 fraction is expected to be dissolved into the pore fluid due to its high solubility.

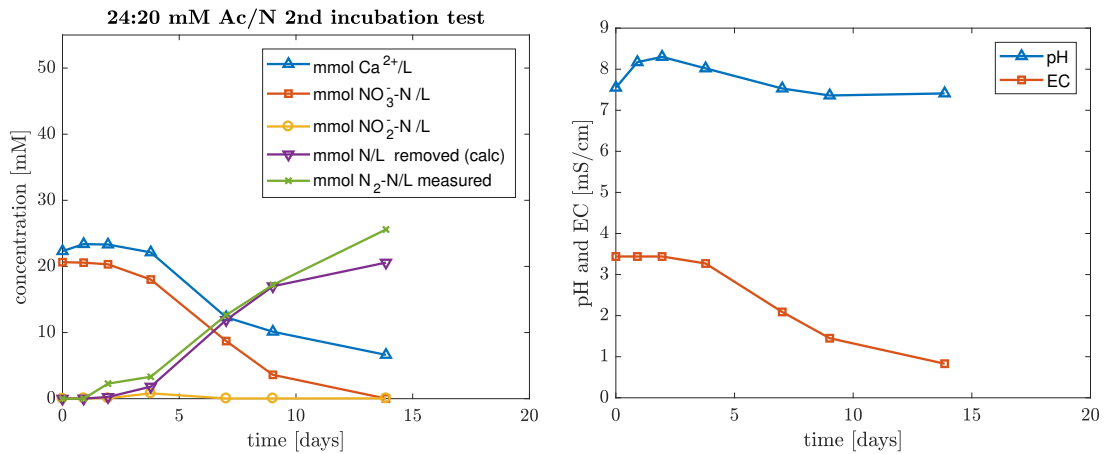
The electrical conductivity (EC) reduces in conjunction with the reduction of salts in solution (Ca^{2+}). The pH increases slightly during the initial reaction phase due to denitrification, but starts to stabilise as the precipitation of calcium carbonate occurs, which acts as buffer due to the increase of hydrogen ions released during the reaction. The same phenomena are noticed when a higher concentration of calcium acetate and -nitrate solution is used. As expected, the higher concentration lengthens the nitrate reduction period.

A.1. INCUBATION TEST RESULTS

a.)



b.)



c.)

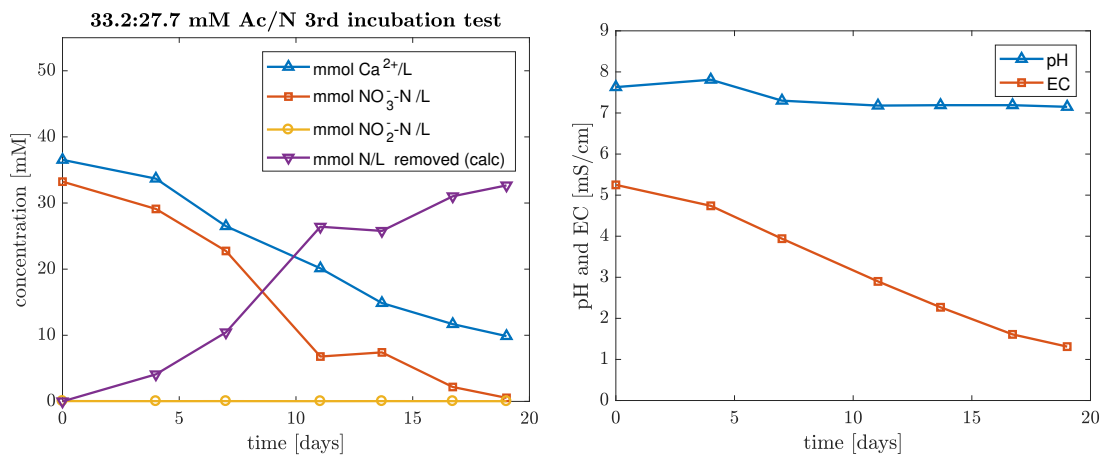


Figure A.1: Comparison of changes in chemical composition of denitrifying bacteria incubation test over time with constant Ac/N =1.2 at T=25 and P=1 atm : a.) 1st Incubation 24:20 mM Ac-N inoculated with 40ml/l bacteria inoculum from Pham et al.'s (2016) 6th incubation; b.) 2nd Incubation 24:20 mM Ac-N inoculated with 40ml/l inoculum from 1st incubation; c.) 3rd Incubation 33:27.5 mM Ac-N inoculated with 40ml/l inoculum from 2nd incubation

Appendix B

Test Specimen

B.1 Particle size distribution - Sieving

The particle size distribution for Geba and M6-MILLISIL, determined through dry sieving and hydrometer, respectively are indicated in figure B.1. The Particle size distribution of Toyoura sand is added as reference from Hyodo et al.'s (2013) work. Standard Proctor test results similar to the Geba-M6 84-16 were achieved in Gallage et al.'s (2016) study of Toyoura sand (Figure 4.1).

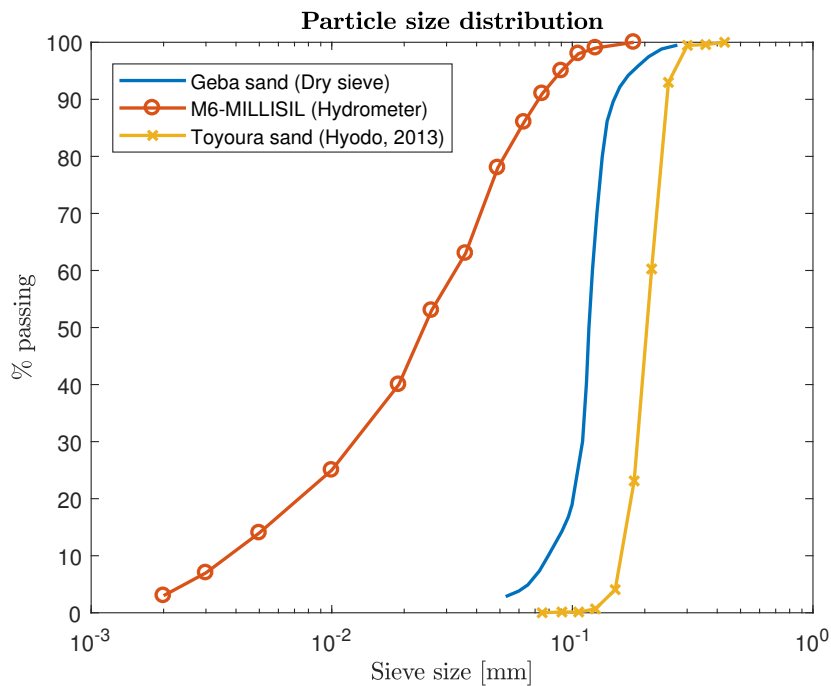


Figure B.1: Particle size distribution determined by dry sieving (BS-1377) from Krapfenbauer (2016)

The distributions are combined in the different ratios to determine the PSD of the mixed specimens:

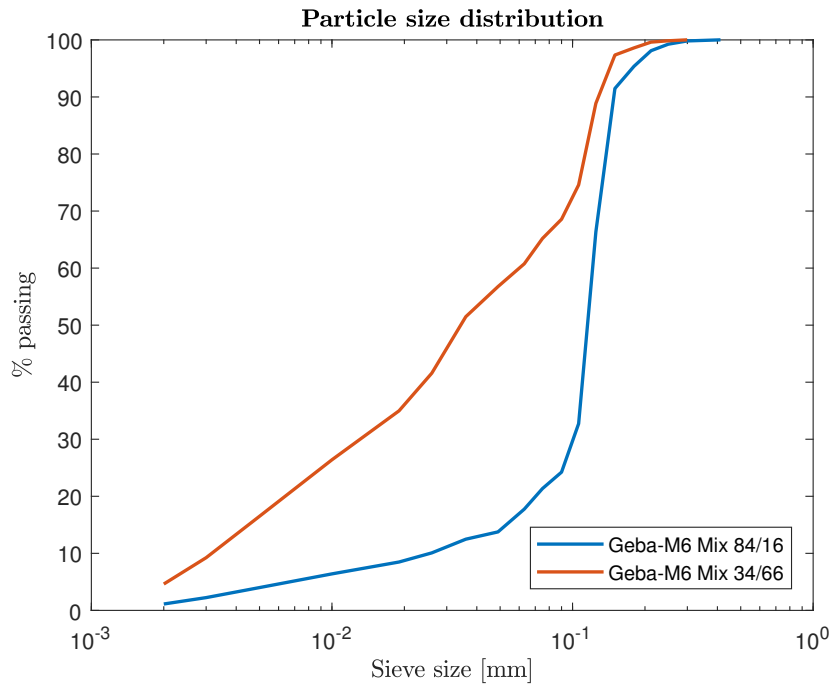


Figure B.2: Particle size distribution of M6-MILLISIL silica flour determined through hydrometer test

Table B.1: Particle size information from sieve and hydrometer curves (μm)

	Geba	M6-MILLISIL
D_{90}	148	72 (95*)
D_{60}	121	33
D_{50}	117	24 (30*)
D_{10}	80	5 (5*)

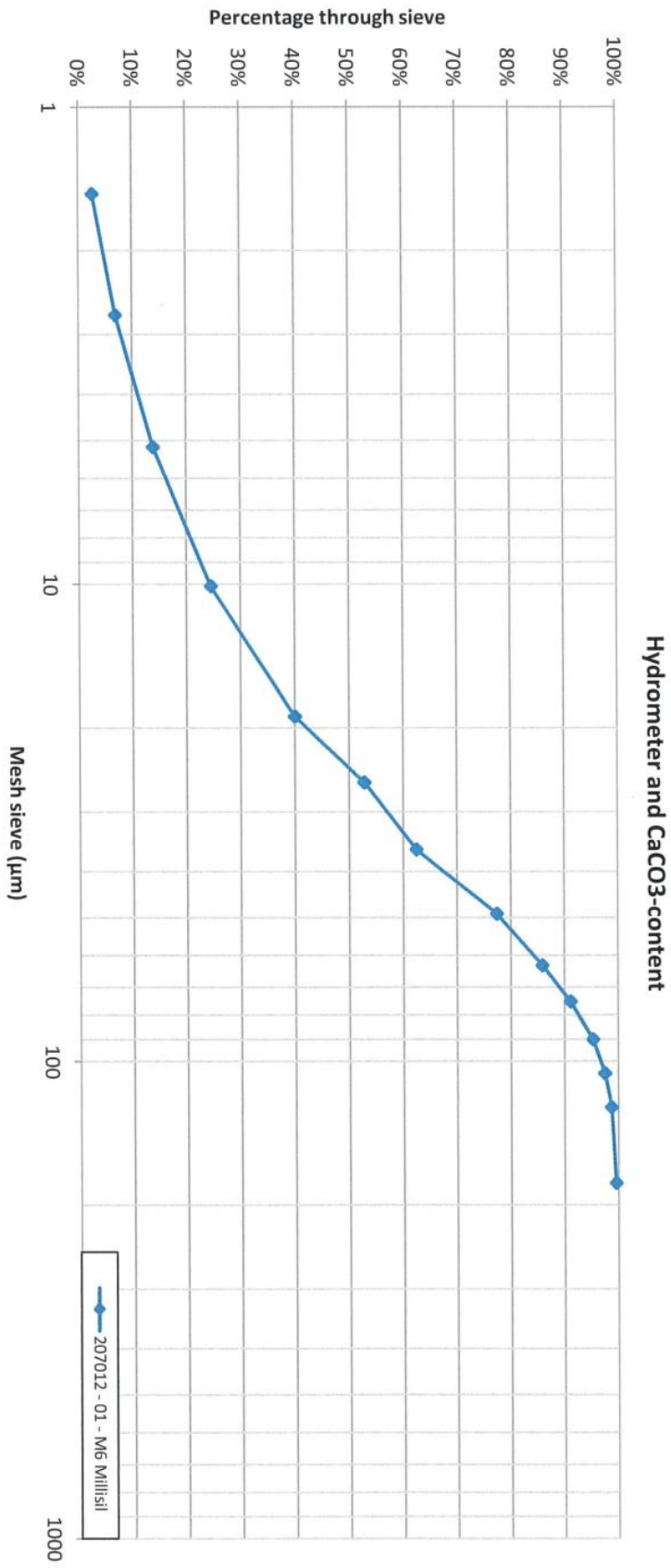
*From technical specification sheet (Sibelco M6 MILLISIL brochure)

Table B.2: Density information (Sibelco M6-MILLISIL/Geba Technical Data Brochures)

	M6-MILLISIL	Geba
Density [kg/dm^3]	2.65	2.65
Bulk density [kg/dm^3]	1	1.35
Specific gravity G_s	2.65	2.65

B.2 Hydrometer M6

A hydrometer test is conducted according to NEN-EN-ISO 17892-4 (2016) on the M6-MILLISIL fraction to determine the size distribution of the fines fraction. The results are available in Figures B.3 and B.4:



Sieve		Sample:												
Name		D10	D20	D30	D40	D50	D60	D70	D80	D90	% > 2mm	DMF (total)	D60/D10	
		µm	µm	µm	µm	µm	µm	µm	µm	µm				
1	207012 - 01 - M6 Millisil	4	8	13	19	24	33	42	53	72	0.00%	30	9.2	
2														
3														
4														

Figure B.4: Hydrometer results: PSD for M6 MILLISIL based on BS1377

B.3 Chemical analysis

The chemical analysis information is obtained from the product brochures

Table B.3: Chemical Analysis of M6-Millisil (Sibelco M6-MILLISIL/Geba Brochures)

	M6-MILLISIL (XRF)	Geba (DIN51001)
<i>SiO₂</i>	99.50%	99.00%
<i>Fe₂O₃</i>	0.03%	0.08%
<i>Al₂O₃</i>	0.20%	0.29%
<i>TiO₂</i>	0.03%	0.16%
<i>K₂O</i>	0.04%	0.03%
<i>CaO</i>	0.02%	0.02%
<i>Na₂O</i>		0.01%
<i>MgO</i>		0.01%
<i>BaO</i>		0.02%
Loss on ignition	0.12%	0.20%
pH	7	7*

*Measured to be pH 5 in a LS5 by volume test in 10 mM *CaCl₂*

B.4 Proctor test data

The data for water content measurements and dry density calculations for Standard and Modified Proctor tests on both Geba-M6 84-16 and Geba-M6 34-66 soil mixtures are provided in this section. Multiple water content measurements are conducted for in a single point. The water content is then averaged and plotted together with the dry density on the Proctor plane.

Table B.4: Standard Proctor Geba-M6 84-16 water content measurements

test#-layer	container mass [g]	m_i [g]	m_e [g]	w [-]
1-1	2.14	32.1	30	0.075376884
1-2	2.13	47.83	44.56	0.077068112
1-3	2.16	45.04	42	0.076305221
2-1	2.16	35.29	32.01	0.109882747
2-2	2.16	68.84	62.33	0.108193452
2-3	2.16	68.23	61.68	0.110047043
3-1	2.15	59.85	53.1	0.132482826
3-2	2.15	49.8	44.16	0.134253749
3-3	2.15	63.5	56.16	0.135900759
4-1	2.15	19.28	16.56	0.188757807
4-2	2.15	25.9	21.88	0.203750634
4-3	2.15	18.33	16.78	0.105946685
5-1	2.12	22.79	19.53	0.187248708
5-2	2.15	27.96	23.37	0.216305372
5-3	2.13	23.26	20.62	0.142779881
6-1	2.11	33.73	28.24	0.21010333
6-2	2.11	37.84	31.19	0.228679505
6-3	2.11	30.51	26.32	0.17306898

Table B.5: Standard Proctor Geba-M6 84-16 dry density determination

test#	total mass [kg]	mass cont kg	p [kg/L]	w [-]	p_d [kg/l]
1	6.07051	4.3753	1.695013033	7.62500725	1.574924896
2	6.13957	4.3753	1.764065009	10.9374414	1.590143947
3	6.226	4.3753	1.850484967	13.42124448	1.631515308
4	6.244	4.3753	1.868482875	16.61517085	1.602263978
5	6.222	4.3753	1.846485431	18.21113203	1.562023305
6	6.208	4.3753	1.832487058	20.39506047	1.522061662

Table B.6: Modified Proctor Geba-M6 84-16 water content measurements

test#-layer	container mass [g]	m_i [g]	m_e [g]	w [-]
1-1	2.15	23.16	22.2	0.047880299
1-2	2.14	23.36	22.39	0.047901235
1-3	2.17	18.79	18.03	0.047919294
2-1	2.17	22.06	20.68	0.074554295
2-2	2.17	24.28	22.73	0.075389105
2-3	2.17	19.93	18.66	0.077016374
3-1	2.16	21.05	19.23	0.106619801
3-2	2.16	42.19	38.48	0.102147577
3-3	2.16	27.82	25.34	0.106988783
4-1	2.16	23.63	21.19	0.128218602
4-2	2.16	34.62	30.96	0.127083333
4-3	2.16	37.51	33.5	0.1279515
5-1	2.13	20.9	18.28	0.162229102
5-2	2.16	34.2	30.2	0.142653352
5-3	2.14	33.95	30.4	0.12561925
6-1	2.12	51.12	43.06	0.196873473
6-2	2.12	32.56	28.5	0.153904473
6-3	2.12	43.21	38.17	0.139805825

Table B.7: Modified Proctor Geba-M6 84-16 dry density determination

test#	total mass [kg]	mass cont kg	p [kg/L]	w [%]	p_d [kg/l]
1	6.02474	4.3753	1.649248351	4.790027588	1.573860022
2	6.08878	4.3753	1.71328091	7.565325786	1.59278178
3	6.15253	4.3753	1.777023503	10.52520538	1.607799322
4	6.223	4.3753	1.847485315	12.77511451	1.638203005
5	6.223	4.3753	1.847485315	14.35005681	1.61564005
6	6.18626	4.3753	1.810749584	16.35279239	1.556257952

Table B.8: Standard Proctor Geba-M6 34-66 water content measurements

test#-layer	container mass [g]	m_i [g]	m_e [g]	w [-]
1-1	2.14	20.64	18.77	0.112447384
1-2	2.13	62	56.36	0.104001475
2-1	2.16	34.74	30.96	0.13125
2-2	2.16	60	53.33	0.130349814
3-1	2.15	35.78	31.3	0.153687822
3-2	2.15	71.53	62.41	0.151344175
4-1	2.15	42.13	36.33	0.169689877
4-2	2.15	53.47	45.71	0.178145087
5-1	2.12	58.03	48.95	0.193892804
5-2	2.15	46.79	39.44	0.197103781
6-1	2.11	48.93	41.42	0.191045535
6-2	2.11	42.8	36.13	0.196061141

Table B.9: Standard Proctor Geba-M6 34-66 dry density determination

test#	total mass [kg]	mass cont kg	p [kg/L]	w [-]	p_d [kg/l]
1	6.18236	4.3753	1.80706	0.10822443	1.630590295
2	6.265	4.3753	1.8897	0.130799907	1.67111793
3	6.341	4.3753	1.9657	0.152515998	1.705572853
4	6.32	4.3753	1.9447	0.173917482	1.656590033
5	6.287	4.3753	1.9117	0.195498292	1.599082167
6	6.297	4.3753	1.9217	0.193553338	1.610066294

Table B.10: Modified Proctor Geba-M6 34-66 water content measurements

test#	container mass [g]	m_i [g]	m_e [g]	w [-]
1	2.17	23.48	21.86	0.082275267
2	2.17	42.57	38.91	0.099618944
3	2.16	35.58	32.09	0.116605413
4	2.16	52.79	46.66	0.137752809
5	2.14	55.77	48.22	0.163845486

Table B.11: Modified Proctor Geba-M6 34-66 dry density determination

test#	total mass [kg]	mass cont kg	p [kg/L]	w [-]	p_d [kg/l]
1	6.252	4.3753	1.8767	0.082275267	1.734032051
2	6.311	4.3753	1.9357	0.099618944	1.760337079
3	6.37	4.3753	1.9947	0.116605413	1.786396499
4	6.388	4.3753	2.0127	0.137752809	1.769013431
5	6.347	4.3753	1.9717	0.163845486	1.694125228

Appendix C

Substrate solution

C.1 Treatment Composition

Table C.1: Substrate solution constituents 16.6 mM $Ca(NO_3)_2$ - 19.9 mM $Ca(C_2H_3O_2)_2$ used in all treatments

Compound	Chemical Formula	Stock solution concentration [M]	solute concentration [mM]	mL/volume
Calcium nitrate	$Ca(NO_3)_2$	1	16.6162	5.649508
Calcium acetate	$Ca(C_2H_3O_2)_2$	1	19.93944	6.7794096
Ammonium sulfate	$(NH_4)_2SO_4$	0.01	0.003	0.102
Magnesium sulfate	$MgSO_4$	0.01	0.0024	0.0816
Monopotassium phosphate	KH_2PO_4	0.01	0.006	0.204
Dipotassium phosphate	K_2HPO_4	0.01	0.014	0.476
			ml/L	
Trace element	SL12B			1 0.34
soil/bacteria inoculum		0.1 L/L		34
demi water				292.367482
prepare solution volume [ml]				340
Ac/N ratio	1.2			

C.2 Areometer/Hydrometer density test

The relative density of the substrate solution used in all treated Rowe cell test was determined using a Areometer with range 1-1.05 (Figure C.1)(Fischer, Germany). The results are presented in Table C.2.

The relative density of the material in Table C.1 was determined as 1.0033. Demi water was analysed and had an relative density of 0.9995. The assumption that the density of the substrate solution was the same as that of water, remains valid.

Table C.2: Areometer results

Liquid	Specific gravity
Substrate solution 16.6mM $Ca(NO_3)_2$ - 19.9 mM $Ca(C_2H_3O_2)_2$	1.0033
Demineralised water	0.9995

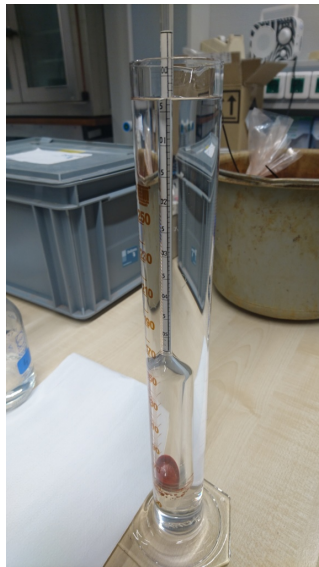


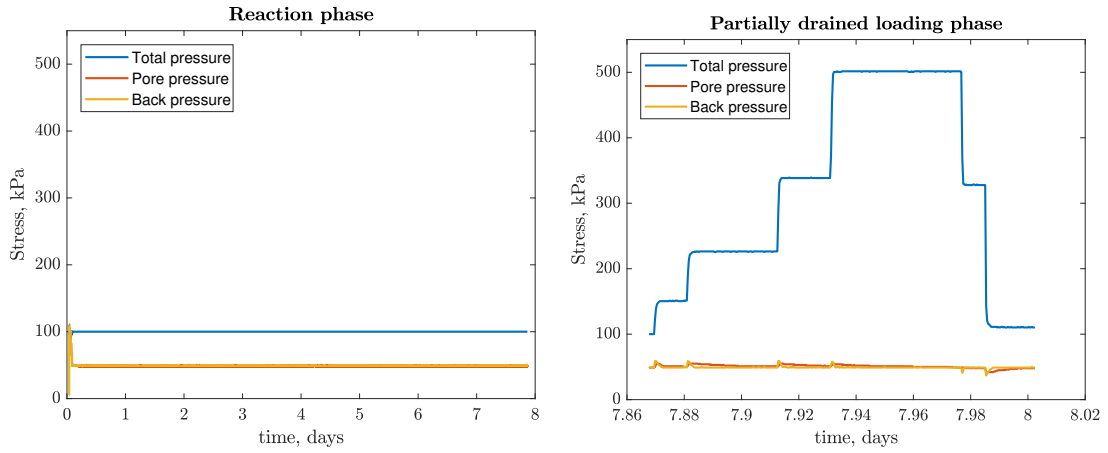
Figure C.1: Areometer (hydrometer) test used to determine the Relative density of the inoculated substrate solution as in Table C.1

Appendix D

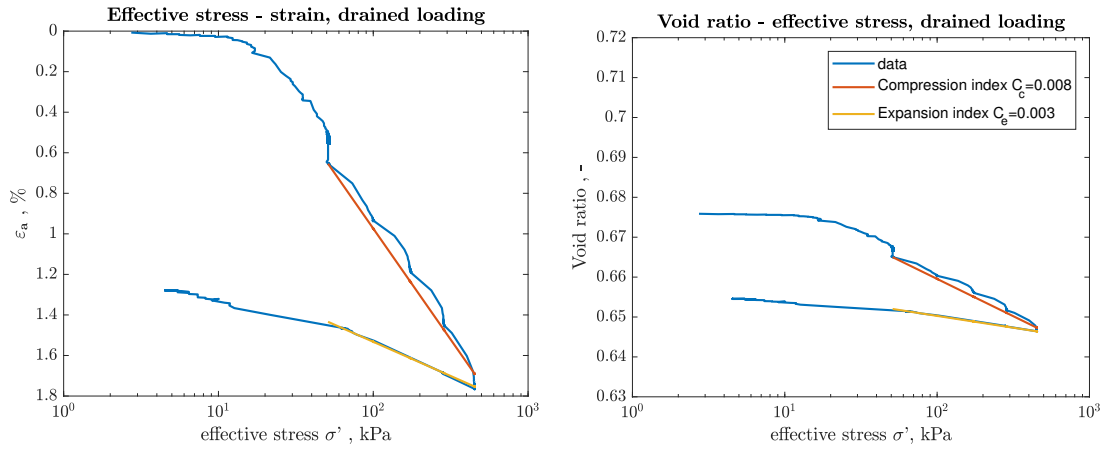
Hydraulic Cell test Results

D.1 Control 1

a.)



b.)



c.)

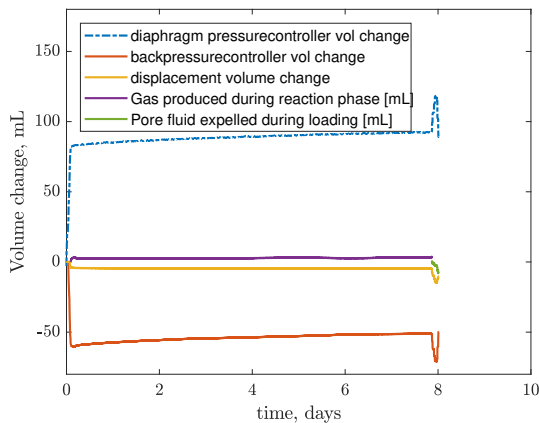


Figure D.1: a.) Total and pore pressure throughout test for the reaction phase (left) and partially drained loading phase (right); b.) Effective stress - axial strain plot (left) and effective stress - void ratio with C_c and C_e (right); c.) Volume change measurements recorded throughout reaction and loading phases

D.2 Control2

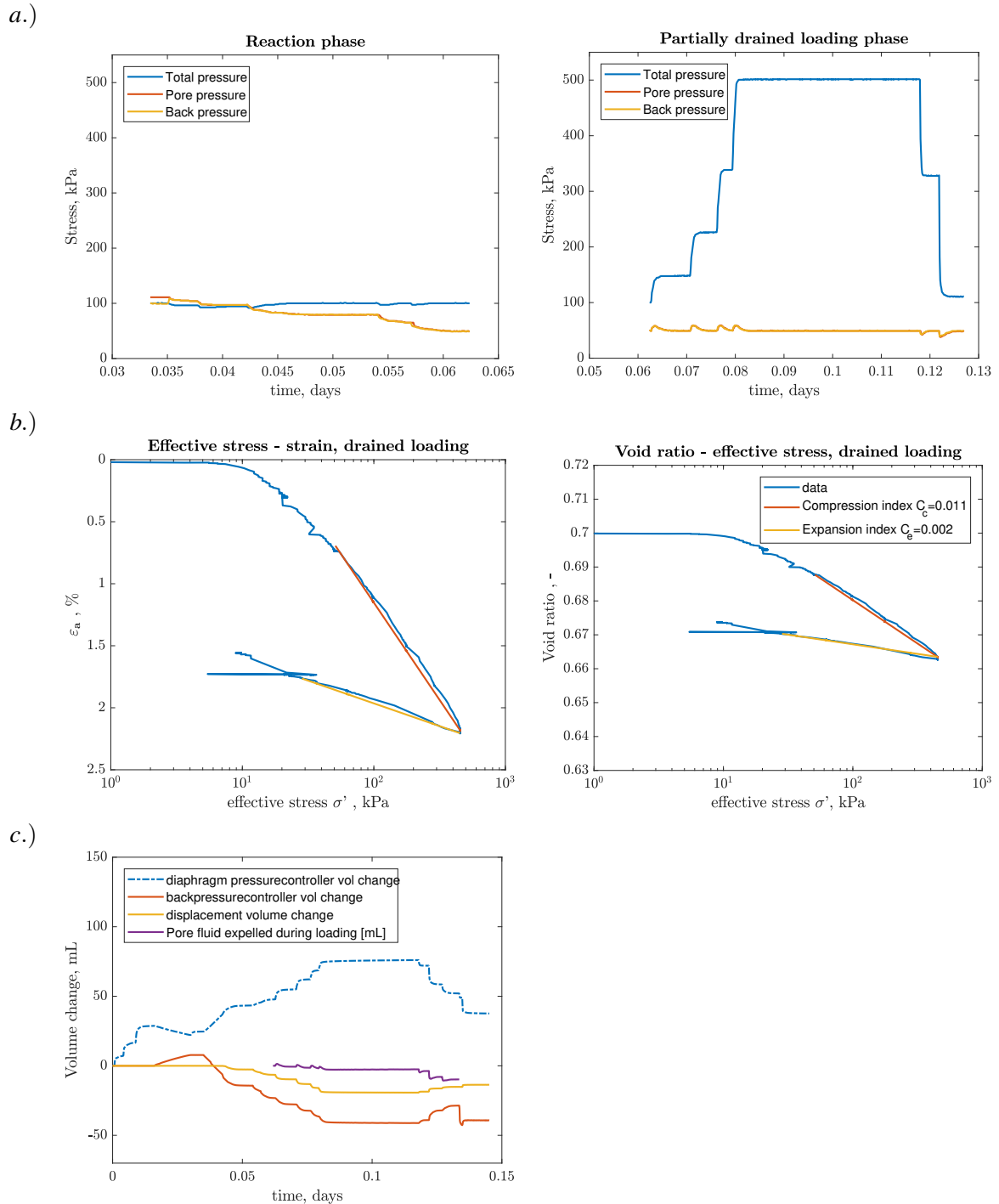


Figure D.2: a.) Total and pore pressure throughout test for the reaction phase (left) and partially drained loading phase (right); b.) Effective stress - axial strain plot (left) and effective stress - void ratio with C_c and C_e (right); c.) Volume change measurements recorded throughout reaction and loading phases

D.3 Control3

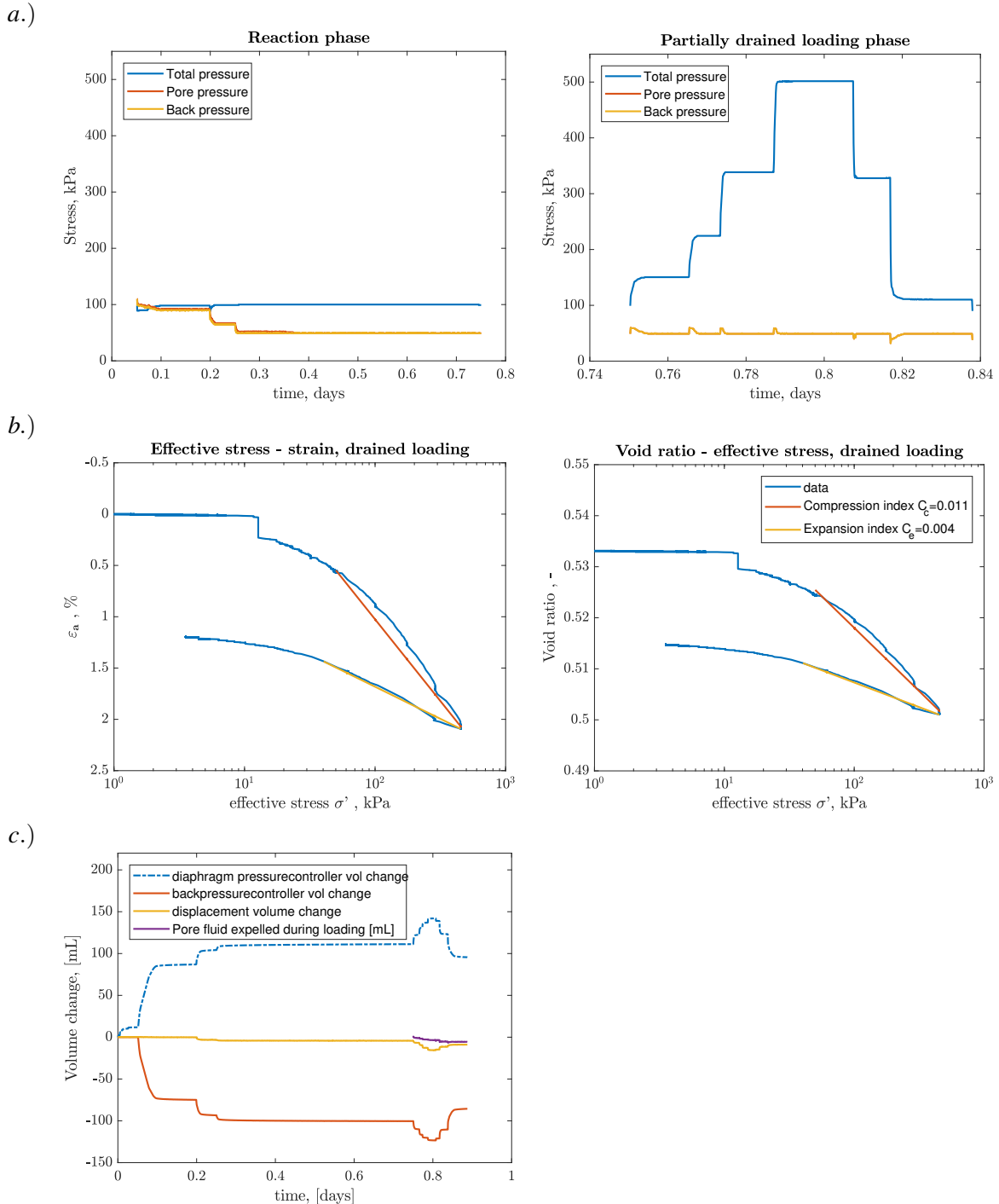


Figure D.3: a.) Total and pore pressure throughout test for the reaction phase (left) and partially drained loading phase (right); b.) Effective stress - axial strain plot (left) and effective stress - void ratio with C_c and C_e (right); c.) Volume change measurements recorded throughout reaction and loading phases

D.4 Bac1

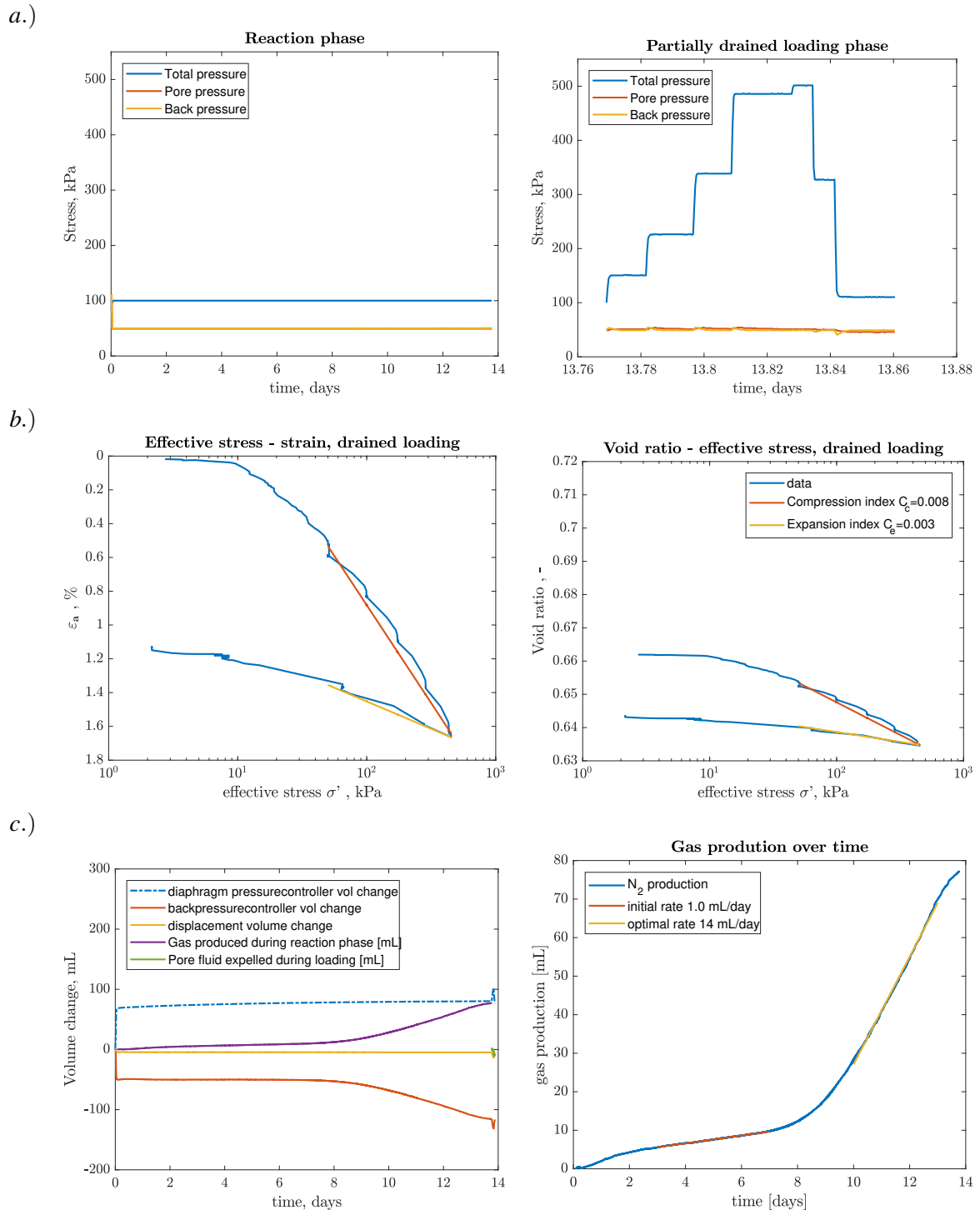
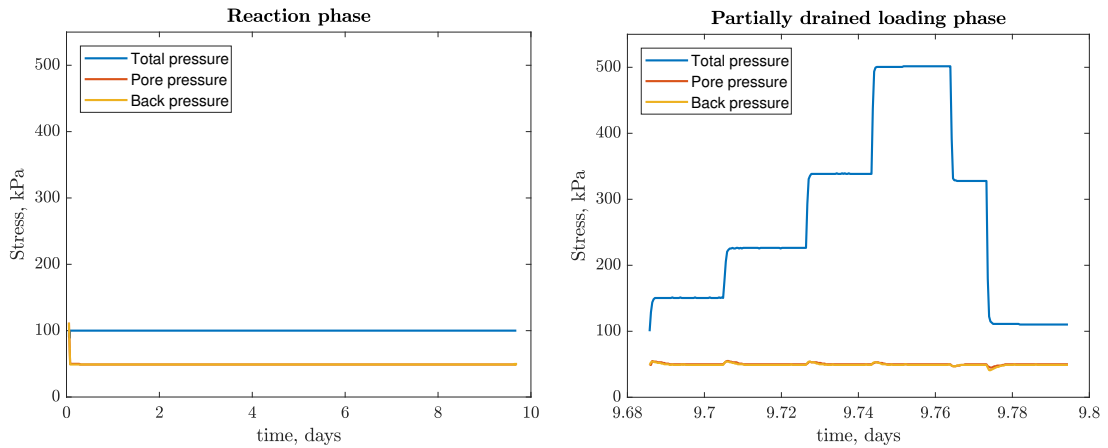


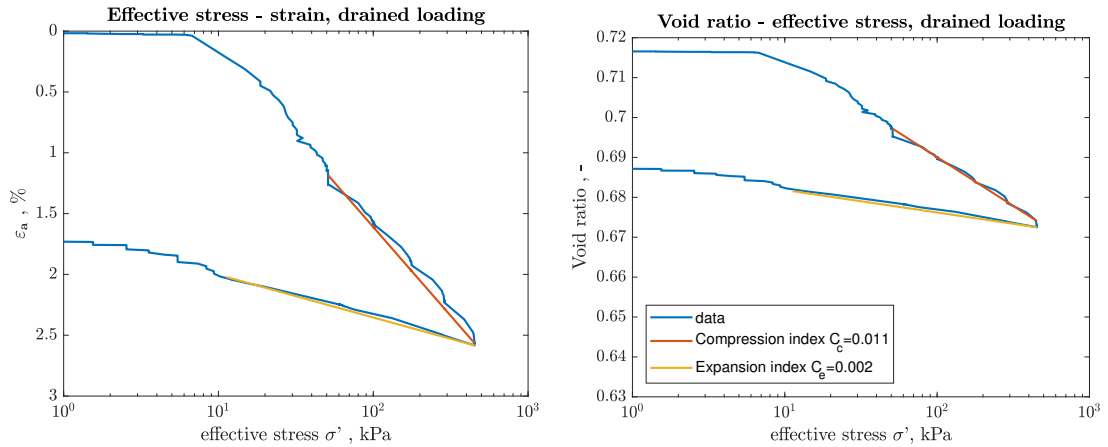
Figure D.4: a.) Total and pore pressure throughout test for the reaction phase (left) and partially drained loading phase (right); b.) Effective stress - axial strain plot(left) and effective stress - void ratio with C_c and C_e (right); c.) Volume change measurements recorded throughout reaction and loading phases (left) and gas production over time with initial- and optimal gas production rates indicated

D.5 Bac2

a.)



b.)



c.)

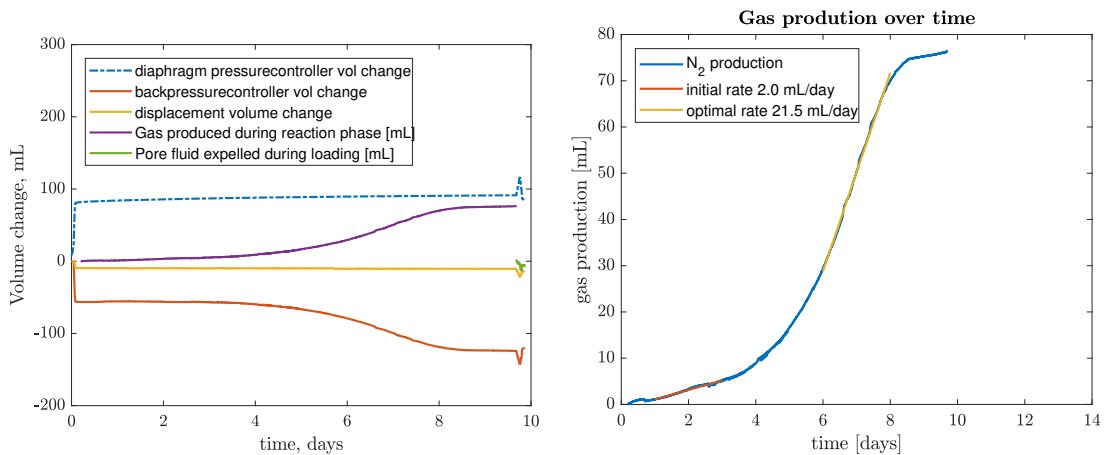


Figure D.5: a.) Total and pore pressure throughout test for the reaction phase (left) and partially drained loading phase (right); b.) Effective stress - axial strain plot (left) and effective stress - void ratio with C_c and C_e (right); c.) Volume change measurements recorded throughout reaction and loading phases (left) and gas production over time with initial- and optimal gas production rates indicated

D.6 Bac3

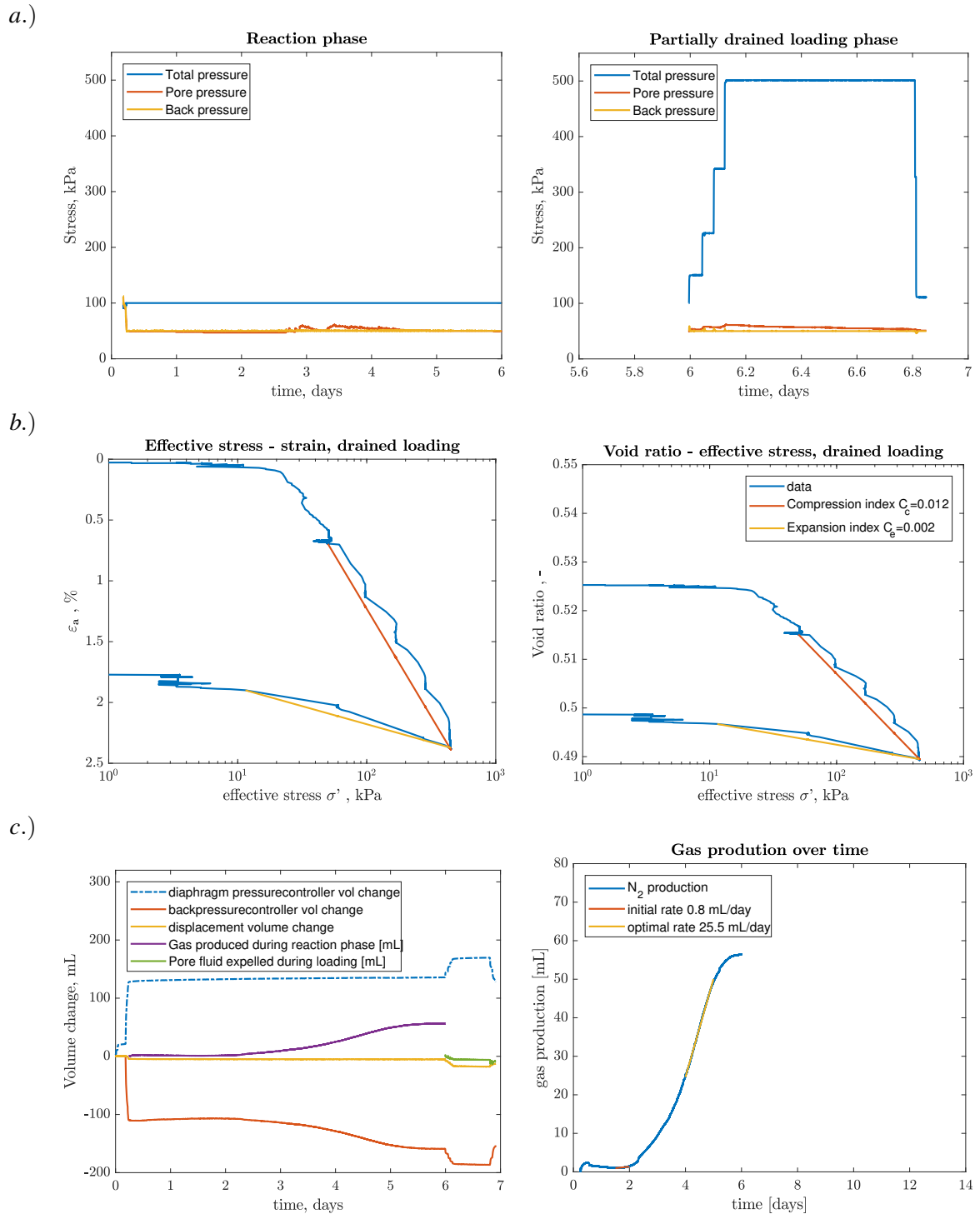


Figure D.6: a.) Total and pore pressure throughout test for the reaction phase (left) and partially drained loading phase (right); b.) Effective stress - axial strain plot (left) and effective stress - void ratio with C_c and C_e (right); c.) Volume change measurements recorded throughout reaction and loading phases (left) and gas production over time with initial- and optimal gas production rates indicated

D.7 Nitrogen balance

Table D.1: Nitrogen balance hydraulic cell test Bac1

Bac1 nitrogen balance	initial	end		gas
	pore fluid	pore fluid	supernatant	
Volume [ml]	331	273.76	n.d.	77.14
Nitrate [mmol $NO_3 - N$]	10.85	0.371		
Nitrite [mmol $NO_2 - N$]	0.01	0.115		
$N_2/NO/N_2O$ gas [mmol-N]		0.2650		9.579
Total	10.87	10.33		
N-gap [mmol]	0.54			
N-gap [%]	5%			

Table D.2: Nitrogen balance hydraulic cell test Bac2

Bac2 nitrogen balance	initial	end		gas
	pore fluid	pore fluid	supernatant	
Volume [ml]	355	303.73	0	76.35
Nitrate [mmol $NO_3 - N$]	11.47	0.045		
Nitrite [mmol $NO_2 - N$]	0.02	0.011		
$N_2/NO/N_2O$ gas [mmol-N]		0.2941		9.481
Total	11.49	9.83		
N-gap [mmol-N]	1.66			
N-gap [%]	14%			

Table D.3: Nitrogen balance hydraulic cell test Bac3

Bac3 nitrogen balance	initial	end		gas
	pore fluid	pore fluid	supernatant	
Volume [ml]	317.5	264.87	n.d.	56.52
Nitrate [mmol $NO_3 - N$]	10.07	0.039		
Nitrite [mmol $NO_2 - N$]	0.02	0.010		
$N_2/NO/N_2O$ gas [mmol-N]		0.2564		7.018
Total	10.09	7.32		
N-gap [mmol-N]	2.77			
N-gap [%]	27%			

D.8 $CaCO_3$ content

The procedures of NEN-EN-ISO 10693 (2014) are implemented to determine the $CaCO_3$ content of each treated test. Three samples are taken distributed over the height and analysed.

Summary of results

Test	Unit	207012	207013	207014	207015	207016	207017
Moisture content	%	0.0	0.0	0.0	0.0	0.0	0.1
Dry matter content	%	100.0	100.0	100.0	100.0	100.0	99.9
CaCO ₃	g/kg.d s		1	0	0	1	0

Test	Unit	207018	207019	207020	207021	207022	207023
Moisture content	%	0.0	0.1	0.0	0.0	0.1	0.0
Dry matter content	%	100.0	99.9	100.0	100.0	99.9	100.0
CaCO ₃	g/kg.d s	1	0	0	0	1	1

Nr.	Monsternaam
207012	01 - M6 - Millisil
207013	02 - M6 - Millisil Blank
207014	03 - Bac2 11
207015	04 - Bac2 12
207016	05 - Bac2 13
207017	06 - Bac3 11
207018	07 - Bac3 12
207019	08 - Bac3 13
207020	09 - M6 - Millisil Blank
207021	10 - Beba Blank
207022	11 - Bac4 11
207023	12 - Bac4 12

Figure D.7: Calcium carbonate content of the treated soil specimens according to NEN-EN-ISO 10693 (2014)

Table D.4: CaCO₃ content for treated tests [g/kg dissolved solids]

Position	Unit	Bac1	Bac2	Bac3
Top	g/kg. d s	0	0	1
Middle	g/kg. d s	0	1	1
Bottom	g/kg. d s	1	0	n.d.
Average	g/kg. d s	0.33	0.33	1

Table D.5: Ca²⁺ Balance Rowe Cell Bac1

Bac1 calcium balance	initial	end
Calcium [mmol-Ca]	10.43	3.593
Supernatant [mmol-Ca]	n.d.	n.d.
Calcium precipitate [mmol CaCO ₃ – Ca]		4.296
Total [mmol-Ca]	10.427	7.889
Ca-gap [mmol]	2.537	
Ca-gap [%]	24%	

Table D.6: Ca^{2+} Balance Rowe Cell Bac2

Bac2 calcium balance	initial	end
Calcium [mmol-Ca]	12.16	3.474
Calcium precipitate [mmol $\text{CaCO}_3 - \text{Ca}$]		4.224
Supernatant [mmol-Ca]	n.d.	0
Total [mmol-Ca]	12.159	7.697
Ca-gap [mmol-Ca]	4.461	
Ca-gap [%]	37%	

Table D.7: Ca^{2+} Balance Rowe Cell Bac3

Bac3 calcium balance	initial	end
Calcium [mmol-Ca]	12.50	3.460
Calcium precipitate [mmol $\text{CaCO}_3 - \text{Ca}$]		12.872
Supernatant [mmol-Ca]	n.d.	n.d.
Total [mmol-Ca]	12.502	16.332
Ca-gap [mmol-Ca]	-3.830	
Ca-gap [%]	-31%	

Appendix E

Alternative Test Set-ups

E.1 Adapted Proctor Cell

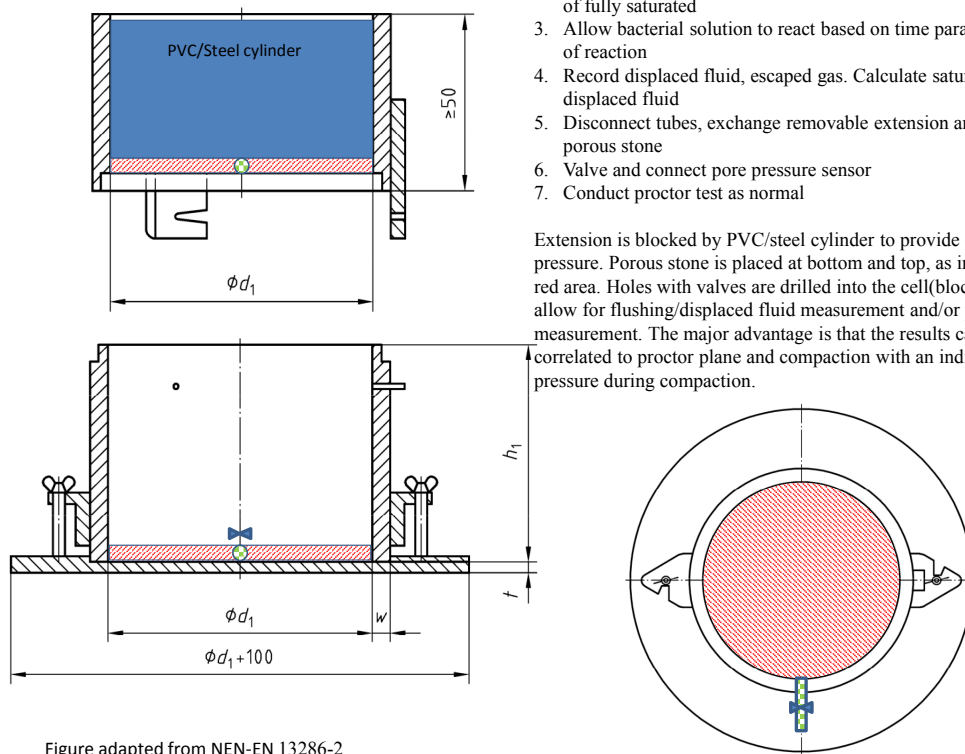


Figure adapted from NEN-EN 13286-2

Protocol:

1. Set up Proctor curves by following nen-en13286-2
2. Mix in place/ flush bacterial solution into soil based on water content of fully saturated
3. Allow bacterial solution to react based on time parameters and kinetics of reaction
4. Record displaced fluid, escaped gas. Calculate saturation based on displaced fluid
5. Disconnect tubes, exchange removable extension and remove top porous stone
6. Valve and connect pore pressure sensor
7. Conduct proctor test as normal

Extension is blocked by PVC/steel cylinder to provide overburden pressure. Porous stone is placed at bottom and top, as indicated by hatched red area. Holes with valves are drilled into the cell(blocky green) wall to allow for flushing/displaced fluid measurement and/or pore pressure measurement. The major advantage is that the results can directly be correlated to proctor plane and compaction with an indication of pore pressure during compaction.

Figure E.1: Adapted Proctor cell to allow desaturation and gas measurements. The removal of the overburden pressure removes the confinement to keep gas phase stable. Test is conducted at atmospheric pressure. Dynamic loading can be applied with a Proctor hammer. Shearing effects assists in compaction if confinement cylinder is removed. If confinement is maintained, the dropped weight acts over the entire surface, similar to the hydraulic cell

E.2 Hydraulic Cell with Flush Through

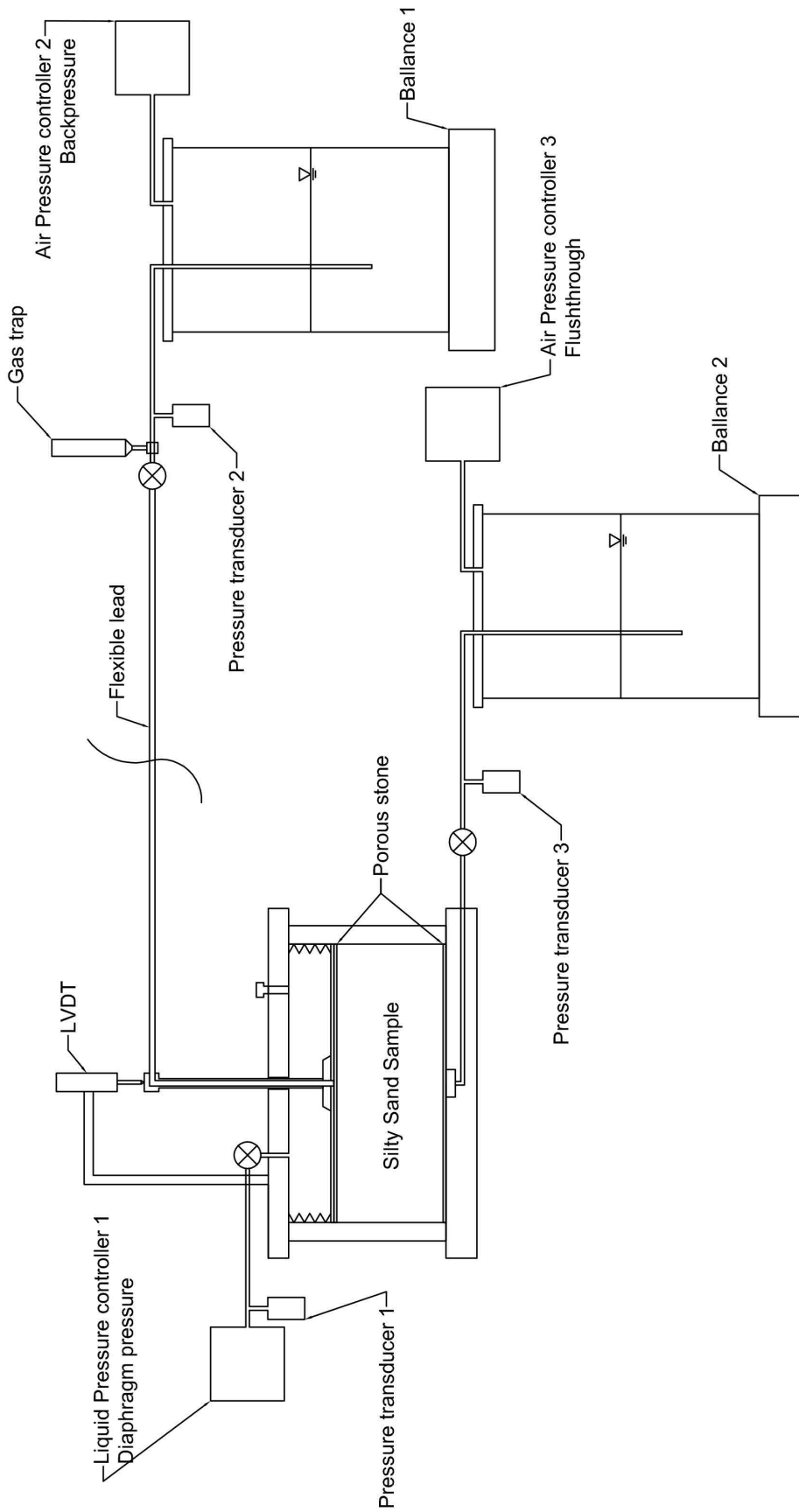


Figure E.2: Hydraulic cell with flush through was initially designed to allow for flush-through of the substrate. The set-up was inspired by Pham's (2017) set-up, with the triaxial replaced by the hydraulic cell. A gas trap was added to the back-pressure line to monitor expelled gas separately. It is assumed that anaerobic conditions are maintained

